AD-A251 945

NAVAL POSTGRADUATE SCHOOL
Monterey, California

DTIC
S ELECTE
JUN 0 5 1992
A D

NONLINEAR RESPONSE OF CYLINDRICAL
SHELLS TO UNDERWATER EXPLOSION:
TESTINGS AND NUMERICAL PREDICTION
USING USA/DYNA3D

by

LCDR P. K. Fox, USN
Professor Y. W. Kwon, Co-Investigator
Professor Y. S. Shin, Principal Investigator

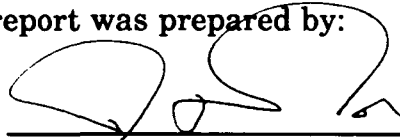June 1, 1991 - March 1, 1992

92-14818

Naval Postgraduate School
Monterey, California

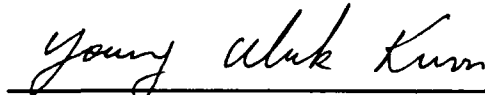Real Admiral R. W. West, Jr.
Superintendent

H. Shull
Provost

This report was prepared for and funded by both Defense Nuclear Agency, Alexandria, VA 20311 and Naval Postgraduate School, Monterey, CA 93943.
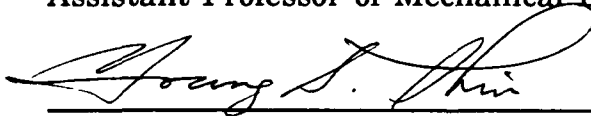
This report was prepared by:

_____
P. K. Fox
LCDR, USN

_____
Y. W. Kwon
Assistant Professor of Mechanical Engineering
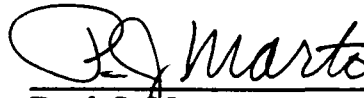
_____
Y. S. Shin
Professor of Mechanical Engineering

Reviewed by:

_____
Anthony J. Healey
Chairman
Dept. of Mechanical Engineering

Released by:

_____
Paul J. Marto
Dean of Research

REPORT DOCUMENTATION PAGE

1a. REPORT SECURITY CLASSIFICATION Unclassified	1b RESTRICTIVE MARKINGS
2a. SECURITY CLASSIFICATION AUTHORITY	3 DISTRIBUTION/AVAILABILITY OF REPORT Approved for public release: Distribution is unlimited.
2b. DECLASSIFICATION/DOWNGRADING SCHEDULE	
4. PERFORMING ORGANIZATION REPORT NUMBER(S)	5 MONITORING ORGANIZATION REPORT NUMBER(S)

6a. NAME OF PERFORMING ORGANIZATION Naval Postgraduate School	6b OFFICE SYMBOL (If applicable) ME	7a NAME OF MONITORING ORGANIZATION Naval Postgraduate School
6c. ADDRESS (City, State, and ZIP Code) Monterey, CA 93943-5000		7b. ADDRESS (City, State, and ZIP Code) Monterey, CA 93943-5000

8a. NAME OF FUNDING/SPONSORING ORGANIZATION Defense Nuclear Agency/NPS	8b OFFICE SYMBOL (If applicable)	9. PROCUREMENT INSTRUMENT IDENTIFICATION NUMBER

8c. ADDRESS (City, State, and ZIP Code) DNA: Alexandria, VA 22310 NPS: Monterey, CA 93943	10 SOURCE OF FUNDING NUMBERS		
	PROGRAM ELEMENT NO.	PROJECT NO	TASK NO	WORK UNIT ACCESSION NO.

11. TITLE (Include Security Classification)
Nonlinear Response of Cylindrical Shells To Underwater Explosion: Testings and Numerical Prediction Using USA/DYNA3D

12. PERSONAL AUTHOR(S)   P. K. Fox, Y. K. Kwon and Y. S. Shin

13a. TYPE OF REPORT Progress Report	13b TIME COVERED FROM 6/91 TO 3/92	14 DATE OF REPORT (Year, Month, Day) 1992, March 1	15 PAGE COUNT 135

16. SUPPLEMENTARY NOTATION   The views expressed are those of the authors and do not reflect the official policy or position of DoD or US Government.

17.	COSATI CODES		18 SUBJECT TERMS (Continue on reverse if necessary and identify by block number)
FIELD	GROUP	SUB-GROUP	Underwater Explosion

19. ABSTRACT (Continue on reverse if necessary and identify by block number)
Nonlinear 3-D Dynamic Analysis Code (VEC/DYNA3D) has been interfaced with Underwater Shock Analysis Code (USA) and capabilities were developed to perform numerical analysis of submerged and semi-submerged marine structures subjected to underwater explosion. A series of numerical analysis were performed to determine the elastic and elasto-plastic responses of cylindrical shell type structures. The results were favorably compared with those of underwater explosion testings. The coupled code USA/DYNA3D makes possible to predict shock-induced damage response of naval structure. In addition, numerical sensitivity analyses were undertaken to determine the importance of various physical and numerical modeling factors. This study showed clearly three types of response modes of cylinder subjected to a side-on explosion: accordion mode, breathing mode and whipping mode.

20 DISTRIBUTION/AVAILABILITY OF ABSTRACT ☒ UNCLASSIFIED/UNLIMITED ☐ SAME AS RPT ☐ DTIC USERS	21. ABSTRACT SECURITY CLASSIFICATION Unclassified
22a. NAME OF RESPONSIBLE INDIVIDUAL Y.W. Kwon/Y.S. Shin	22b TELEPHONE (Include Area Code) 408-646-3385	22c OFFICE SYMBOL

DD FORM 1473, 84 MAR   83 APR edition may be used until exhausted   SECURITY CLASSIFICATION OF THIS PAGE
All other editions are obsolete

☆ U.S. Government Printing Office: 1986—606-24.

Best
Available
Copy

ABSTRACT

The coupling was made between a structural analysis code (VEC/DYNA3D) and an underwater shock analysis code (USA). The coupled computer program (USA/DYNA3D) was verified using a set of benchmark problems which had known analytical solutions. The benchmark problems were elastic analyses of a spherical and an infinite cylinder subjected to a plane wave. The comparison between the numerical and analytical solutions was very good.

An underwater explosion test was performed with an aluminum cylinder subjected to a far field, side on explosion. A pre-shot calculation using USA/DYNA3D determined critical locations to measure both axial and hoop strains of the cylinder. After the experiments, a post-shot calculation was undertaken using the free field pressure obtained from the physical experiment. The numerical results obtained using the elastoplastic analysis were very comparable to the experimental data except for some positions.

A series of numerical experiments were performed to determine the cause of the difference between the numerical and experimental results at some positions. It was found from the experimental data that there might be some rotation in the cylinder relative to the explosive. Considering the rotation in the numerical model improved the comparison. In addition, numerical sensitivity analyses were undertaken to determine the importance of various physical and numerical modelling factors.

Finally, this study showed there were three major response modes of the cylinder subjected to a side on explosion. They were the accordion mode, breathing mode as well as the whipping mode. Large plastic strains occurred at the center of the cylinder on the reverse side to the explosive and near the ends of the cylinder' on the near side to the explosive. The large plastic strains seemed to be related to the whipping motion.

Accesion For	
NTIS CRA&I	☑
DTIC TAB	☐
Unannounced	☐
Justification	
By	
Distribution /	
Availability Codes	
Dist	Avail and / or Special
A-1	

TABLE OF CONTENTS

LIST OF TABLES

I. INTRODUCTION

A research program is underway at the Naval Post Graduate School to study numerical modeling of ship structures subjected to both near and far field underwater explosions. This program is expected to improve the understanding of factors affecting the reliability of numerical models. In addition, it will provide insight into the dynamic response of surface ship and submarine hulls and the physics that lead to failure when a hull is subjected to an underwater shock wave. The current study centers around simple cylinders constructed of a homogenous material. Future studies will include more complex materials and structures as experience increases and the reliability of the numerical models is proven.

This paper describes progress of the research program to date and the expected line of future research. Previous results of this research program were provided in references 1-2. This report will describe the results of two numerical verification tests which were performed to prove the validity of a computer code software link which was developed for this project. It will also compare the numerical results with experimental results obtained from a underwater explosion test of an aluminum cylinder subjected to a side on attack. In addition, analyses were performed to determine the sensitivity of the results to mesh refinement, boundary effects, rotation

1

from expected configuration, and use of different types of shell elements. Results show that the computer code closely models simple known analytic results, and can provide close correlation to experimental results. Most of the inconsistencies between experimental and numerical results are most likely caused by uncertainties associated with physical model fabrication and the underwater explosion test rather than a failure of the numerical method to provide correct answers. Recommendations will be provided to improve control of future underwater explosion tests. Finally, preparations for future testing will be described and recommendations for additional study are provided.

II. NUMERICAL CODE DESCRIPTION AND VALIDATION

A. GENERAL DESCRIPTION OF THE METHOD

The primary purpose of this study was to match numerical results obtained from a computer program with experimental results from an underwater explosion test. For this initial study of a side on attack, a relatively simple model was used. The model consisted of a unstiffened, right circular cylinder constructed of a homogeneous material submerged in water. The cylinder was modelled using a dynamic finite element method (FEM) code called VEC/DYNA3D and the water was modelled using a boundary element method (BEM) code called USA (Underwater Shock Analyzer). The linkage between the two codes was developed in 1991 at the request of the Naval Post Graduate school under funding provided by the Defense Nuclear Agency (DNA).

B. VEC/DYNA3D FINITE ELEMENT METHOD CODE

VEC/DYNA3D [Ref. 3] is an explicit finite element code. It has been used successfully for various types of nonlinear engineering problems since its conception in 1976. VEC/DYNA3D was selected for this study for several reasons. First, as stated above, VEC/DYNA3D is an explicit code. This attribute has two distinct advantages and two disadvantages. The advantages are its relatively high speed and its ability to be

3

implemented on a relatively small stand alone engineering work station. Initial work for this study is being performed on IBM RISC 6000 work stations. Once the USA/DYNA3D interface is proven to be reliable and accurate and experience has been gained in the use of the software, work will begin on more complex models using main frame type computers. Therefore it was important to obtain a code that was able to work significant problems on a small work station and yet be compatible with the main frames expected to be used in the future. DYNA3D is compatible with a full range of engineering work stations and has been implemented on the Los Alamos CRAY computer. Problems including up to 20000 solid elements have been run on work stations with 16 megabytes of random access memory.

The first disadvantage associated with the explicit numerical code is that the code is not inherently stable. This means that any problems dealing with time integration, including the underwater shock problems included in this study must be treated with care. Integration time steps must be matched closely with the size of the elements in the problem. This is performed automatically by DYNA3D in the stand alone mode. However, when coupled with the USA code, this automation is no longer functional. Incorrect selection of integration time steps can lead to significant oscillations and inaccuracies in the final solution. The second problem associated with the explicit codes is the mesh reflection

effect. Non-uniform meshes result in inaccurate solutions due to mesh reflection. Two factors appear to be important in ensuring that correct solution was obtained. The first is mesh size and the second is total mass of neighboring elements. Sensitivity analyses indicate that error in the final solution is relatively small if neighboring elements are kept within ten percent of each other in size. This was used as a rule of thumb in performance of this study. This lead to some inefficiency in obtaining solutions since often refinement had be performed over a larger area of the mesh to obtain a mesh independent solution than might normally be required in an implicit code. The additional area means more total elements and a subsequent increase in computation time to obtain the problem solution. These disadvantages can be overcome through careful planning. In general, they did not significantly overshadow the benefits associated with using an explicit code.

The second reason for selecting VEC/DYNA3D was its wide range of available material models and equations of state including the ability to model strain rate sensitivity, explosive materials and acoustic media. In addition, VEC/DYNA3D has a large degree of interactivity when used with the INGRID pre-processor [Ref. 4] and TAURUS post-processor [Ref. 5]. Changes can be entered with relative ease using the pre-processor and most physical components can be obtained

through knowledgeable use of the post-processor once the calculations are complete.

C. USA BOUNDARY ELEMENT METHOD CODE

The Underwater Shock Analyzer (USA) computer code [Ref. 6] is a boundary element computer code based on the Doubly Asymptotic Approximation (DAA) theory developed by Geers in 1971 (Ref. 7). Through the use of the DAA theory and the boundary element formulation, USA computes the acoustic pressure loading and added mass matrices which represent the fluid surrounding the submerged shell. The acoustic pressure loading and added mass are applied at selected wetted nodes. This formulation has the benefit of significantly decreasing the number of elements required to model the submerged system since external water elements need not be included in the calculations. The reduced number of elements requires substantially less time and storage space to obtain a solution.

However, it must be noted that this code has limitations which result directly from the fundamental assumptions associated with the DAA theory (Ref. 6). First, DAA is not theoretically appropriate for concave or multiple structures or near surface problems involving convex bodies. However, studies show that only results in highly shadowed, closely spaced areas or regions of strong concavity are affected. Secondly, DAA requires that the source of the incident wave be

6

sufficiently removed from the structure since it can only account for acoustic waves and not hydrodynamic flow. Finally, the DAA theory is based on an early time (high frequency) approximation coupled with a late time (low frequency) approximation. Therefore, although the DAA solution will be very good at early times when the high frequency approximation is dominant and at late times when the low frequency approximation is dominant, it can vary significantly from the analytic or exact solution during intermediate times when neither the high or low frequency solution is dominant. A detailed description of DAA theory is provided by reference 7.

D. COMPUTER CODE VERIFICATION

Since the USA/DYNA3D interface was new and had not been tested, some effort was expended on performing a verification of the performance of the code. To perform the verification, two cases with known analytic results were modelled using the USA/DYNA3D code. The first case was a quarter cylinder and the second was an infinite cylinder. Results were satisfactory for both cases and the code interface is believed to be performing correctly.

1. DETAILED DESCRIPTION OF THE SPHERICAL MODEL

The numerical study was performed on a quarter symmetry model of a sphere containing 150 elements. Figure II.1 shows the model and figure II.2 shows the test geometry.

7
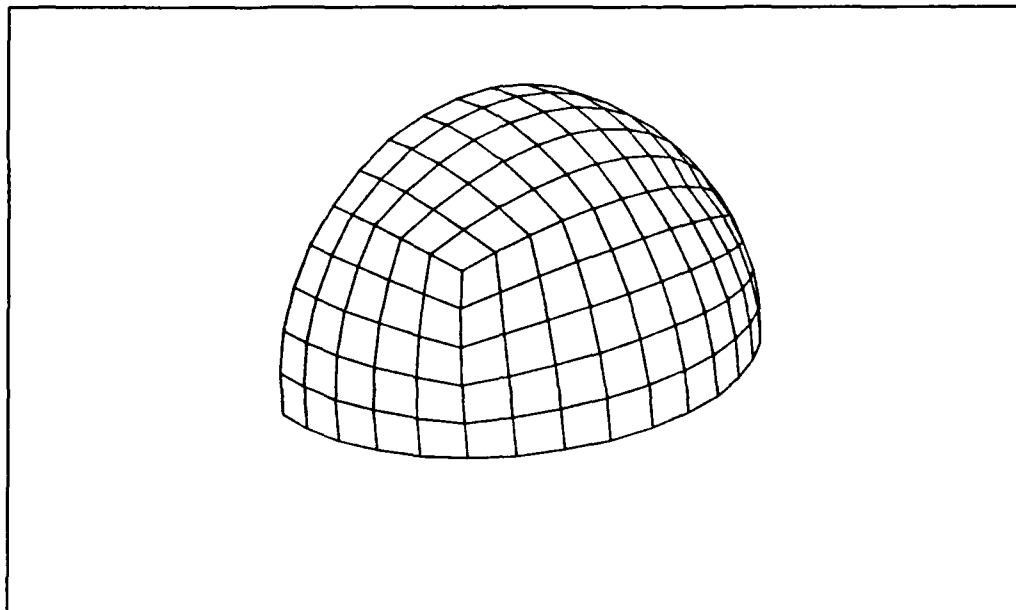
Figure II.1. Elastic sphere test case model.
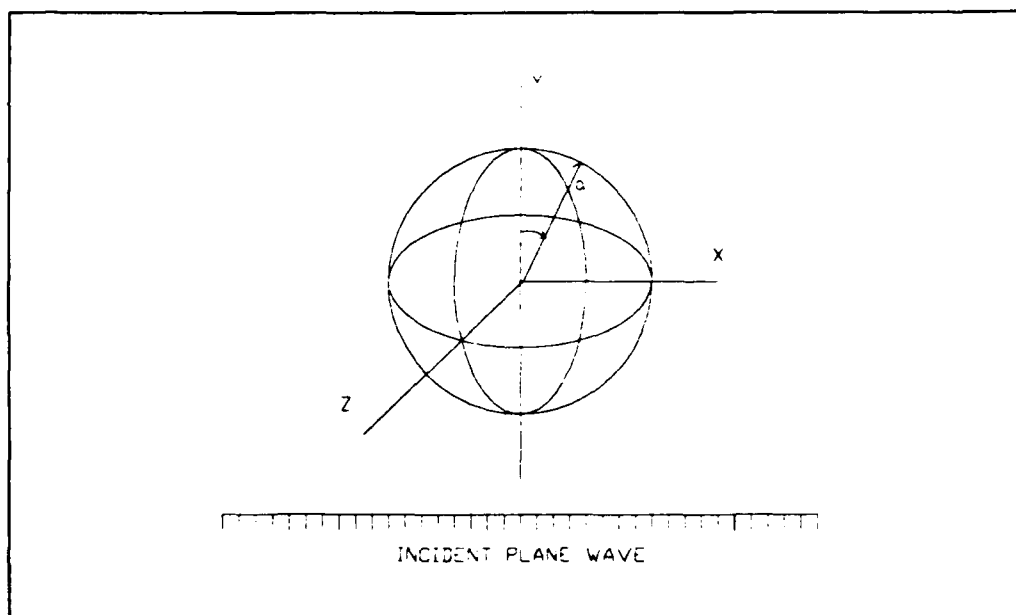
Figure II.2. Elastic cylinder test case geometry.

8

The thickness to diameter ratio of the shell is 1 to 50 and the shell is constructed of steel. The excitation is provided by a very small step pressure wave. As a result, the shell response is considered to be completely elastic. The case was run using the elastic material model of DYNA3D and, since results are being compared to the analytic results found in reference 8, the same material and water properties as those found in reference 8 were used. As stated in reference 8, the exact solution is obtained from separation of variables as shown in reference 9. The material and water properties used are listed below:

Steel Properties

Young's Modulus	$E=206.84$ GPa
Poisson's ratio	$v=0.33$
Mass density	$\rho=7784.5$ kg/m

Water Properties

Sound speed	$c=1461.2$ m/s
Density	$\rho=999.6$ kg/m

The numerical results using the USA/DYNA3D combination for the above test case compare favorably with the exact results. The normalized results are shown in figure II.3. It can be seen that the numerical results lag the exact results, but the difference is negligible. Copies of the INGRID pre-processor input and output as well as the USA pre-processor inputs are provided in Appendix A.

θ = 0

θ = π
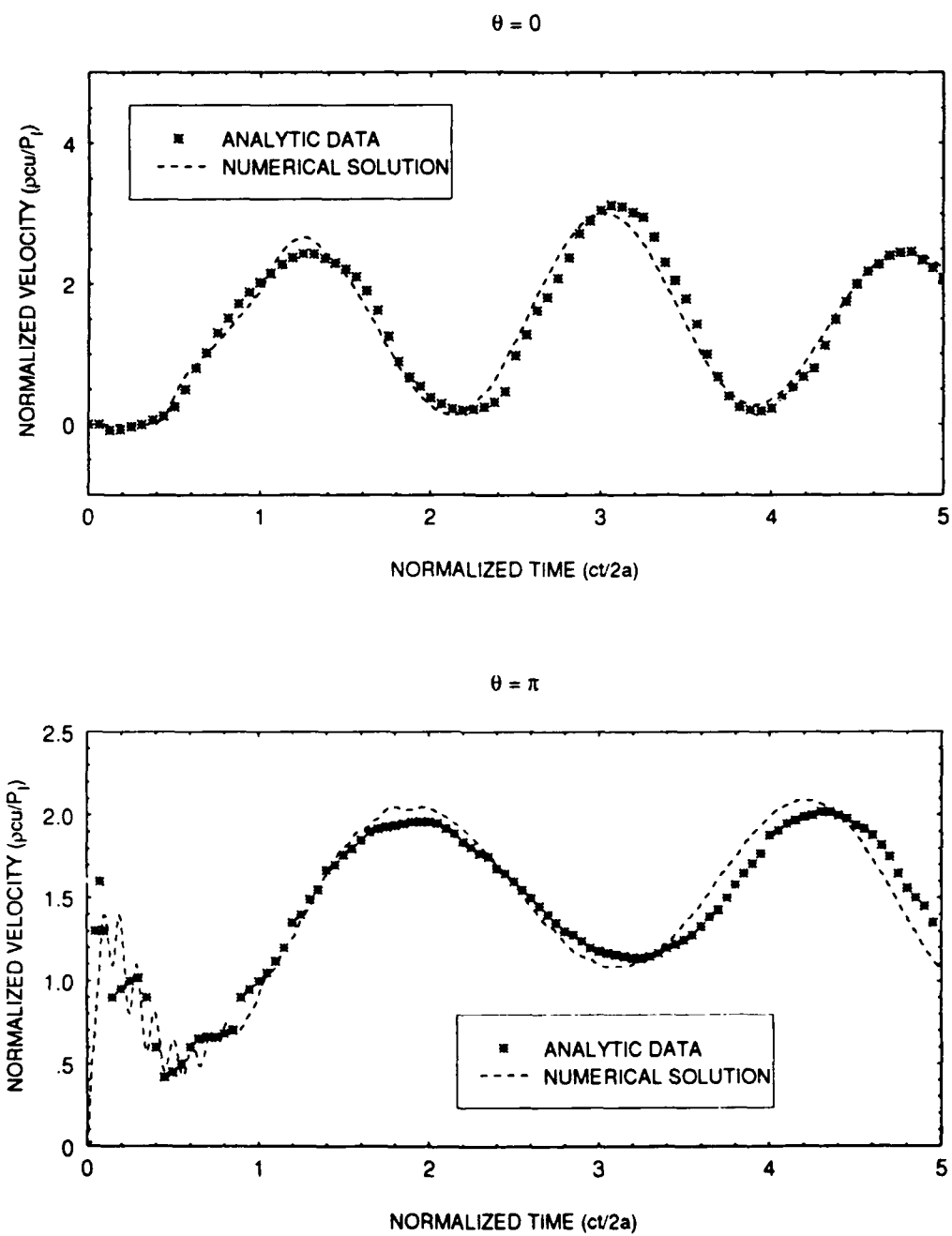
Figure II.3.   Spherical model verification results.

2. DETAILED DESCRIPTION OF THE INFINITE CYLINDER MODEL

The infinite cylinder model was run using the same material and water properties shown above. Figure II.4 shows the geometry used for the analyses and, as shown in figure II.5, a single ring of elements was used to model the infinite cylinder by enforcing symmetry boundary conditions on each end of the model. In addition, since this is a two dimensional problem, the TWODIM option in USA was used to generate the added mass and DAA matrices. Further, the value of the η variable was set to 0.0. η is the factor that accounts for curvature. This resulted in a DAA1 solution for comparison to a known analytic DAA1 solution. The first model attempted had a longitudinal length of 0.1 inches. However, it was discovered that this resulted in a oscillatory solution as shown in the first graph in Figure II.6. A similar oscillation occurred on the reverse side of the cylinder as shown in Figure II.7. After a check of the input data to ensure that the problem was not caused by numerical instability, it was hypothesized that the oscillation was caused by residual three dimensional effects caused by the finite width of the model. As a test of this hypothesis, two additional models were run with widths of 0.01 and 0.001 inches. As shown in Figure II.6 and II.7, reduction in width progressively reduced the oscillations on both the front and back of the cylinder. At 0.001 inches, oscillations are absent.

11
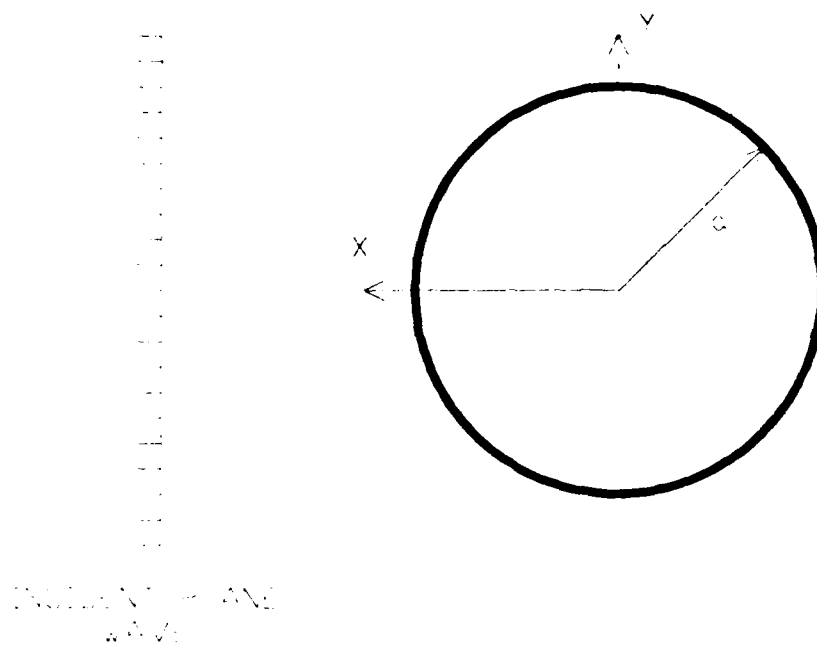
Figure II.4. Infinite cylinder problem geometry.
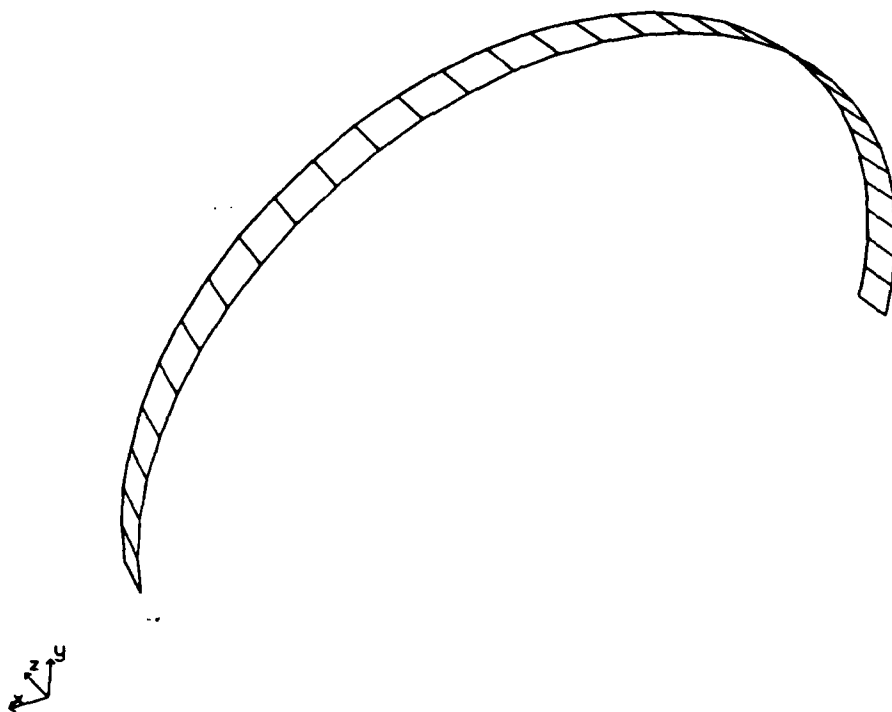
Figure II.5.   Infinite cylinder validation model.

L/a = 0.1, η = 0.0

L/a = 0.01, η = 0.0

L/a = 0.001, η = 0.0
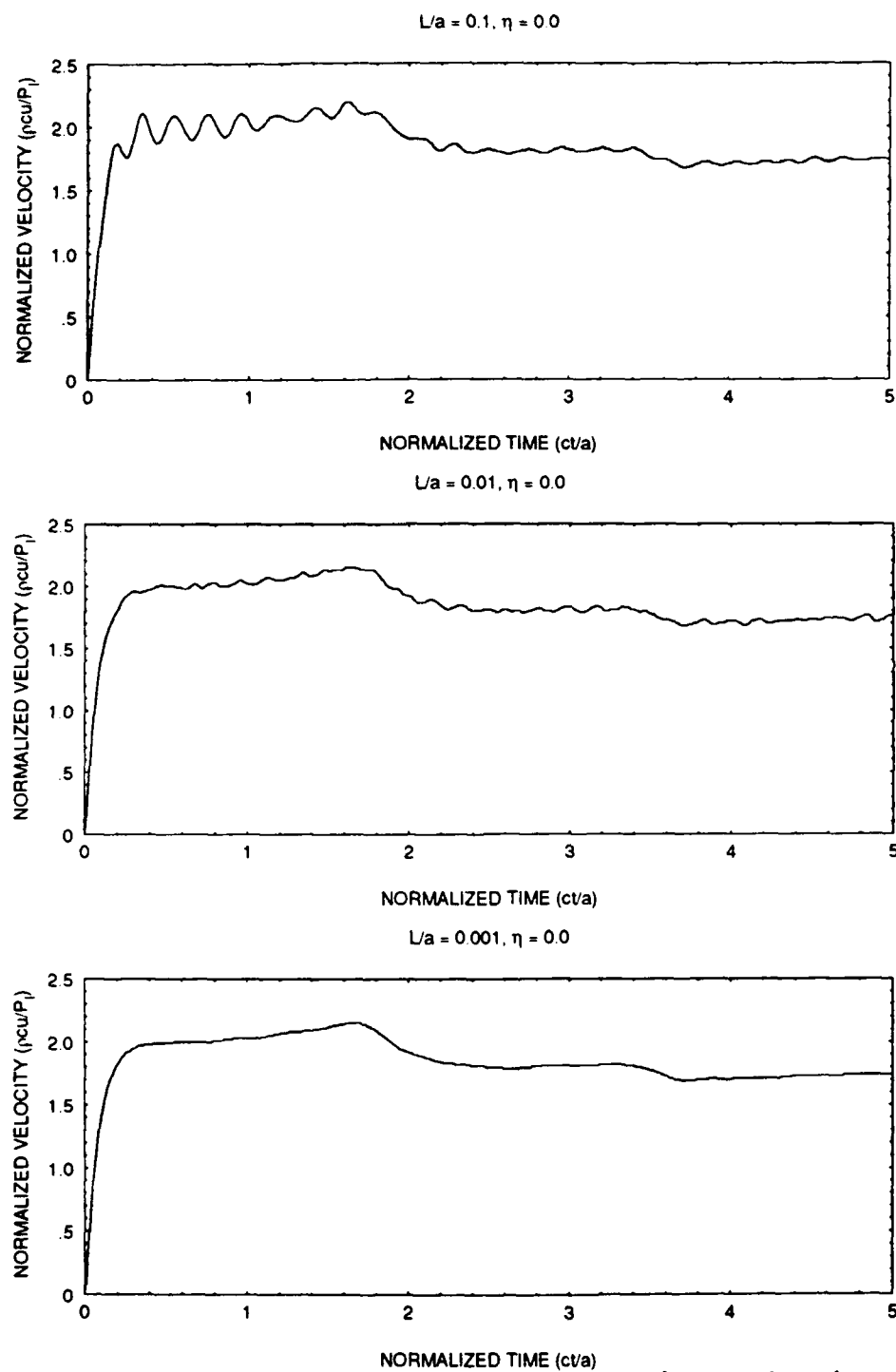
Figure II.6. Infinite cylinder oscillation reduction (near element).

14

L/a = 0.1, η = 0.0

L/a =0.01, η = 0.0

L/a = 0.001, η = 0.0
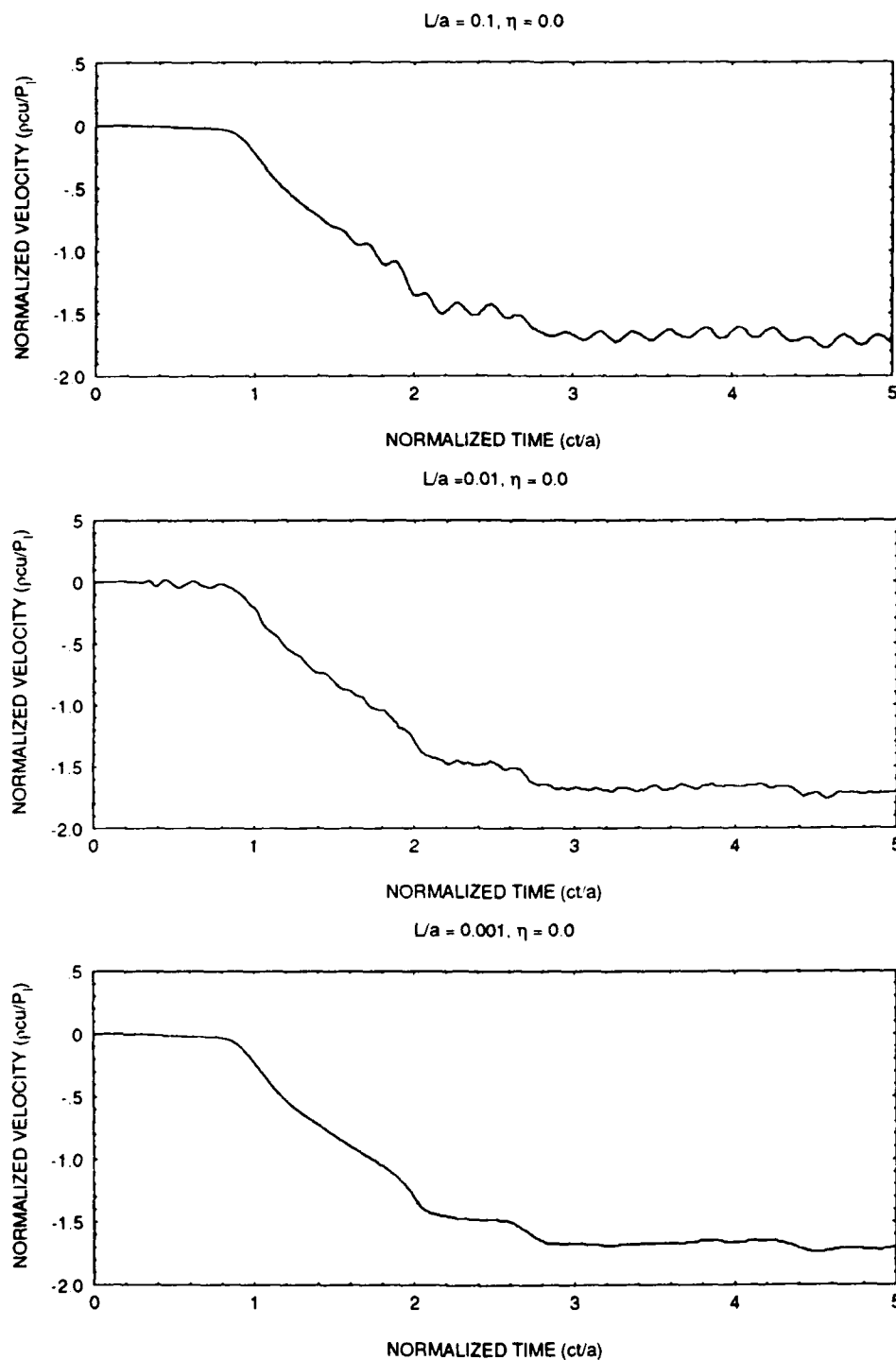
Figure II.7. **Infinite cylinder model oscillation removal
(far element).**

15

The final results from the 0.001 inch model with a η variable value of 0.0 were compared to the analytical exact and analytical DAA1 solutions with favorable results as shown in figure II.8. It can be seen that the results on both the front and back sides of the cylinder lie very close to the analytic DAA1 solution.

A further investigation was conducted to determine what value of the η variable would result in the numerical solution closest to the analytic modal solution. Values of 0.0, 0.25, 0.5, 0.75 and 1.0 were tested. The results are shown in figures II.8 through II.12. Review of the results show that the value of the η variable that provides the results nearest the analytical modal solution varies depending on time and position on the cylinder.

For the front of the cylinder, a DAA2 variable value of 0.0 gives results fairly close to the analytical solution for all times. However, values of 0.25 and 0.5, although they do not match closely at early times, match more closely at late times.

On the reverse side, a value of 0.0 provides a result very near the analytical DAA1 solution, but varies substantially from the analytical modal solution. Values of 0.5 and 0.75 provide results near the analytical modal solution with 0.75 being the best result.

Assuming that interest lies in late time results over

16

NEAR ELEMENT

REMOTE ELEMENT
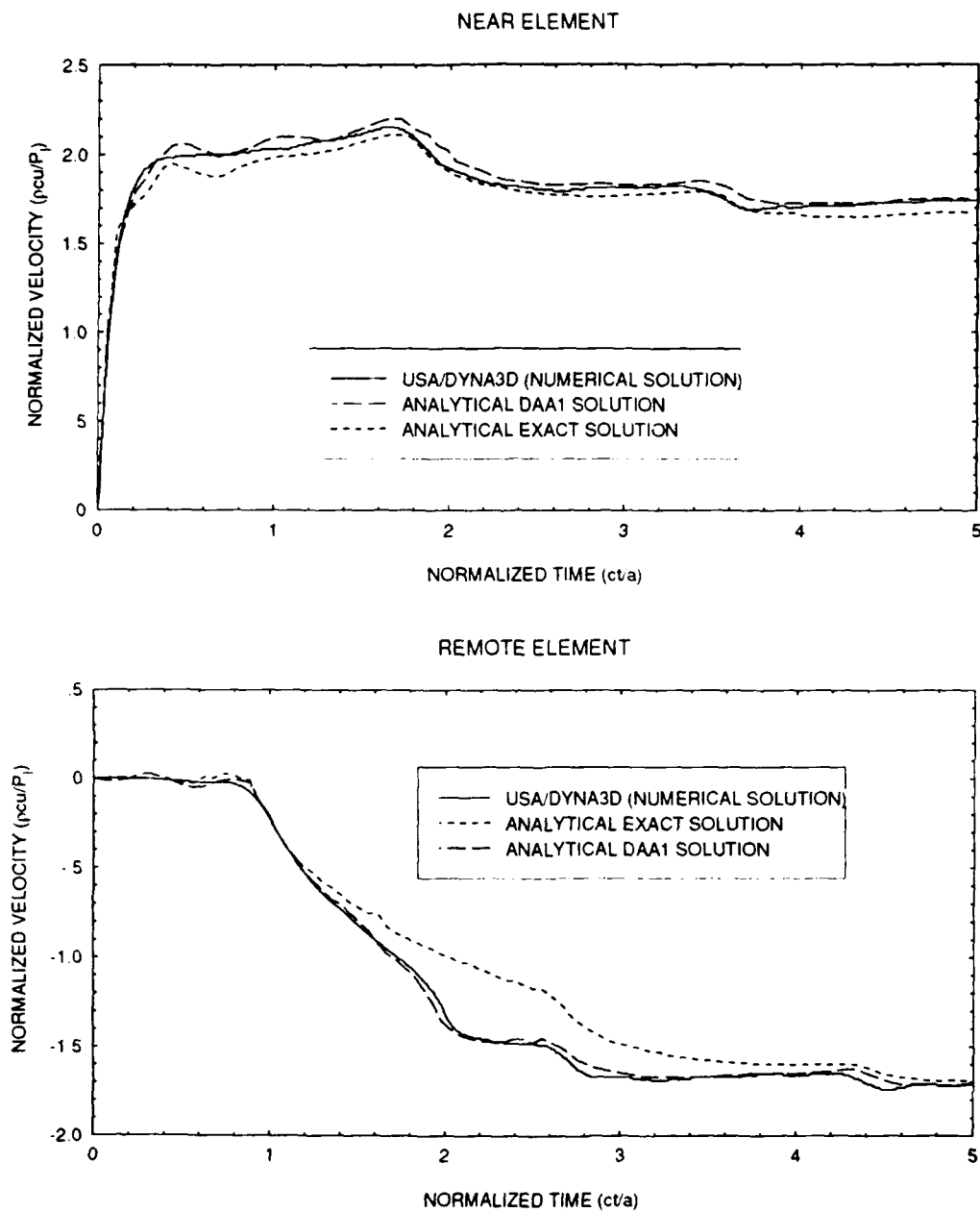
Figure II.8. Infinite cylinder results with η=0.0.

NEAR ELEMENT

REMOTE ELEMENT
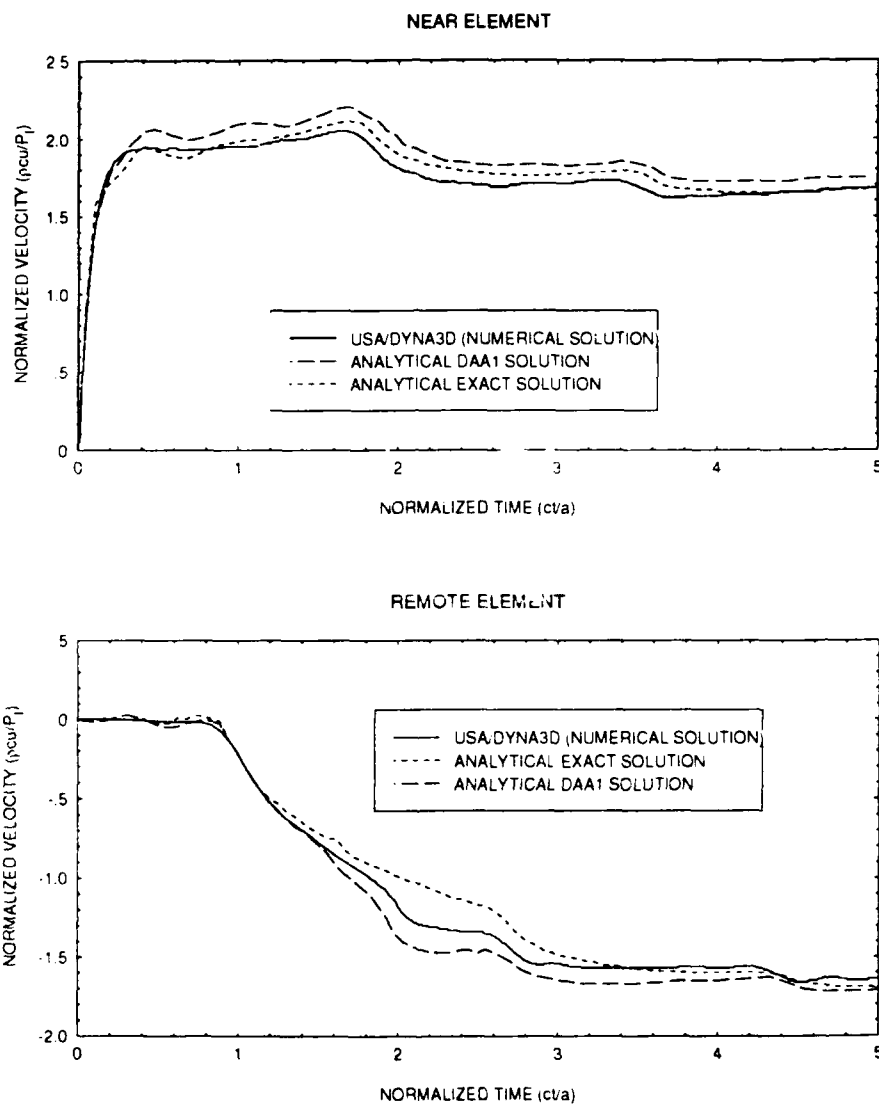
Figure II.9. Infinite cylinder results with η=0.25.

NEAR ELEMENT

REMOTE ELEMENT
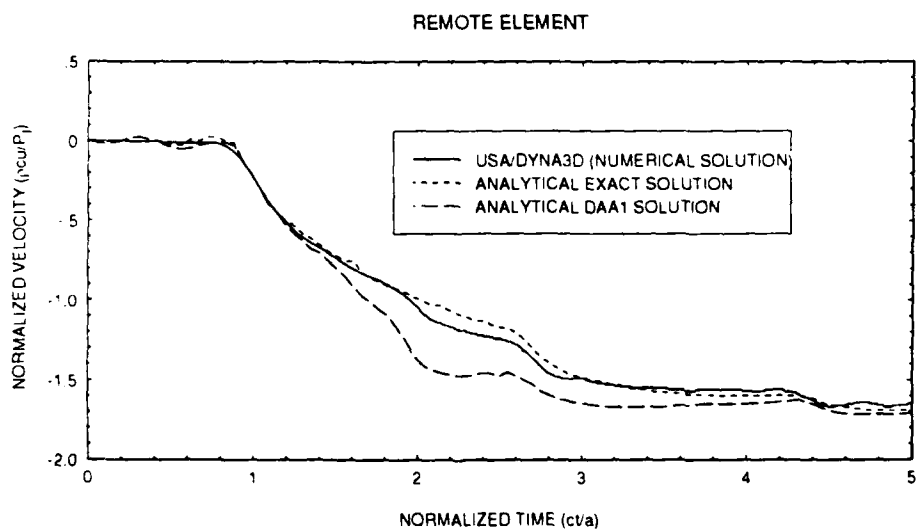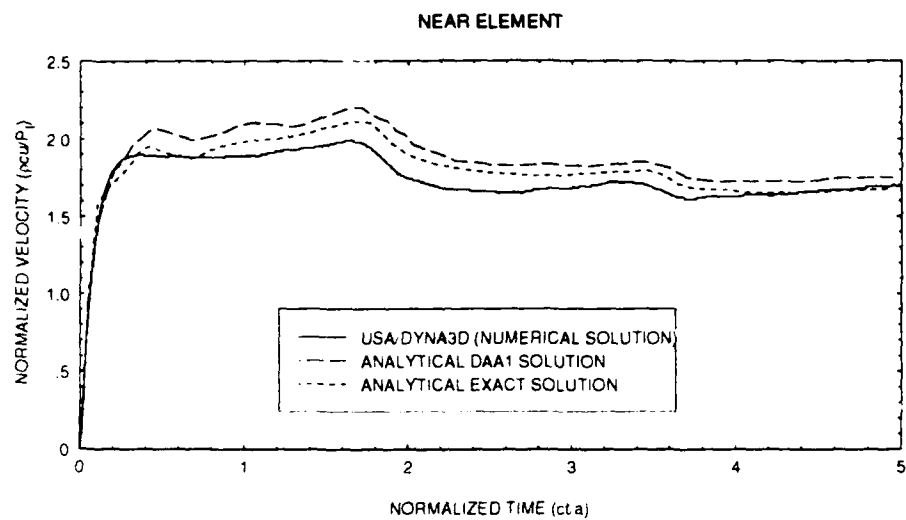
Figure II.10. **Infinite cylinder results with $\eta = 0.50$.**

19
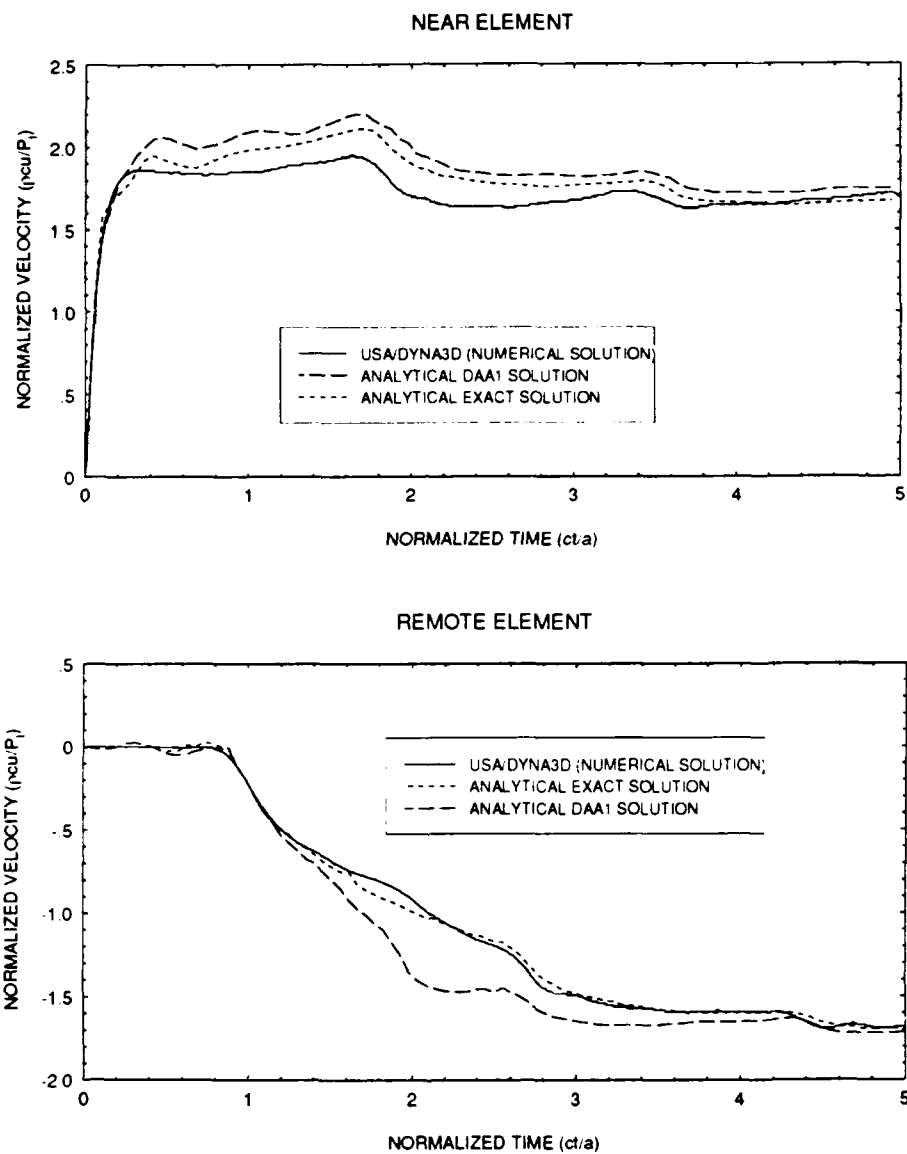
Figure II.11. Infinite cylinder results with $\eta=0.75$.

NEAR ELEMENT

REMOTE ELEMENT
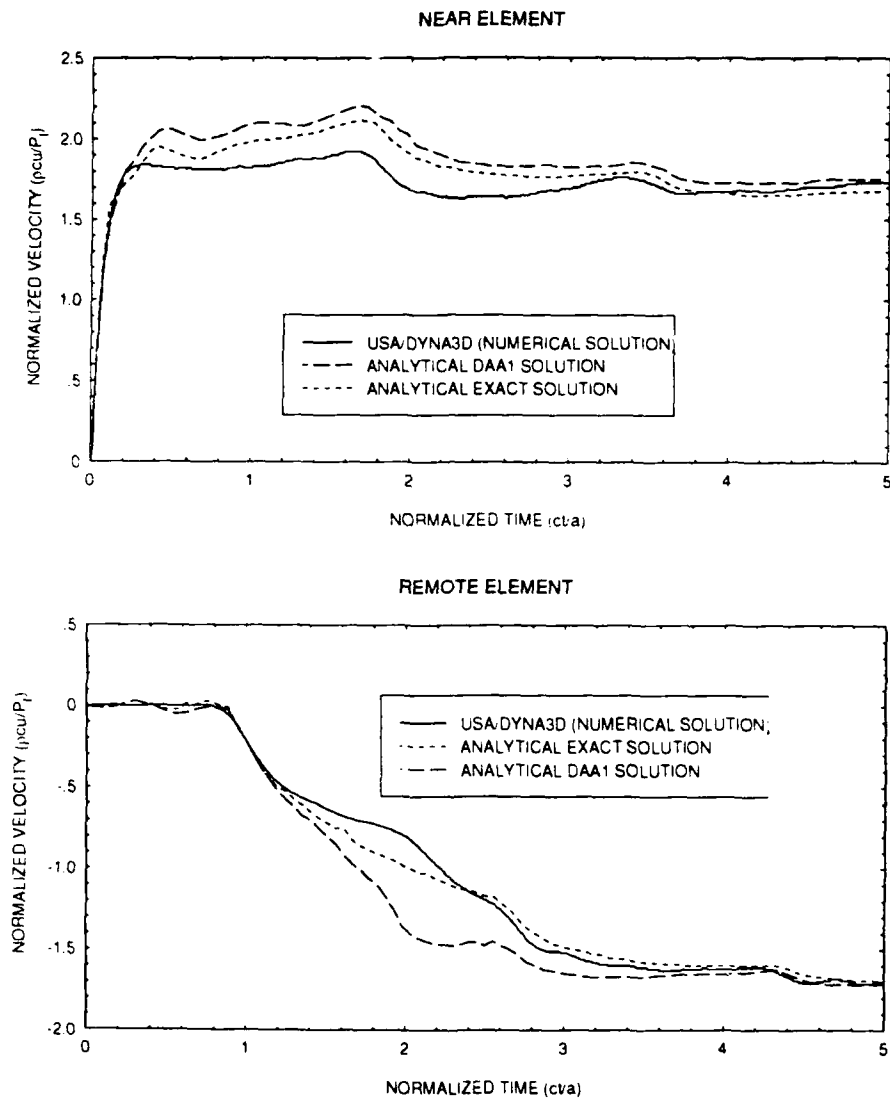
Figure II.12. Infinite cylinder results with η=1.0.

the entire cylinder, the results show that the best overall value of η for an infinite cylinder lies between 0.5 and 0.75. More compact bodies will have best results with higher η values.

The INGRID pre-processor input and output for the infinite cylinder verification, as well as the USA code pre-processor input are provided in Appendix B.

III. EXPERIMENTAL METHOD AND DESCRIPTION OF MODELS

A. DESCRIPTION OF PHYSICAL MODEL USED FOR THE FAR FIELD STUDY

The physical model was an unstiffened right circular cylinder with the following characteristics.

Dimensions:

Length	42 inches	(1.067 m)
Diameter	12 inches	(0.305 m)
Weight	60.5 pounds	(27.5 Kg)

Materials:

Shell	1/4 inch thick 6061-T6 Aluminum (0.64 cm)
End Plates	1 inch thick 6061-T6 Aluminum (2.54 cm)

The cylinders used for this test were constructed from commercially available material. Fabrication was performed at the Naval Postgraduate School. The end plates were welded to the shell using a Tungsten Inert Gas (TIG) process.

The 6061-T6 aluminum was selected on the basis of its high strength and strain rate insensitivity. The material properties of the aluminum used for the shell were verified using the MTS machine at the Naval Postgraduate School. Results of tensile testing determined that the material

23

properties were near nominal with a Young's modulus of 10800 ksi (75.6 GPa) and yield strength of 43 ksi (300 MPa).

B. UNDERWATER EXPLOSION TEST

The underwater explosion test was performed at the Dynamic Testing Incorporated (DTI) facilities in Rustburg, Virginia. The facility is in a quarry and the depth of the water is approximately 130 feet (39.6 m) at the location of the test. As a result, bottom reflection was not a factor in the test.

The charge used for the test was 60 pounds (27.3 Kg) of HBX-1. The peak pressure generated by the charge was 2360 psig (16.3 MPa) which was substantially lower than the calculated peak pressure of 2680 psig (18.5 MPa) for the 60 pound (27.3 Kg) charge at a 25 foot (7.62 m) standoff distance. The test charge was activated by a radio control device.

The test depth for both the charge and the cylinder was 12 feet (3.66 m). This depth allowed the bubble generated by the explosion to vent at the surface prior to encountering the cylinder and eliminated the possibility of a bubble pulse. In addition, the 12 foot (3.66 m) depth provided a clear pressure cutoff.

The cylinder was held in place with a crane rig and the charge was suspended from a float. Distance and alignment of the charge to the cylinder was established and maintained using a tensioned span wire from the charge float to the

24

cylinder support rig. Post-shot calculations found the arrival time of the shock wave to be consistent with a distance of 25 feet (3.66 m) and sound of speed in water of 4800 ft/sec (1463 m/s). Test profile and arrangement are provided as figures III.1 and III.2.

Strain measurement was performed using CEA-06-250UW-350 strain gages. These are general purpose strain gages with an optimum range of ± 1500 microstrain and are good for both static and dynamic test measurements. The strain gages were bonded to the cylinder using a M bond 200 by a instrumentation technician employed by DTI. All pre-shot calibration and connection were performed by DTI technicians.

The test called for 14 total strain gages (seven to measure hoop strains and seven to measure axial strains). Of the fourteen strain gages, three failed. The dynamic range of the test exceeded the optimum range of the strain gages by a significant factor. This is the most probable cause of the high strain gage failure rate. The instrumentation diagram for the test is provided as figure III.3. The strain gage located at B1 was placed nearest the charge during the test. Strain gage output was filtered at 2000 Hz. Locations noted on figure III.3 will be used for reference throughout the remainder of the report.

Slight damage to the cylinder was noted upon completion of the test. Post-shot investigations found all strain gages firmly attached to the cylinder at the locations specified in

25
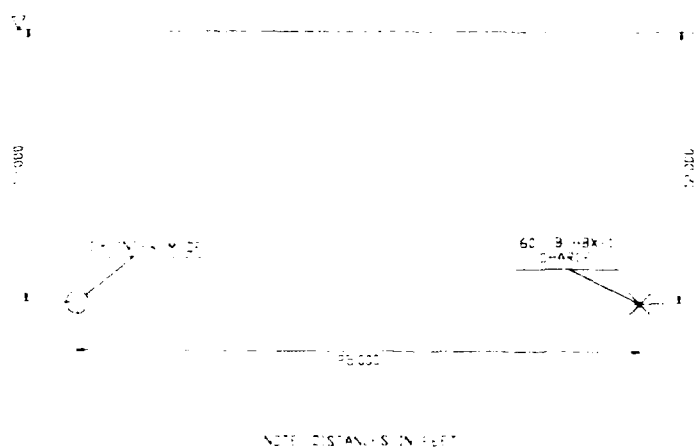
Figure III.1. Undex test profile.

PRESSURE TRANSDUCER

NOTE: DISTANCES IN FEET
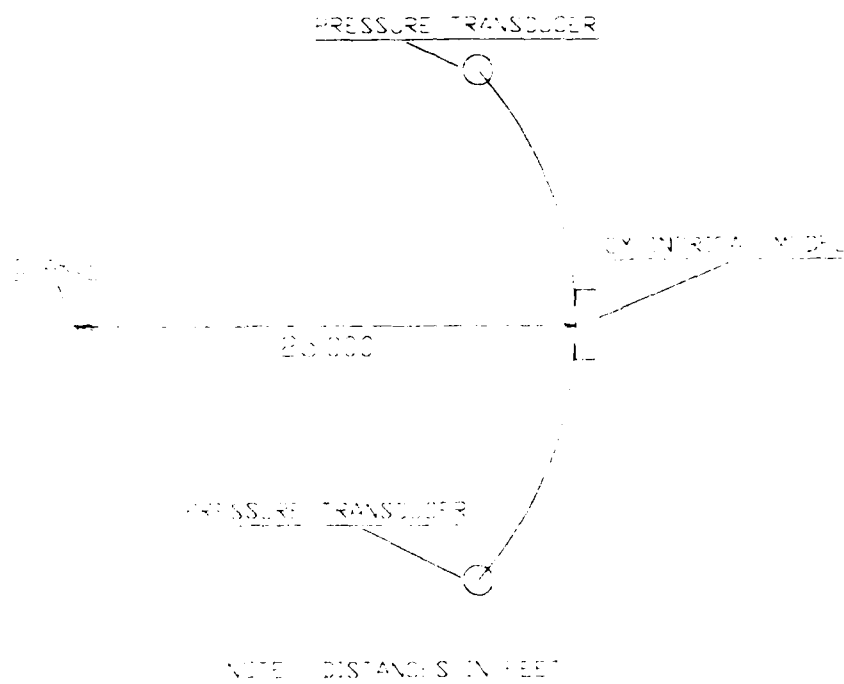
Figure III.2. Undex test general arrangement.

27

Figure III.3. Undex test instrumentation diagram.

the instrumentation diagram. However, some water intrusion was noted under the protective coating of several of the strain gages. This intrusion may also have played a part in the strain gage failures. The results of the test were forwarded to the Naval Postgraduate School. A copy of the report is enclosed as Appendix C.

C. NUMERICAL MODEL

This study was performed using two primary mesh densities. The low density, full model mesh (figure III.4) was used for rotation, shell type and quadrature sensitivity analyses. The high density quarter model was used to perform direct comparison to experimental results and examine end effects.
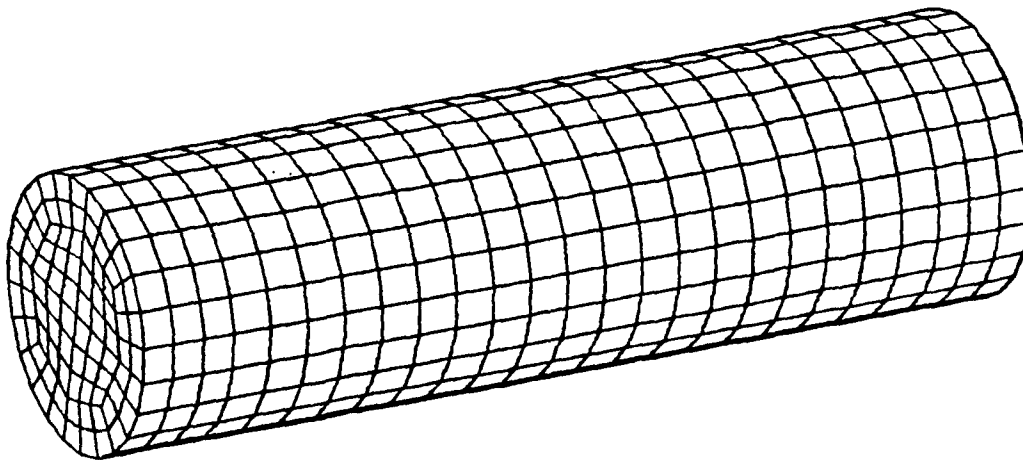
Figure III.4. Low density, full model

The computational efficiency of the quarter model allowed a more refined mesh without a subsequent increase in

29

computational time or random access memory storage capability. A sample quarter model was run and results checked against a full model with the same mesh configuration to certify that the symmetry boundary conditions used to form the quarter model were valid. The refined mesh quarter model is shown in figure III.5.
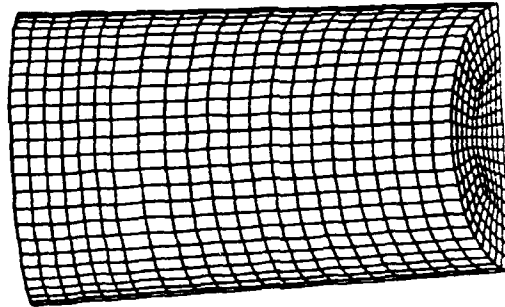
Figure III.5. Refined mesh model.

In addition to the two model noted above, several additional quarter models with varying mesh density were run to verify mesh size independence of the quarter model results. It was found that the most critical locations for the mesh sensitivity check were the locations with the highest strain. The areas with the highest strain were located near each end on the side of the cylinder located nearest the explosive charge. Figure III.6 shows the strain pattern on the surface

of cylinder side nearest the charge. The high strain locations are symmetrically located 16.5 inches (0.42 m) from the axial midpoint of the cylinder. The other region of significant plastic strain was located on the surface of the reverse side of the cylinder at the axial midpoint. Figure III.7 shows the effective plastic strain pattern for this location. Effective plastic strain is defined by the relation:

$$\overline{\varepsilon_p} = \frac{\sqrt{2}}{3} [(\varepsilon_{1p} - \varepsilon_{2p})^2 + (\varepsilon_{2p} - \varepsilon_{3p})^2 + (\varepsilon_{3p} - \varepsilon_{1p})^2]^{\frac{1}{2}}$$

where ε_{1p}, ε_{2p} and ε_{3p} represent the principal plastic strain components [Ref. 10]. The near side high strain regions cover a much smaller area than the reverse side region. That is, much higher strain gradients occurred on the near side compared to other locations on the cylinder. This condition plays a significant roll in mesh design and integration time increment selection.

Figures III.8 through III.10 show the results of the mesh sensitivity test. It was found that strains in the axial direction were more sensitive to mesh density than hoop strain results. Figure III.8 shows the strain at the surface of the cylinder at the point nearest the charge (location B1). This

31

time = .59796E-02
fringes of eff. plastic strain
min= 0.000E+00 in element   768
max= 6.431E-03 in element   442

fringe levels
9.000E-04
1.800E-03
2.700E-03
3.600E-03
4.500E-03
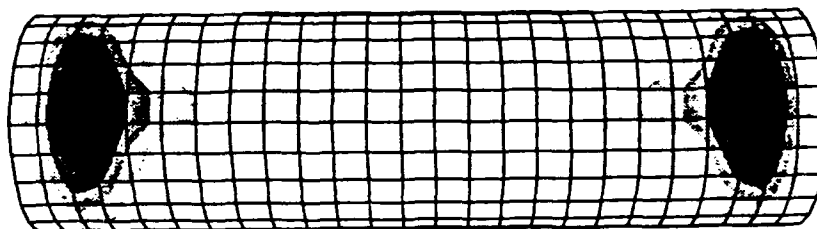
Figure III.6. Effective plastic strain pattern on cylinder side nearest the explosive charge.

time = .59796E-02
fringes of eff. plastic strain
min= 0.000E+00 in element   768
max= 6.431E-03 in element   442

fringe levels
9.000E-04
1.800E-03
2.700E-03
3.600E-03
4.500E-03
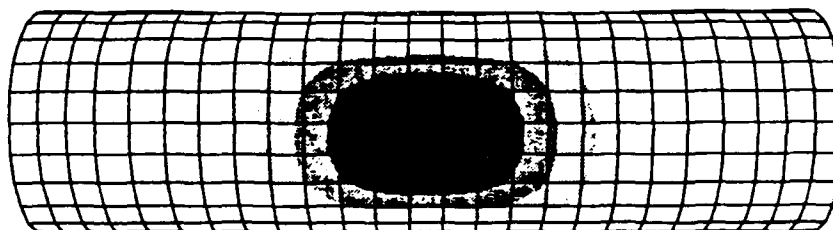
Figure III.7. Effective plastic strain pattern on cylinder side most remote from the charge.

32

location has no permanent plastic strain. It can be seen that there is no significant difference between the results for the three mesh densities checked. Figure III.10 shows strain results for the surface of the shell at the point most remote from the charge in the circumferential direction at the axial midplane (location B3). This location had the second highest strain of the positions checked. Although there is a slight difference between the three different mesh results, it is apparent that these differences are insignificant when compared to the overall plastic strain. Figure III.9 shows the strain results for the locations that experienced the highest plastic strains (locations A1 and C1). The difference in the hoop direction is noticeable but small enough to be neglected. However, the results in the axial direction are significant with a 30 percent variance between the average plastic strains for the high density mesh and medium density mesh. Additional refinement was not possible due to random access memory limitations on the system used to perform the analysis. On the basis of the above results it was determined that the medium mesh model was adequate for comparison of numerical to experimental results for all hoop strains and all axial strains except at the locations near the end on the side nearest the charge. The high density mesh was used for the axial strain comparison at the remaining locations. Care was taken to ensure that the mesh was as uniform as possible for both the full and the quarter mesh models to avoid problems

33

HOOP STRAIN

AXIAL STRAIN
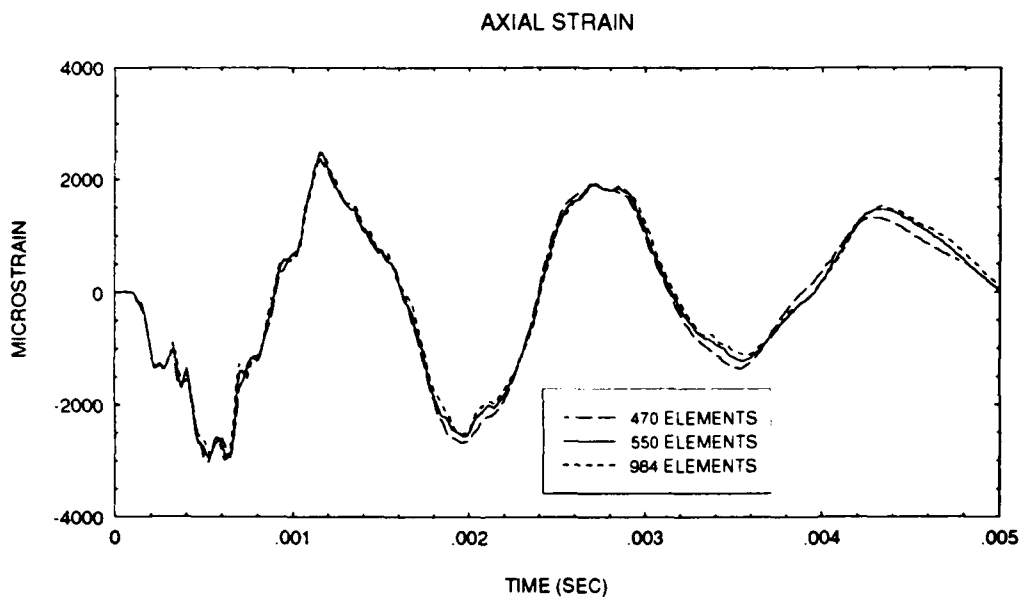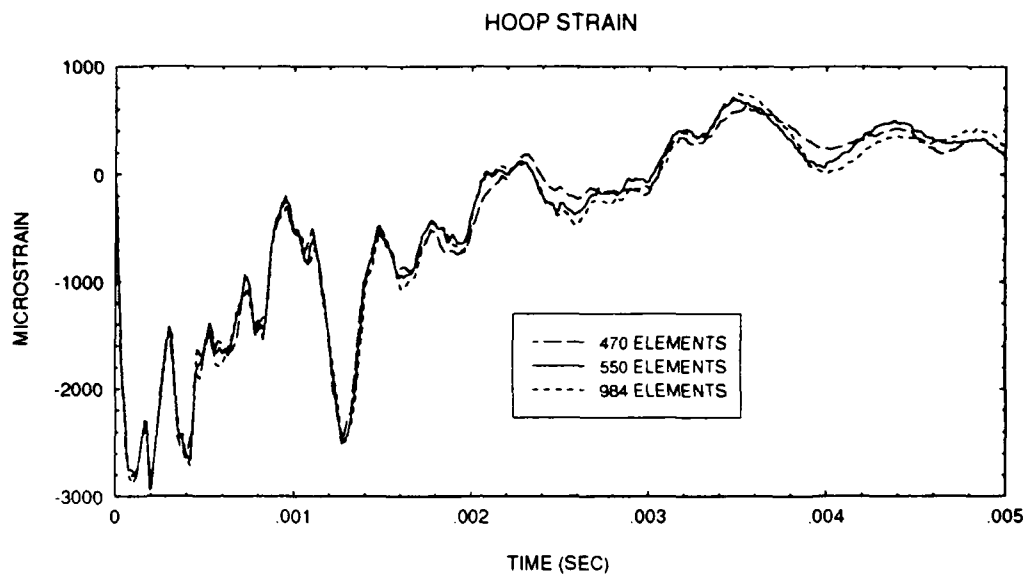
Figure III.8. Mesh sensitivity comparison for surface of shell located nearest the explosive charge (location B1).

34

HOOP STRAIN

AXIAL STRAIN
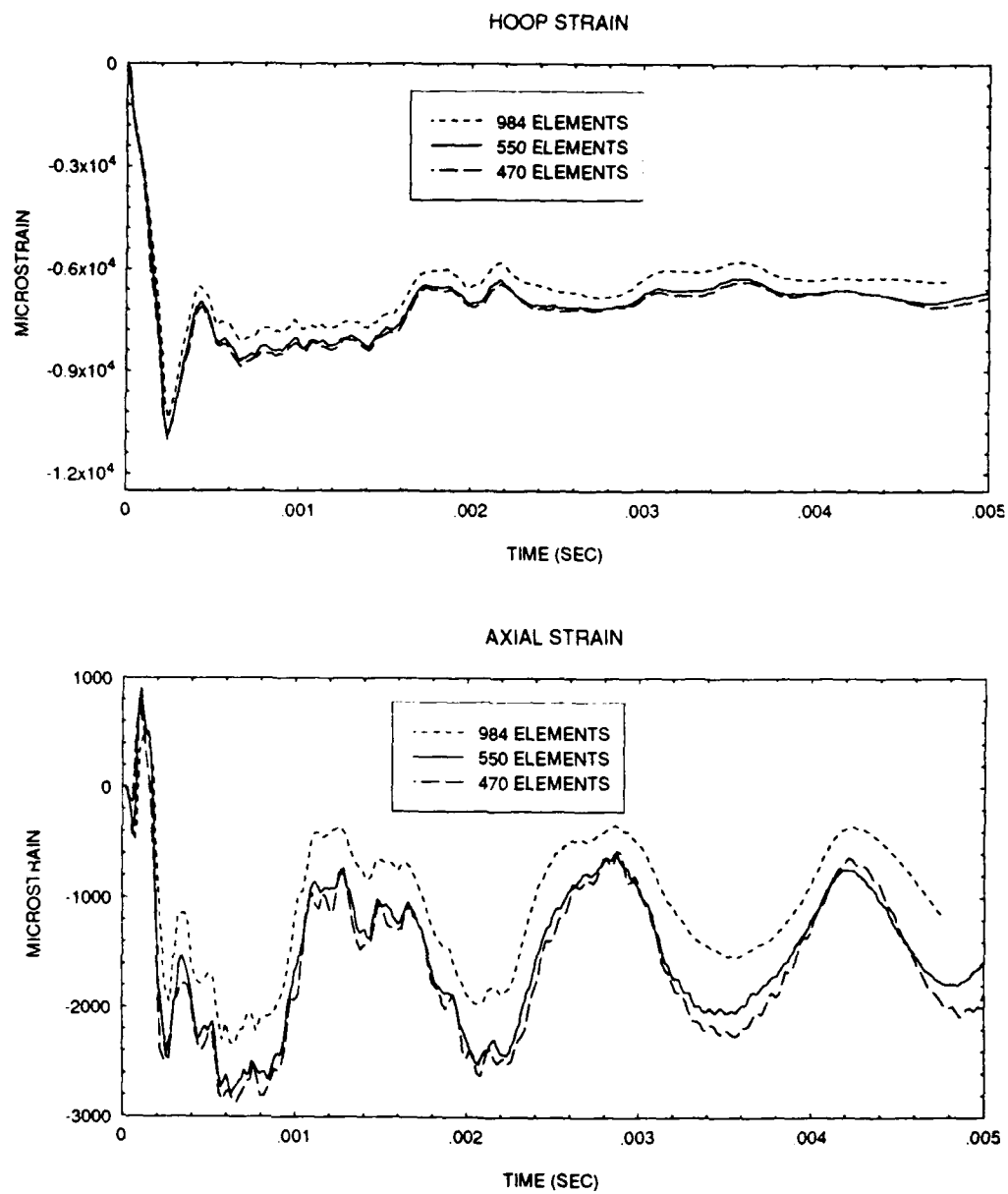
Figure III.9. Mesh sensitivity comparison for position with largest plastic strain (locations A1 and C1).

HOOP STRAIN

AXIAL STRAIN
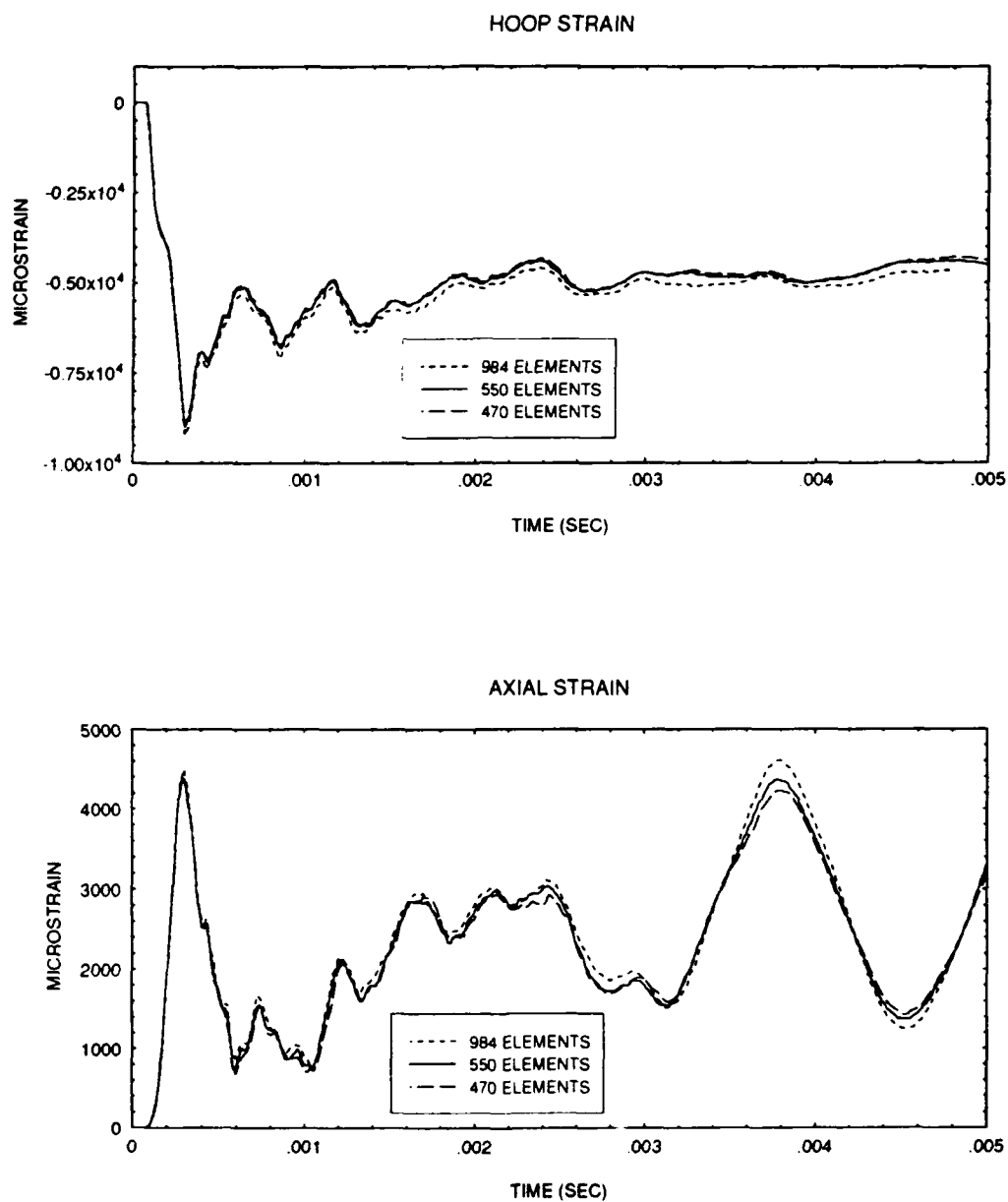
Figure III.10. Mesh sensitivity comparison for point on cylinder most circumerentially remote from the charge (location B3).

with mesh reflection as noted earlier in this report.

Thin shell elements were used for both the shell and end plates. Since relatively small out of plane displacements were encountered in the test model, it was determined that the four node Belytschko/Lin/Tsay shell formulation [Ref 11], which is the default formulation for VEC/DYNA3D, was adequate for the analysis. A Hughes/Liu [Ref. 12] shell model and a eight node brick shell model were also run for comparison.

The Belytschko/Lin/Tsay shell was selected over the Hughes/Liu shell and 8 node brick shell formulation because of its higher relative computational efficiency.

The aluminum was treated as a kinematic/isotropic elastic/plastic material with no strain rate sensitivity. Research has shown that shock velocities much higher than the velocities encountered in the test are required to induce strain rate sensitivity in 6061-T6 aluminum.

The pressure input for the model was obtained from the free field pressure transducer time record of the underwater explosion test. The 17000 point trace was numerically condensed to 100 points and entered into the TIMINT pre-processor of USA using the VARLIN (variable linear) option. Figure III.11 shows the pressure profile used for the analysis. Free surface effects were neglected and the speed of sound in water used for the test was 4800 ft/sec (1463 m/s) since the test was performed in fresh water at approximately 40 degrees Fahrenheit (4.5 degrees centigrade).

37
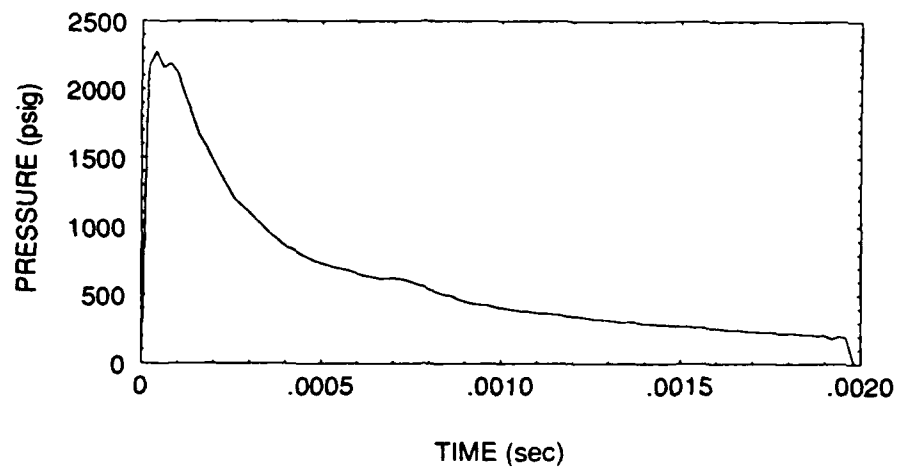
Figure III.11. Undex pressure profile.

IV. FAR FIELD STUDY RESULTS

A. EXPERIMENTAL TO NUMERICAL COMPARISON

As described earlier in the report, an underwater explosion test was conducted at the Dynamic Testing, Incorporated facility in Rustburg, Virginia. The test included a side-on attack of a cylinder with a stand off distance of 25 feet (7.62 m) using a 60 pound (27.3 Kg) HBX-1 charge. Fourteen strain gages were attached to the cylinder, of which eleven provided useable data. Four statements can be made about the results. First, the numerical results compared well with the experimental results qualitatively. That is, the numerical response had the same general shape as the experimental results and it predicted compression and tension correctly. There was one exception to the above statement at position B3 (Figure IV.9). The numerical model indicated a tensile axial strain at position B3 while the experimental data indicated a compressive strain. Physically, it can be observed that the shock wave is spherical and initially strikes the cylinder center. This places the cylinder in bending. Therefore, tensile strain is expected in the axial direction on the reverse side of the cylinder. It is believed that the poles on the axial strain gage at position B3 were reversed resulting in an error in sign of the data returned by

the strain gage. As a result, the negative of the experimental strain is plotted versus the numerical results in Figure IV.9 with satisfactory results.

Second, there were variations in magnitude between the numerical results and the experimental data. Further, magnitudes matched the experimental results more closely at the position nearest the charge and error increased as distance from the point nearest the charge increased in both the axial and circumferential directions. In addition, numerical and experimental results match more closely in areas with lower values of total strain. Finally, axial strains were affected more than hoop strains. Charge size factors were eliminated as a possible cause of the magnitude differential since the measured pressure profile was used to perform the post underwater explosion test numerical calculations. In addition, the possibility of the charge being located closer to the shell than the specified standoff distance was eliminated by comparing the actual shock wave travel time measured from the strain gage traces to the expected shock wave travel time calculated for the speed of sound in water for fresh water at 40 degrees Fahrenheit (4.4 degree centigrade). The results indicated less than two inches difference between the calculated and measured values for stand off distance.

Third, the frequency of oscillation of the numerical data was lower than the experimental data. The higher frequency

40

oscillation in the physical model compared to the numerical model indicates that the experimental model is "stiffer" than the numerical model. This is an unexpected result, since numerical finite element solutions are normally expected to be stiffer than the physical model. In addition, the numerical results for axial strain tended to "ring" at all locations. The "ringing" is not a significant factor for hoop strains. It should also be noted that the "ringing" is heaviest at the front and back of the cylinder at the center. The causes of the "ringing" and the high stiffness of the physical model have not been determined and are a topic of additional study.

Finally, there is an unexpected asymmetry in the experimental results. The axial strain gage at position C1 (figure IV.10) measured 50% lower than the axial strain gage at A1 (figure IV.1) and the hoop strain gage at position C2 (figure IV.11) measured nearly 50 percent higher than the hoop strain gage at position A2 (figure IV.2). Failure of strain gages at positions A1, C1, and C2 prevented additional comparisons. The asymmetric results can result from two factors. The shell may have been rotated from the expected orientation by underwater currents or by forces placed on the cylinder and rigging by the instrumentation cables or there could have been a failure in the bonding between the strain gage and the cylinder surface on one or more strain gages.

Figures IV.1 through IV.11 provide the results of the numerical to experimental data comparison.

41
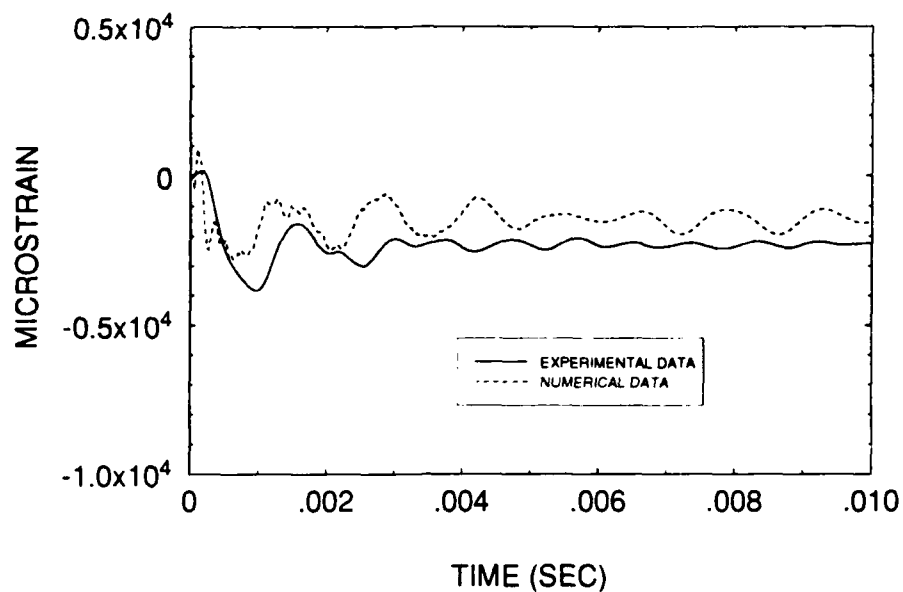
Figure IV.1. Experimental/numerical comparison for position A1 axial strain.
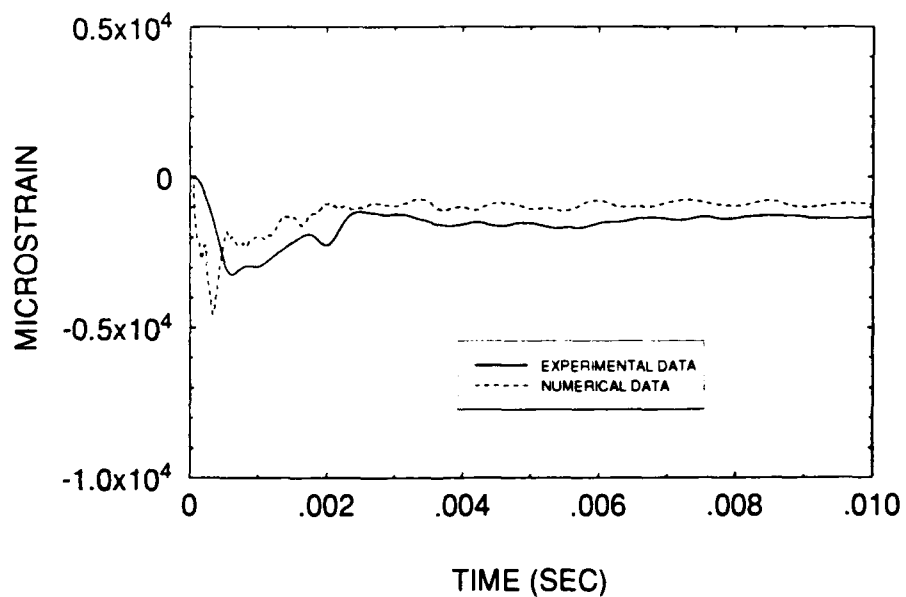
Figure IV.2. Experimental/numerical comparison for position A2 hoop strain.

42
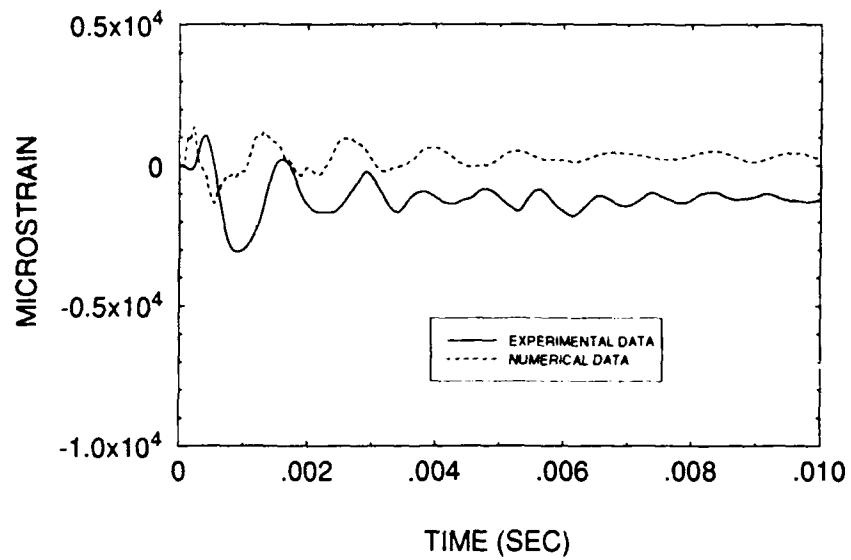
Figure IV.3. Experimental/numerical comparison for position A2 axial strain.
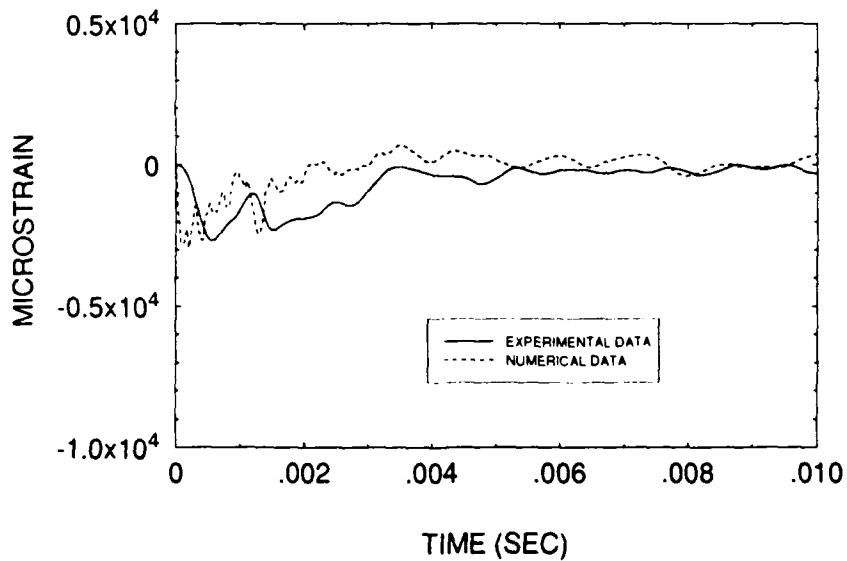
Figure IV.4. Experimental/numerical comparison for position B1 hoop strain.
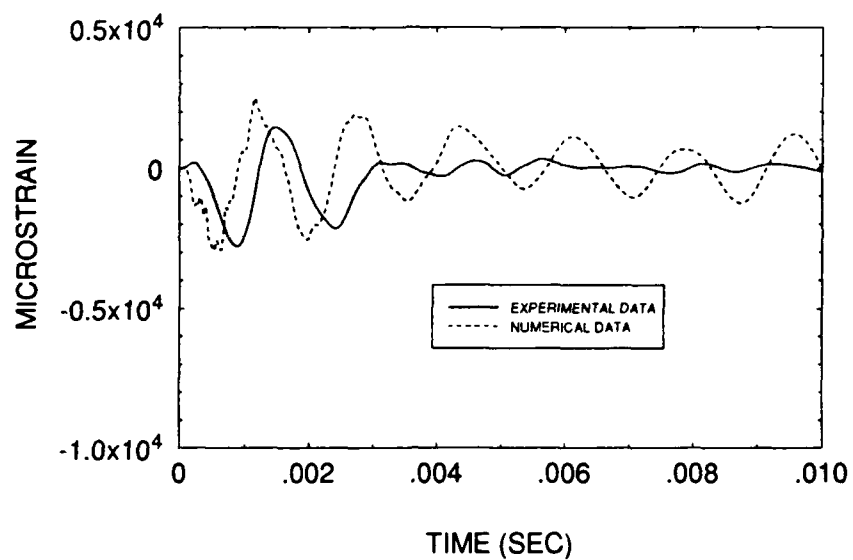
Figure IV.5. **Experimental/numerical comparison for position B1 axial strain.**
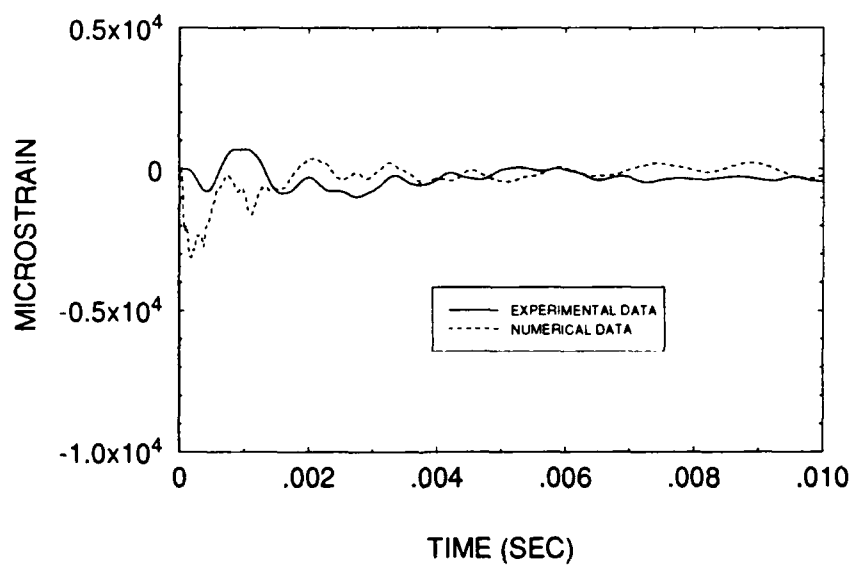
Figure IV.6. **Experimental/numerical comparison for position B2 hoop strain.**

44
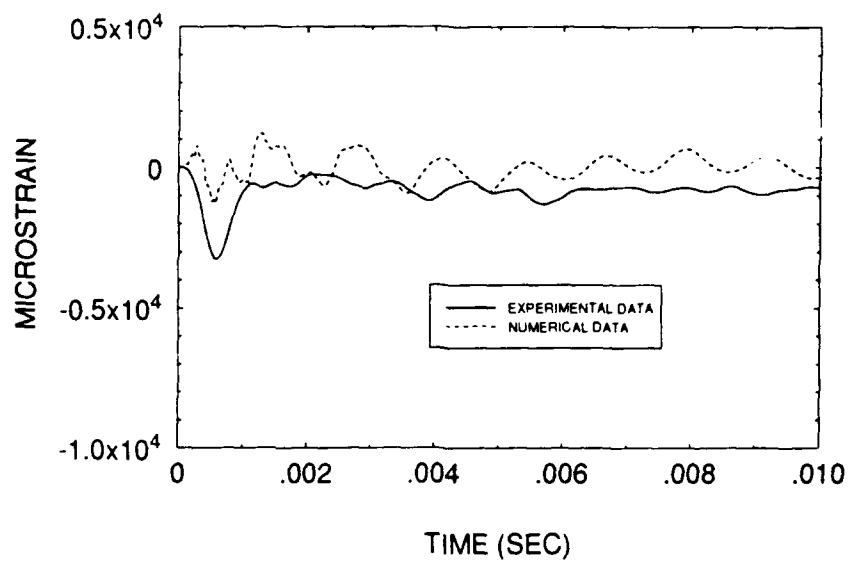
Figure IV.7. Experimental/numerical comparison for position B2 axial strain.
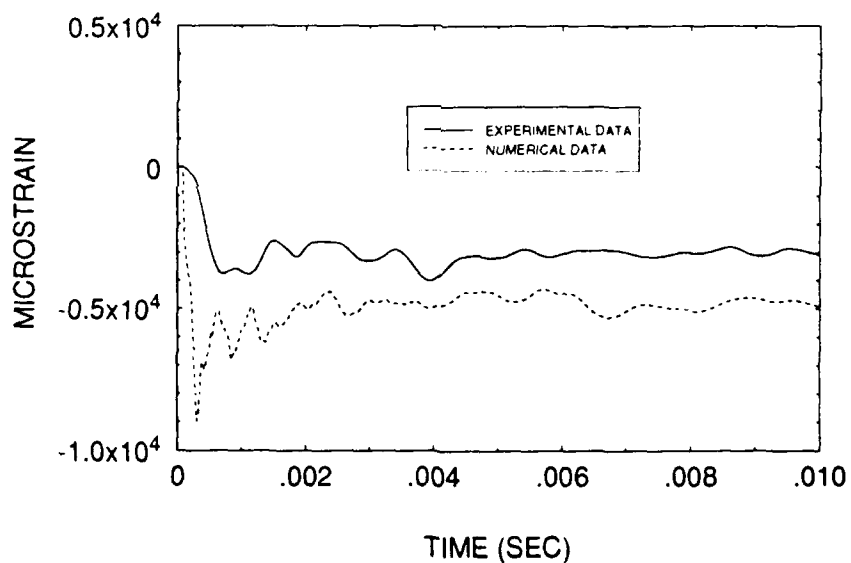
Figure IV.8. Experimental/numerical comparison for position B3 hoop strain.

45
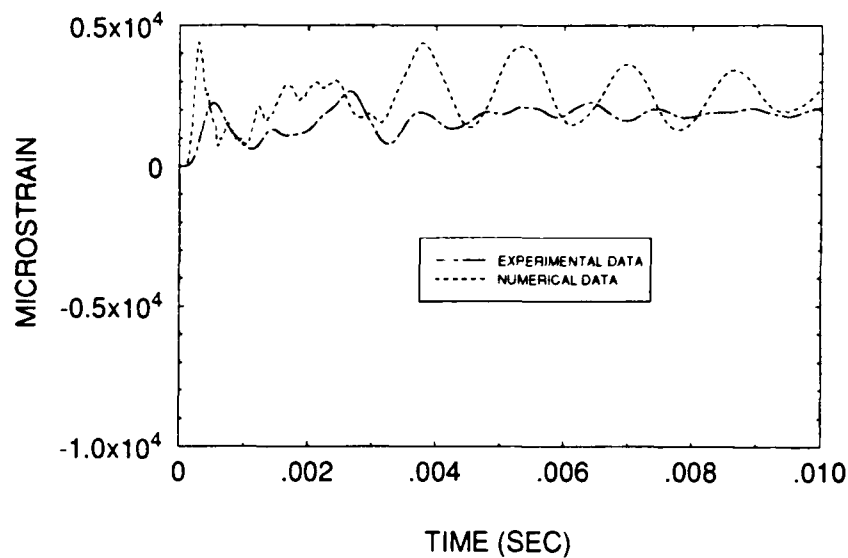
Figure IV.9. Experimental/numerical comparison for position B3 axial strain.
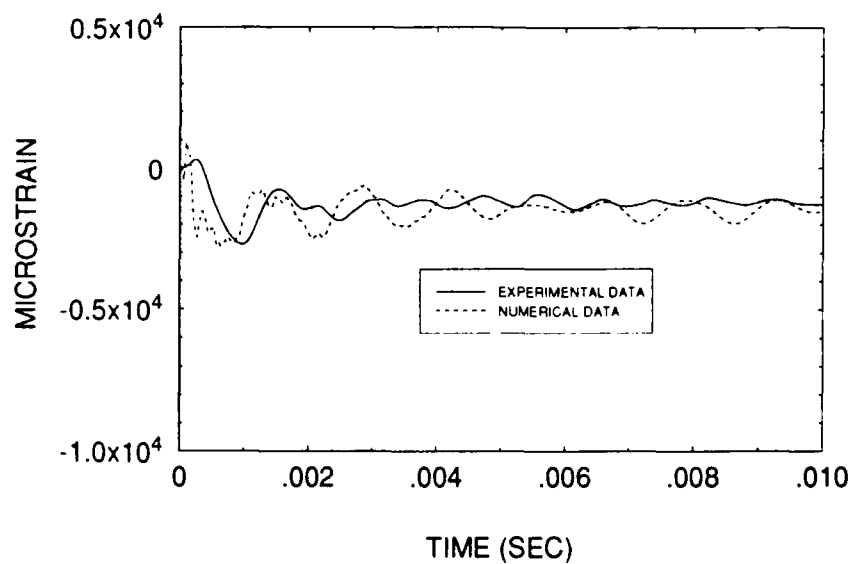
Figure IV.10. Experimental/numerical comparison for position C1 axial strain.

46
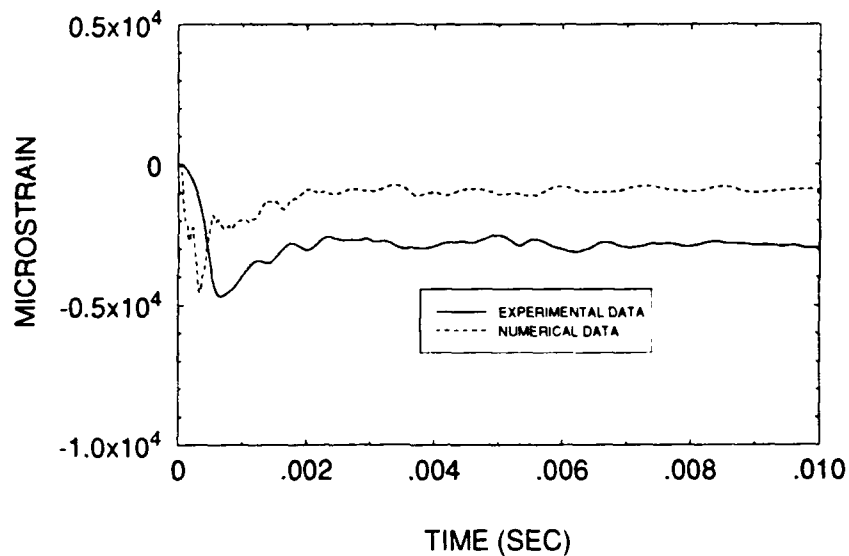
Figure IV.11. Experimental/numerical comparison for position C2 hoop strain.

B. SENSITIVITY ANALYSES

A series of sensitivity analyses were performed in an effort to explain the differences between the numerical and experimental results noted in the previous section. In addition, these analyses provided additional insight into the relative importance of various factors in the performance of underwater explosion tests and the associated calculations. Seven sensitivity analyses were performed. The first was the mesh sensitivity test. The results of this analysis have already been discussed. The other six analyses were, end effect, shell element formulation, integration time increment length, quadrature, rotational position and η value

47

sensitivity checks. The results of these analyses are provided in the following subsections.

1. END EFFECT SENSITIVITY ANALYSIS

As previously noted, the most severe deformation occurred at locations near the end of the cylinder (positions A1 and C1). Two processes cause this phenomena. First, the relatively large mass of the end plates apply large inertial forces to the cylinder shell near the end plates. Second, the one inch thick end plates are very stiff and their lack of flexibility causes the weaker material of the shell near the end plates to deform in response to applied forces. A examination of the numerical and experimental data reveals that these effects are concentrated near the end plates and result in large strain gradients. This means that elements on either side of a selected element near the end of the cylinder can have significantly different strain values. Accurate placement of strain gages within this region and careful mesh design along with adequately short time integration increments are critical in obtaining satisfactory results in a numerical to experimental data comparison. In addition, as stated earlier, the end plates are attached to the shell using a Tungsten Inert Gas process. This welding process results in high temperatures near the end of the cylinder. Since the aluminum for this model is at a peak hardened condition, this process could result in a change of the material properties

near the end of the cylinder that can only be restored by performing the age hardening process again after the welding is complete. These factors can result in an uncertainty in the expected strain compared to what might occur under ideal circumstances.

The mesh sensitivity results clearly display the importance of mesh design within this region. However, even with proper design, the large gradients can result in significant differences between the predicted and actual strains since the strain computed for the element is an average of the strain over the entire element vice a strain at a specific point. The best possible results would be obtained in these regions with large gradients if the mesh could be refined such that the size of the elements is the same size as the gage length of the strain gage. However, this would result in a prohibitively large number of elements and a subsequent increase in problem solution times. These problems can be overcome by placing strain gages in areas that are expected to have consistently increasing or decreasing strains and then ensuring that the mesh is designed so that the strain gage location is at the center of the element. If possible, large gradient regions should be avoided. If strain gages must be placed in a high gradient region, then the strain gages should be placed to one side or the other of the minimum or maximum strain location. Placement at the minimum or maximum point will result in an error since the average for

the element will lie above a minimum or below a maximum if the element is not the same size as the gage length of the strain gage.

In this study, the strain gages located at A1 and C1 were located at the point of highest compressive strain. Therefore, a study was performed to determine the relative importance of the noted location factors. Figures IV.12 through IV.16 show the results of this study. Strains of two additional elements nearer the end were compared to the measured strain and the actual strain gage location. Elements nearer the end plate were selected since the welding effects
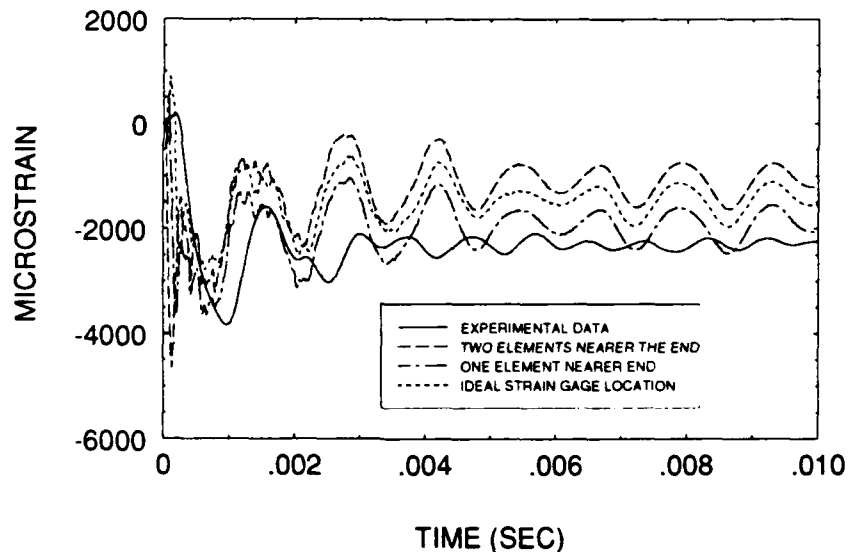
Figure IV.12.   End effect sensitivity results.
(A1 axial)
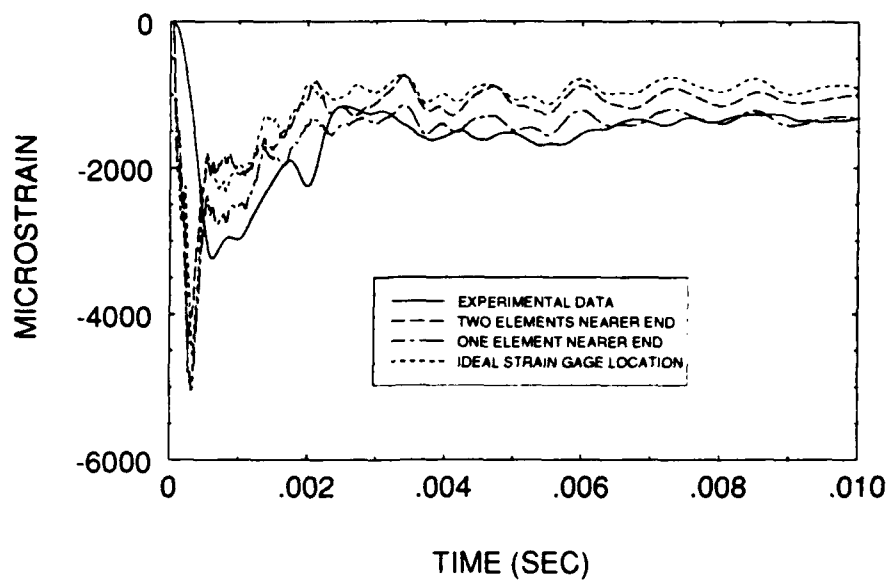
Figure IV.13. End effect sensitivity results.
(A2 Hoop)
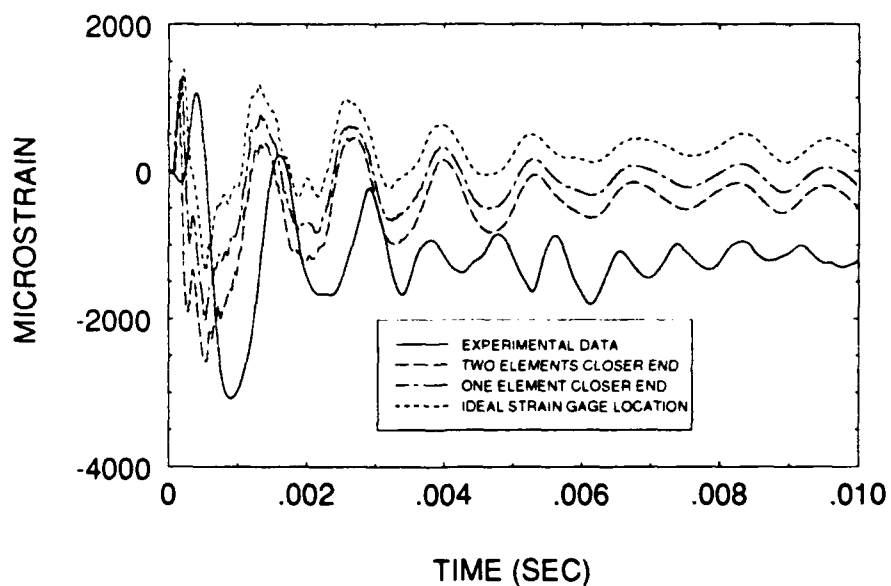
Figure IV.14. End effect sensitivity results.
(A2 Axial)
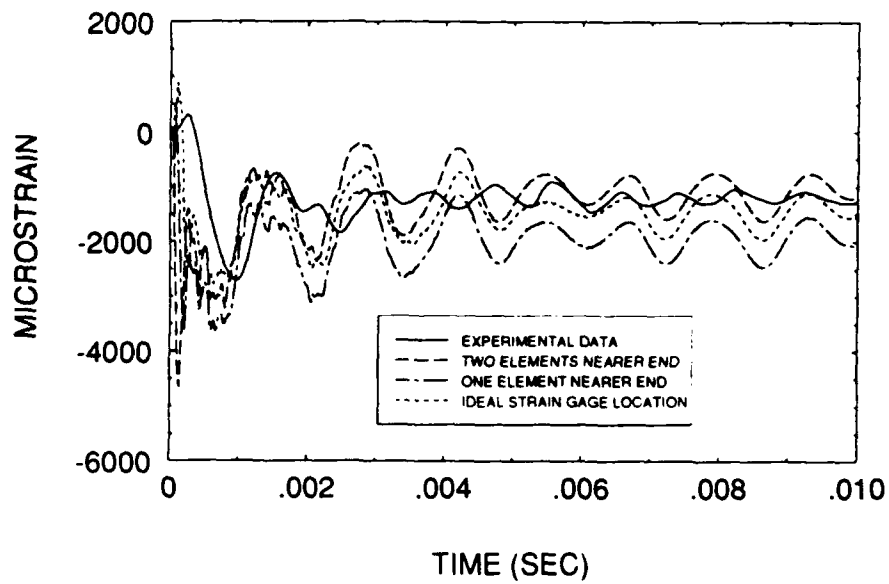
Figure IV.15. End effect sensitivity results. (C1 Axial)
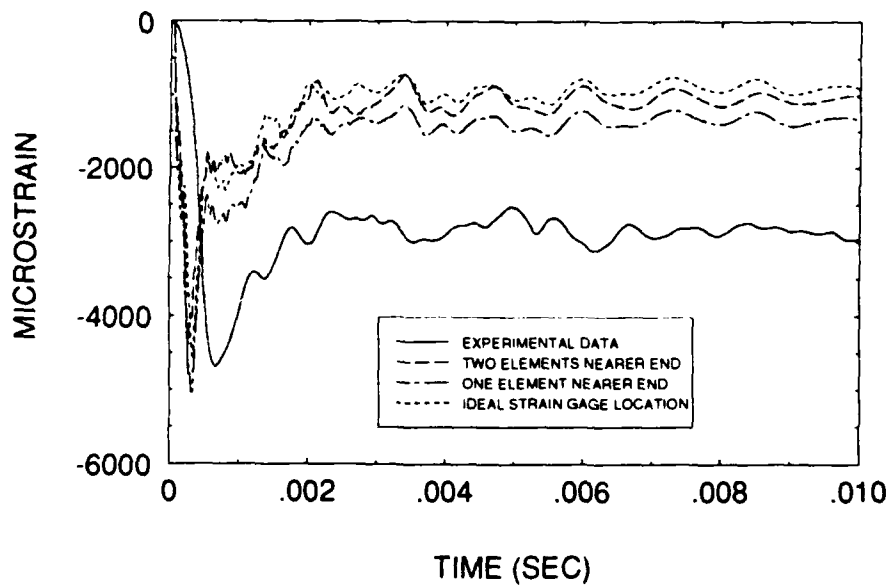
Figure IV.16. End effect sensitivity results. (C2 Hoop)

described in the previous paragraph would tend to move the high strain location nearer to the end plate by weakening the material near the end plate. Only the positions with useable experimental results are shown. In four of the five cases (positions A1 axial, A2 hoop, C1 axial and C2 hoop), if asymmetry effects are taken into account, the element one nearer to the end from the actual strain location provides a better estimate of the actual strain measured during the underwater explosion test. At the fifth location (A2 axial), the second element closer to the end provides the best results. These results require additional study to separate and quantify the effect of the phenomena.

2. SHELL FORMULATION, QUADRATURE RULE AND INTEGRATION TIME INCREMENT SENSITIVITY ANALYSES

In addition to the above end effects, there was some concern that the mid plane reference for the thin shell element would result in a greater flexible length than the actual physical model. This concern was based on the fact that the mass and stiffness of the end plates is concentrated into a planar surface co-located with the mid plane of the end plate in the thin shell analysis. This resulted in the shell portion of the structure being one inch longer in the numerical model than the physical model. This problem could have been avoided by using the Hughes/Liu formulation and shifting the reference plane to the inner surface of the

53

shell. To resolve this issue a study was conducted to compare the performance of different types of thin and thick shell element formulations.

Results from the Belytschko/Tsay/Lin shell formulation were compared to results from the same model using the Hughes/Liu shell formulation. As stated earlier, the Belytschko/Lin/Tsay shell has the advantages of increased computational efficiency and a high degree of stability with large deformations at the expense of reduced accuracy at high levels of plastic strain. The major difference between the two formulation stems from the fact that the element normal direction is updated periodically in the Hughes/Liu formulation. The Belytschko/Lin/Tsay formulation assumes negligible out of plane deformations, and therefore, does not update the shell normal. As a result, the inaccuracy of the Belytschko/Lin/Tsay formulation will increase as shell deformation becomes significant.

The models used to compare the two formulations were identical in all aspects with the exception of the shell formulation. The center line plane was used for the reference on both models. The results confirmed that the strain levels encountered in this underwater explosion test were small enough to support use of the Belytschko/Lin/Tsay formulation. However, it was apparent that differences did occur for positions with significant plastic strain in the axial direction (Positions A1, A2, B3, C1, and C2). Although the

differences in these cases were not significant enough to require use of the Hughes/Liu formulation, it is also noted that higher strain may result in larger differences. Therefore the Belytschko/Lin/Tsay formulation should not be used in cases where significant denting occurs unless stability problems occur while using the Hughes/Liu formulation.

As stated earlier, the presence of high strain gradients near the end plates causes small changes in end condition or distance to be significant. When it became apparent that end effects would be important in the results an investigation was performed to determine if an eight node brick shell formulation would provide more accurate results near the end of the cylinder. The thin shell formulation results as well as the experimental results were compared to results from a model computed using eight node brick shell elements. All three formulations are compared to experimental results in figures IV.17 through IV.27. The following information can be gleaned from the plotted results. First, it is apparent that the greatest differences occur near the positions with the highest strains. At the same time, it can be noted that there is virtually no difference at the locations with no permanent strain. Second, as shown in figures IV.17, IV.18, IV.24, IV.25 and IV.27, it is clear that there is a significant difference between the eight node brick shell results and the Belytschko/Lin/Tsay results at the

55

locations with high levels of permanent plastic strain. However, contrary to the expected results, the eight node brick shell results move further from the expected values than the other formulations. It is also noted that the Hughes/Liu formulation lies between the eight node brick shell and the Belytschko/Lin/Tsay formulation.

Additional research was performed to determine the cause of the disparities. The study revealed that the eight node brick shell is sensitive to integration time increment and will move marginally closer to the thin shell results if time integration is cut in half. However, the overall shift is only about 10 percent of the total difference. Quadrature rule (number of points used in the Gauss quadrature numerical
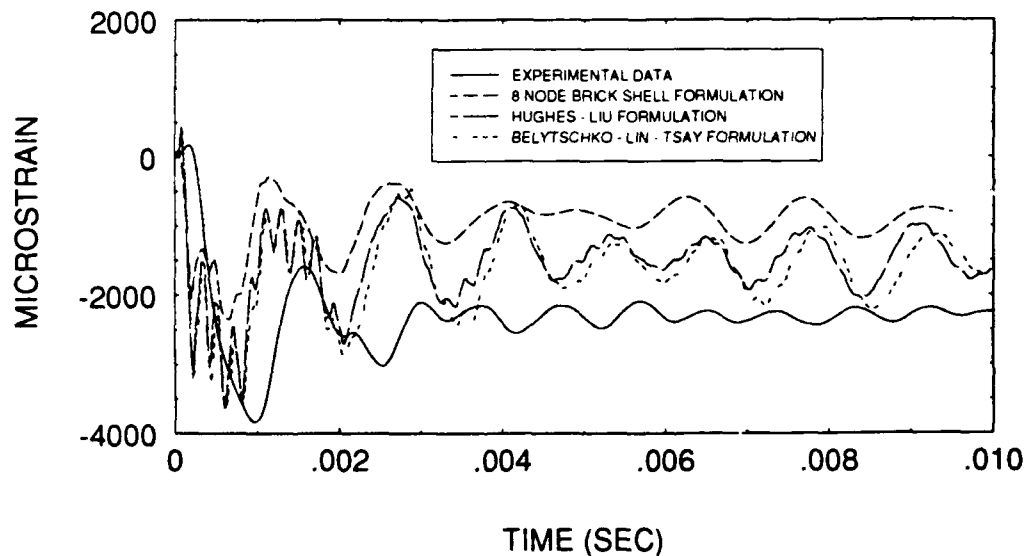
Figure IV.17. Shell formulation sensitivity results. (Al Axial)

56
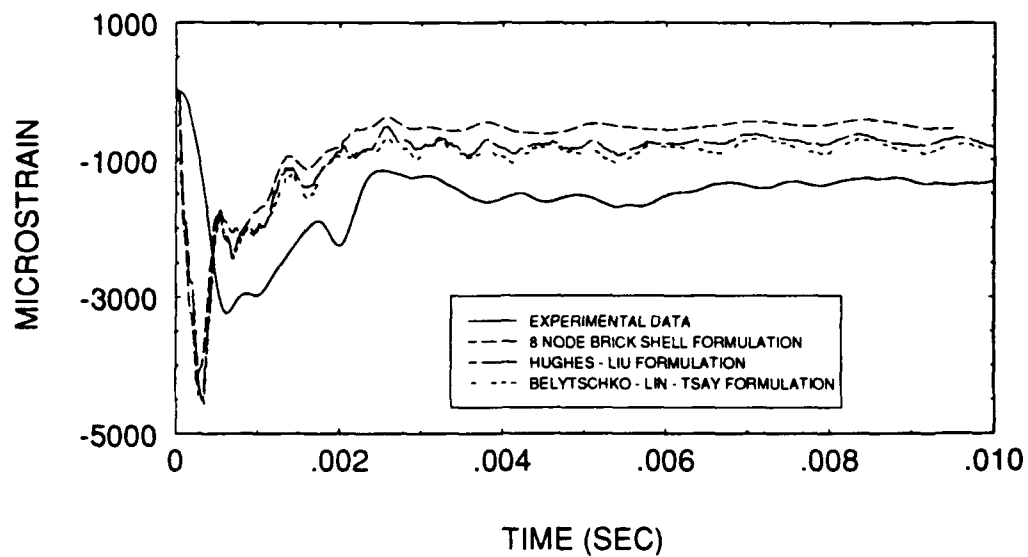
Figure IV.18. Shell formulation sensitivity results. (A2 Hoop)
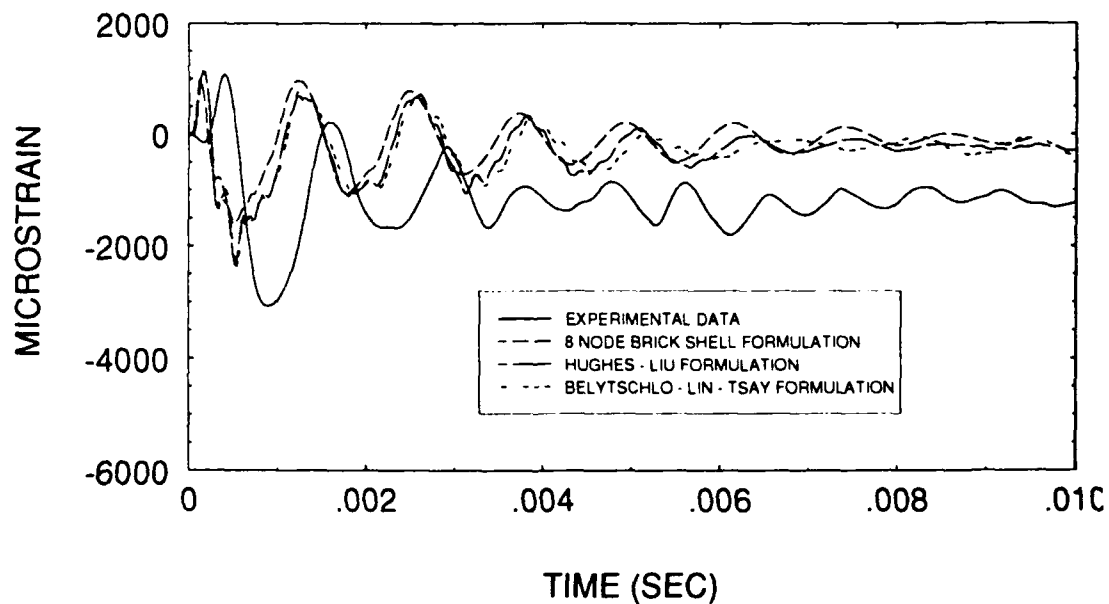
Figure IV.19. Shell formulation sensitivity results (A2 Axial)
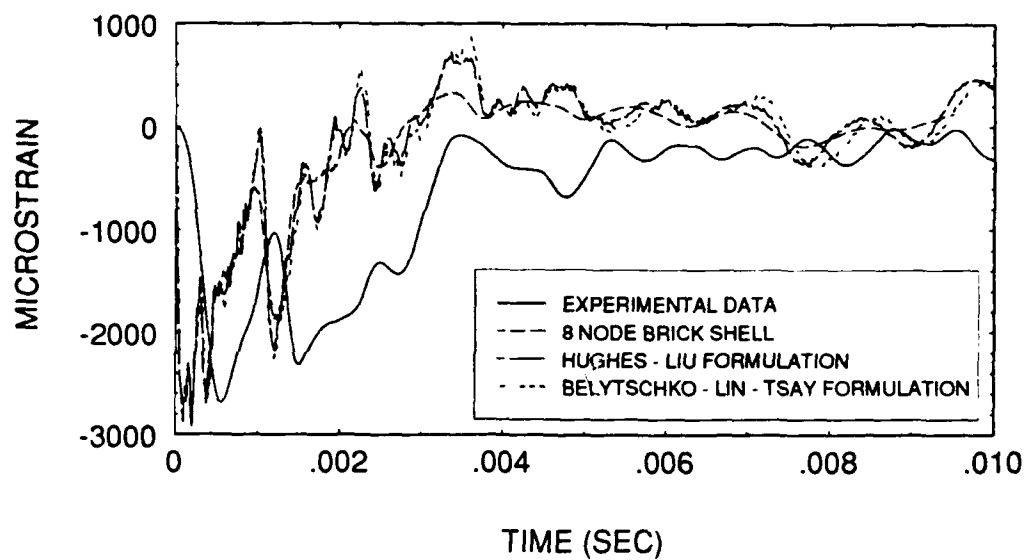
Figure IV.20. Shell formulation sensitivity results. (B1 Hoop)
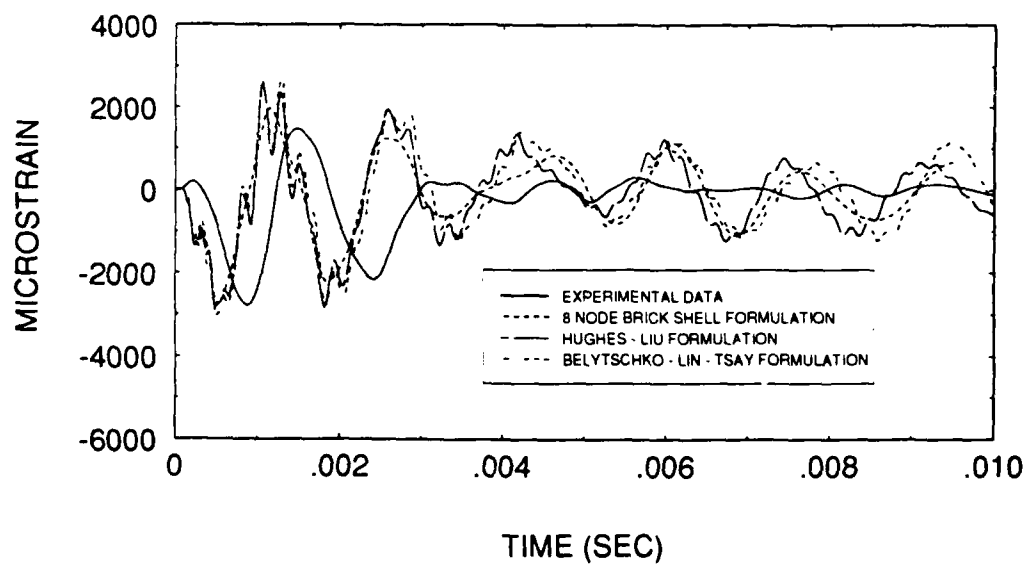
Figure IV.21. Shell formulation sensitivity results. (B1 Axial)
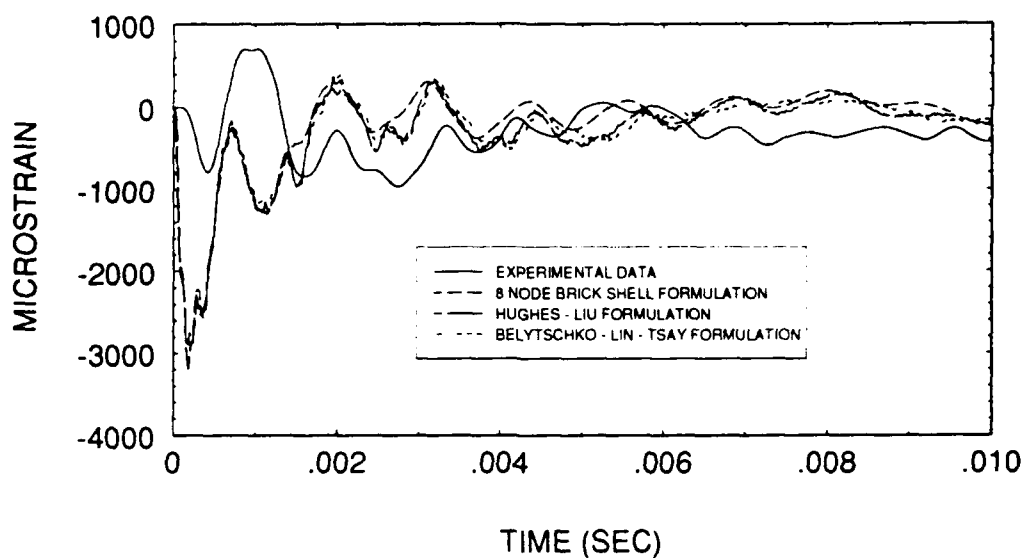
**Figure IV.22.   Shell formulation sensitivity results.
(B2 Hoop)**
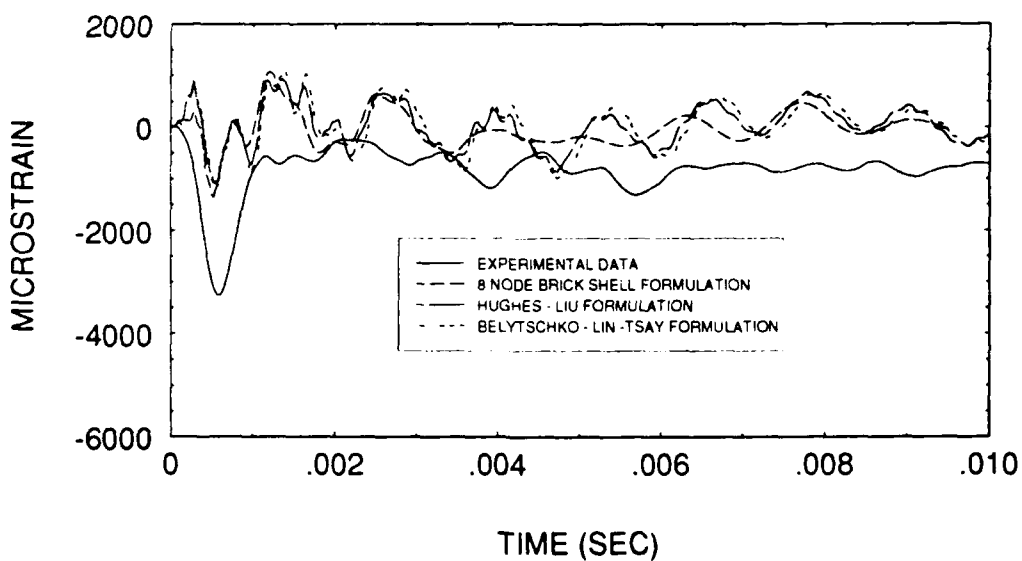
**Figure IV.23.   Shell formulation sensitivity results.
(B2 Axial)**
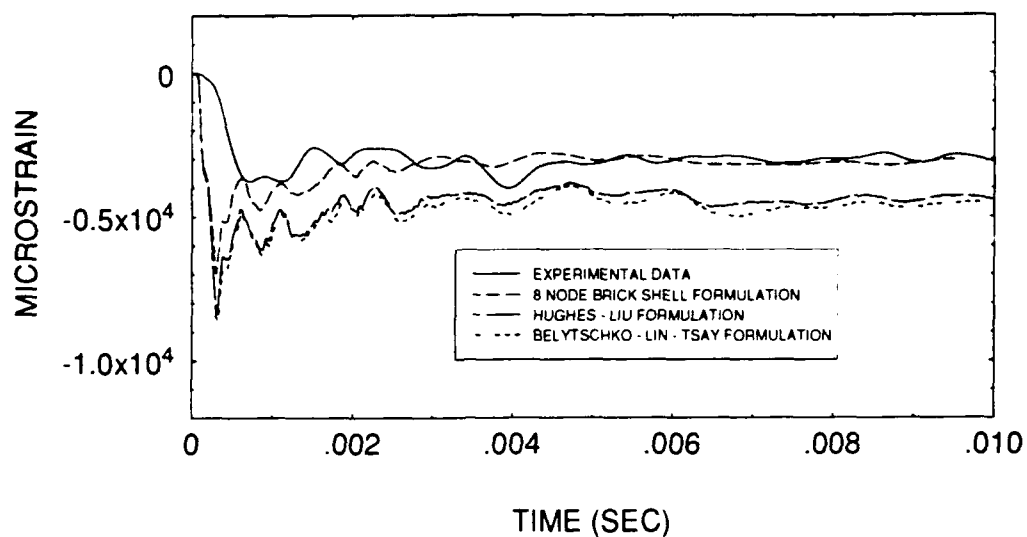
Figure IV.24. Shell formulation sensitivity results. (B3 Hoop)
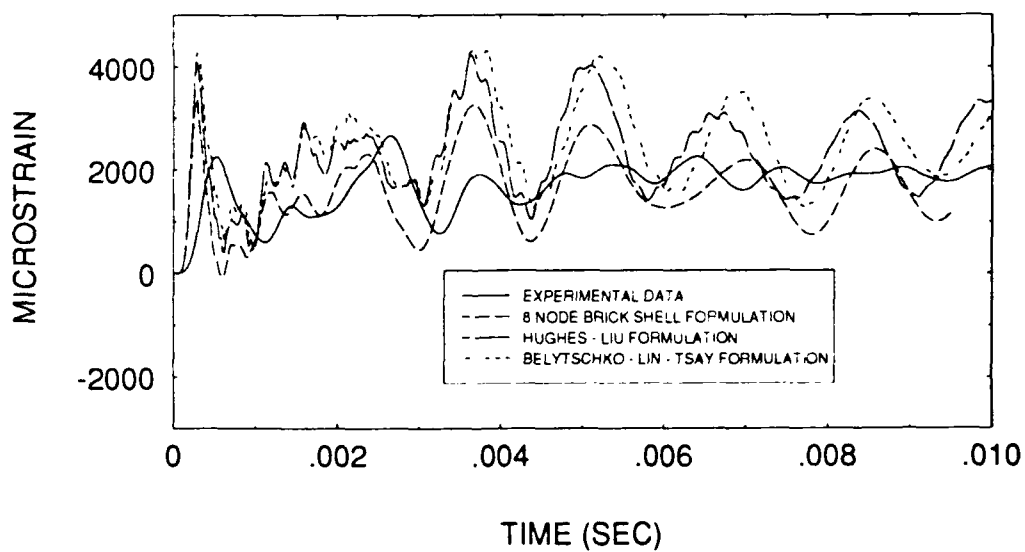
Figure IV.25. Shell formulation sensitivity results. (B3 Axial)
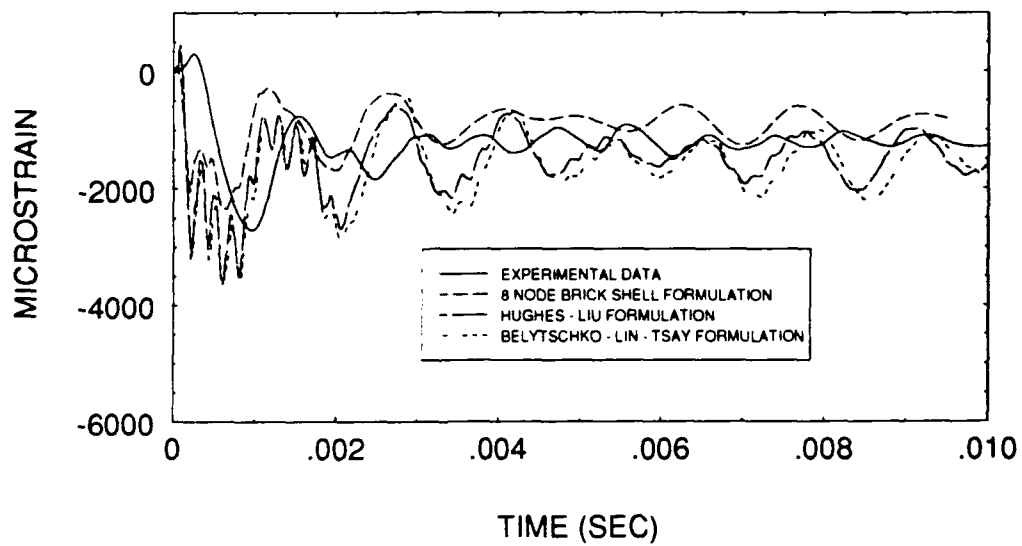
Figure IV.26. Shell formulation sensitivity results. (C1 Axial)
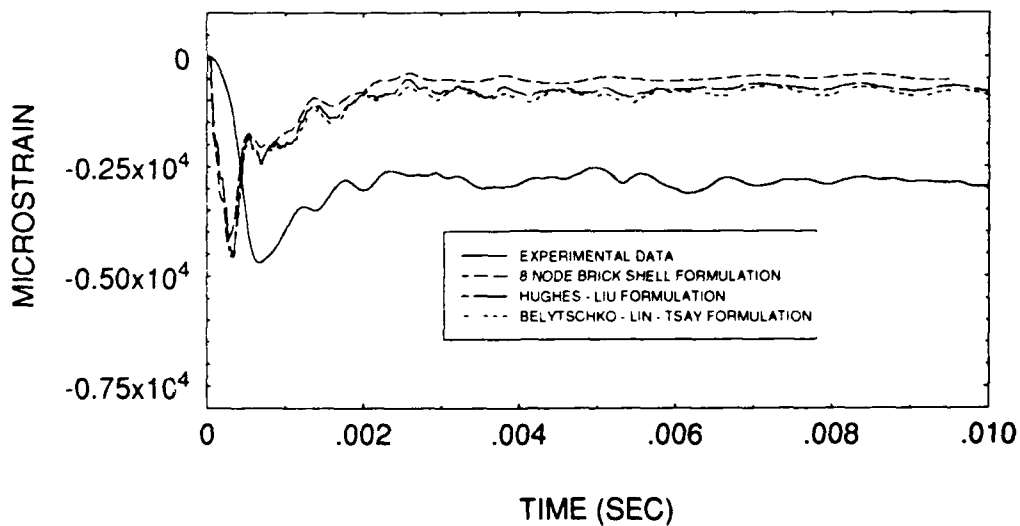
Figure IV.27. Shell formulation sensitivity results. (C2 Hoop)

integration scheme) proved to be a more significant effect. Use of five point quadrature moved the three results closer together while having the most profound effect on the Belytschko/Lin/Tsay formulation. Again, the affect of quadrature rule affected the thick shell results only marginally. Figure IV.28 shows the combined results for the location with greatest plastic deformation.
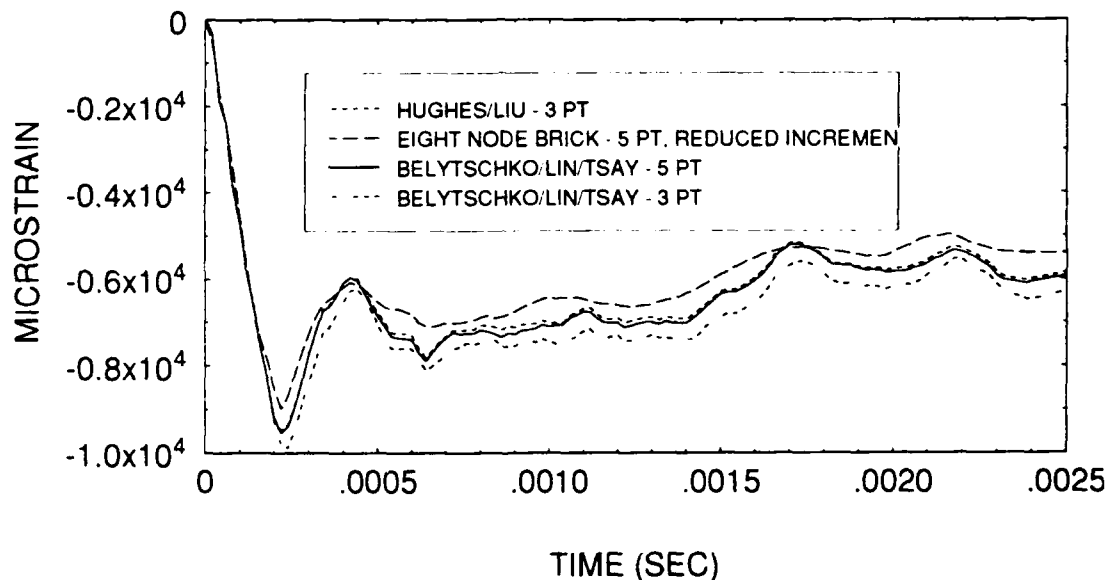
Figure IV.28. Effect of changing quadrature rule and time integration increment at location of highest strain (A1 and C1 hoop).

In summary, all three formulations appear to be satisfactory as long as care is used in designing the mesh and selecting the integration time and quadrature integration

rule parameters. Specifically, when using Belytschko/Lin/Tsay formulations in areas with relatively high strain, the number of quadrature points should be increased until stable results are achieved. When using eight node brick shell elements, integration time increment must be selected with care but number of quadrature points seems to be less critical. The Hughes/Liu formulation appeared to be relatively insensitive to both quadrature rule and integration time increment.

Reference 13 provides some useful thumbrules for selection of time increments. The following criteria are recommended.

$$\Delta t \approx 0.9 \frac{V}{(A_b c)} \text{ for brick shells}$$

$$\Delta t \approx 0.9 \frac{A_s}{Dc} \text{ for thin shells}$$

V - element volume

Δt - time increment

A_s - maximum surface area

D - maximum diagonal

c - speed of sound in the material

A_b - maximum area of any surface

The above criteria were found to be adequate except for the highest strain areas where the thick shell element rule did

not provide stable solutions. In areas such as Al and Cl, a value of the integration time increment half of the above recommendation proved to be satisfactory for the eight node brick shell.

3. ROTATION SENSITIVITY ANALYSIS

A sensitivity analysis was performed to determine the effect of an in plane rotation away from the expected symmetric orientation in an effort to explain the cause of the asymmetric results of the underwater explosion test. It was hypothesized that an unplanned rotation greater than ten degrees would have been detected by the personnel performing the test. Four different models were run within this range representing rotations of 0.0, 2.5, 5.0 and 10.0 degrees. The results are shown along with experimental results where available in figures IV.29 through IV.42. The following observations are made concerning the results. First, the most dramatic affects are on the reverse side of the cylinder at position B3 (Figures IV.37 and IV.38). The results show that the differential between the numerical and experimental results at position B3 can be explained by a six to eight degree rotation from the symmetric configuration. Rotational effects at locations B1 and B2 on the centerline (Figures IV.33 through IV.36) are insignificant. Hoop strain at position C2 (Figure IV.41) is approximately 60 percent
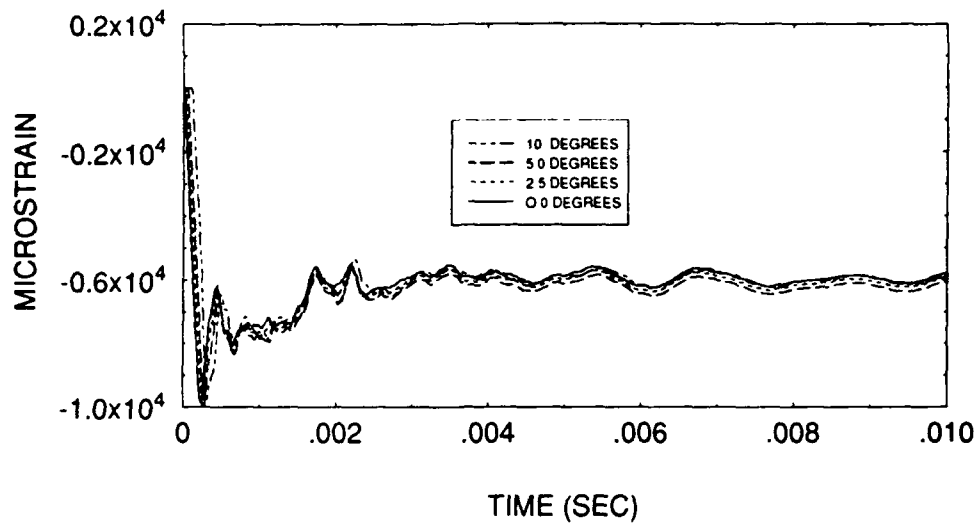
Figure IV.29. Rotation sensitivity results.
(A1 Hoop)
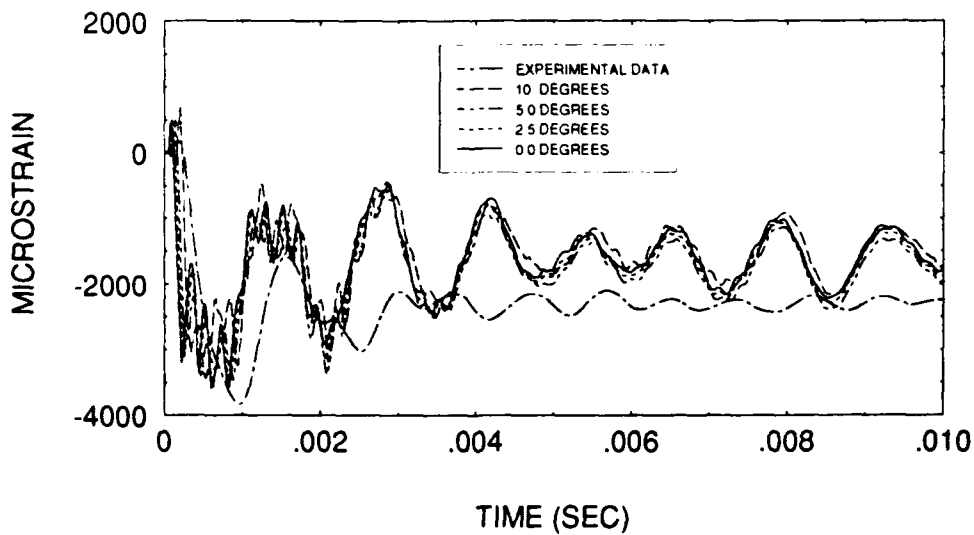
Figure IV.30. Rotation sensitivity results.
(A1 Axial)
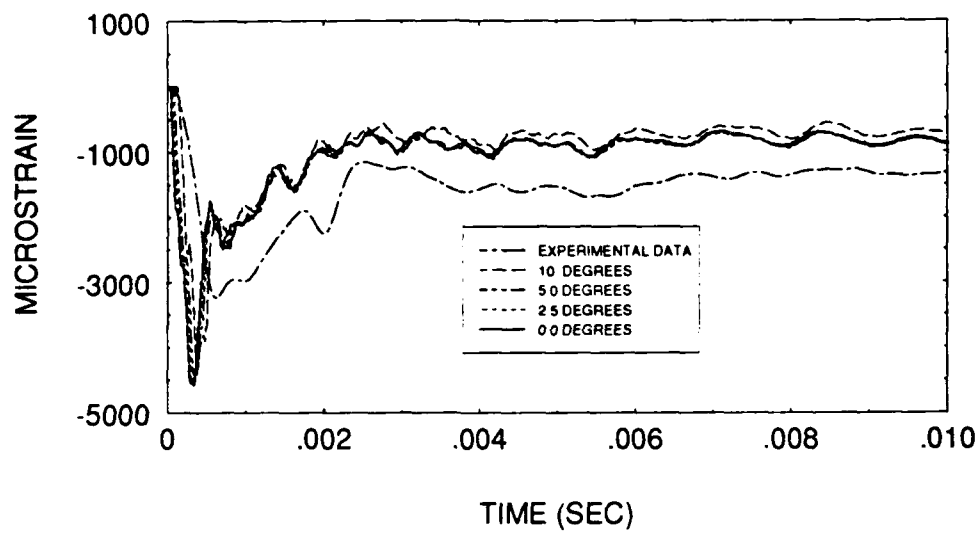
Figure IV.31. Rotation sensitivity results.
(A2 Hoop)
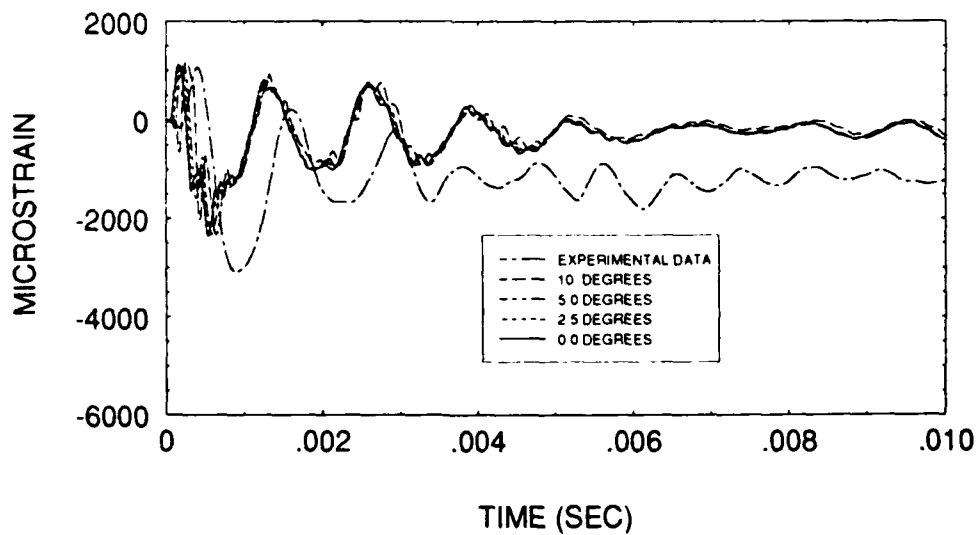
Figure IV.32. Rotation sensitivity results.
(A2 Axial)

66
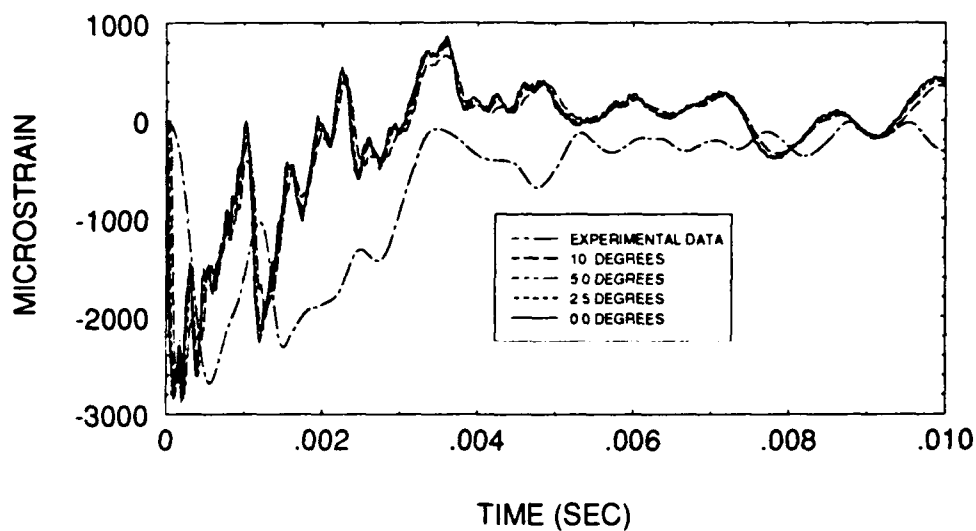
Figure IV.33. **Rotation sensitivity results.**
(B1 Hoop)
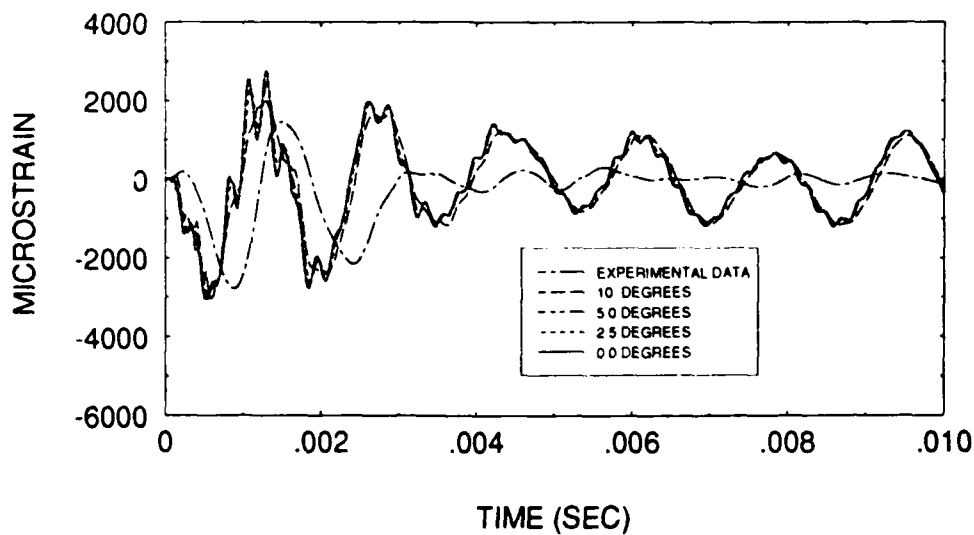
Figure IV.34. **Rotation sensitivity results.**
(B1 Axial)
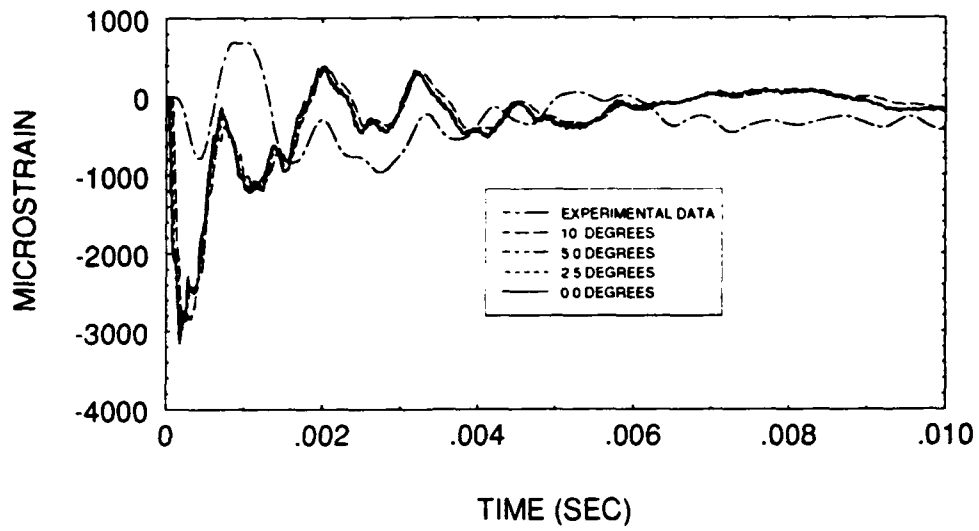
Figure IV.35. Rotation sensitivity results.
(B2 Hoop)
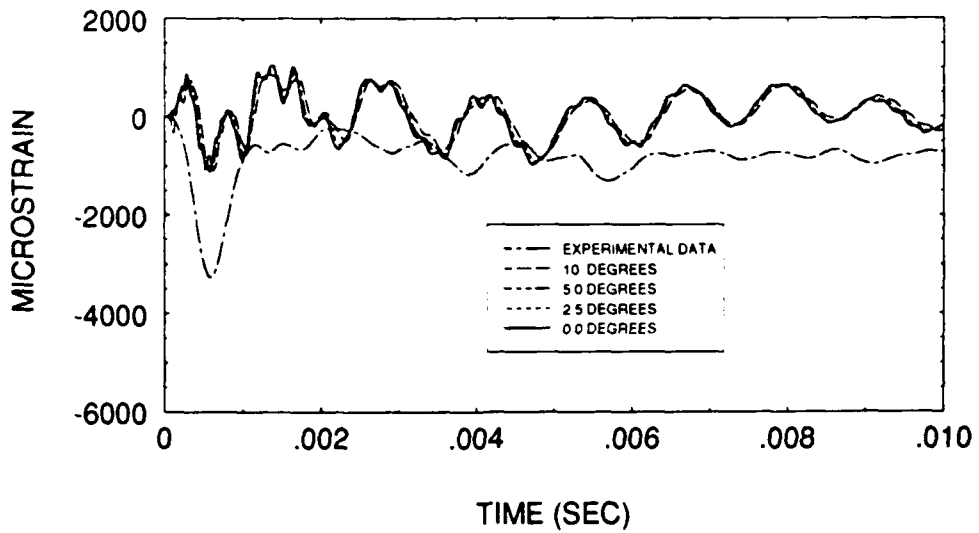
Figure IV.36. Rotation sensitivity results.
(B2 Axial)

68
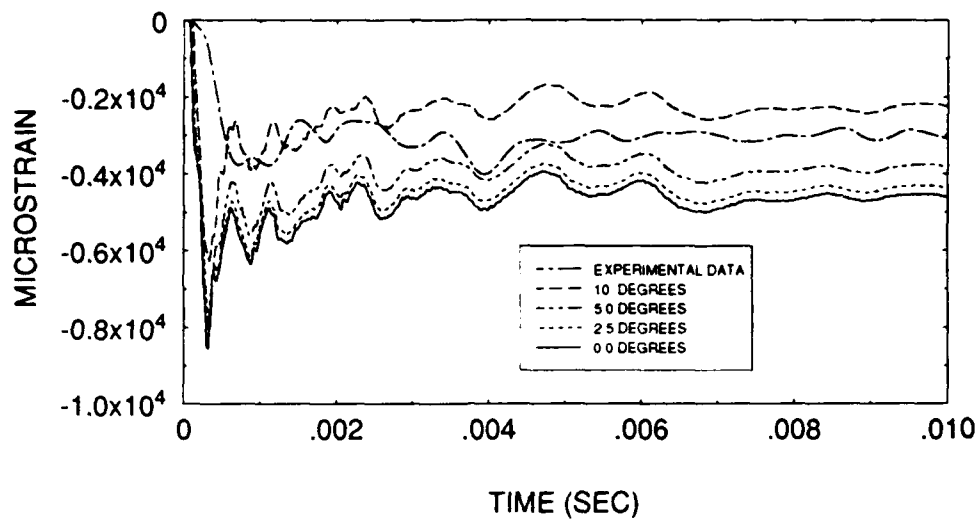
Figure IV.37.   Rotation sensitivity results.
(B3 Hoop)
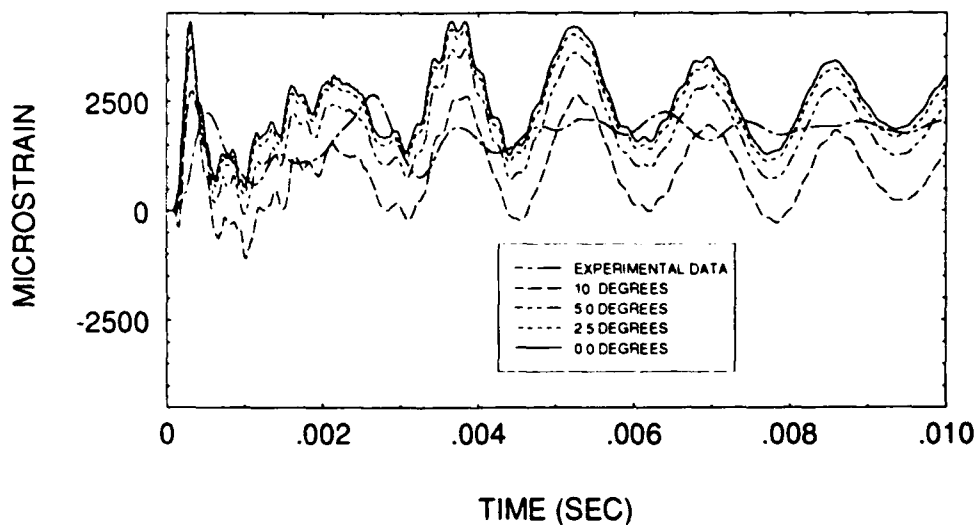
Figure IV.38.   Rotation sensitivity results.
(B3 Axial)
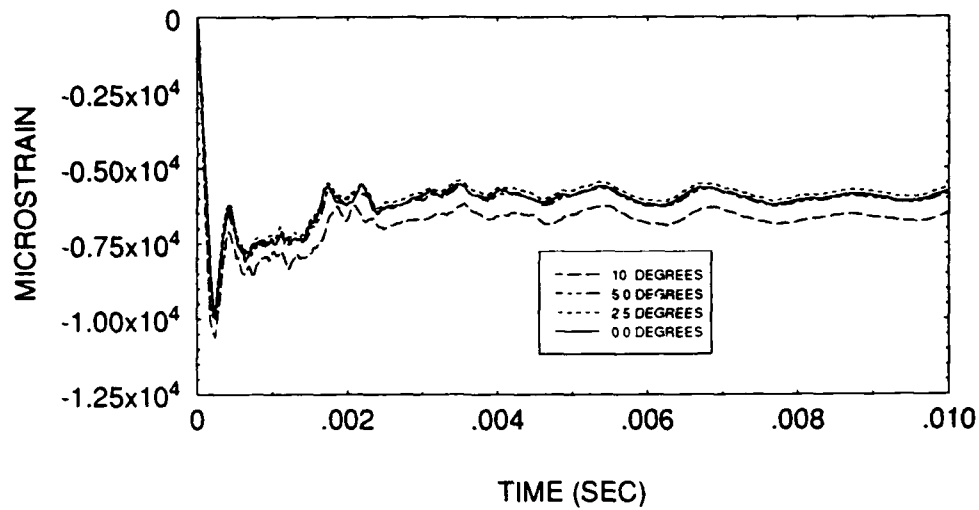
Figure IV.39.   Rotation sensitivity results.
                 (C1 Hoop)
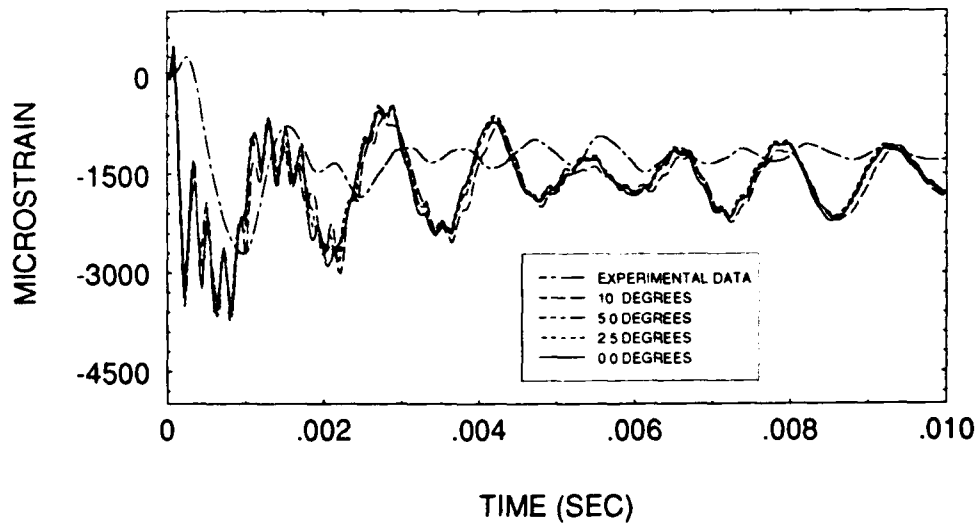
Figure IV.40.   Rotation sensitivity results.
                 (C1 Axial)

70
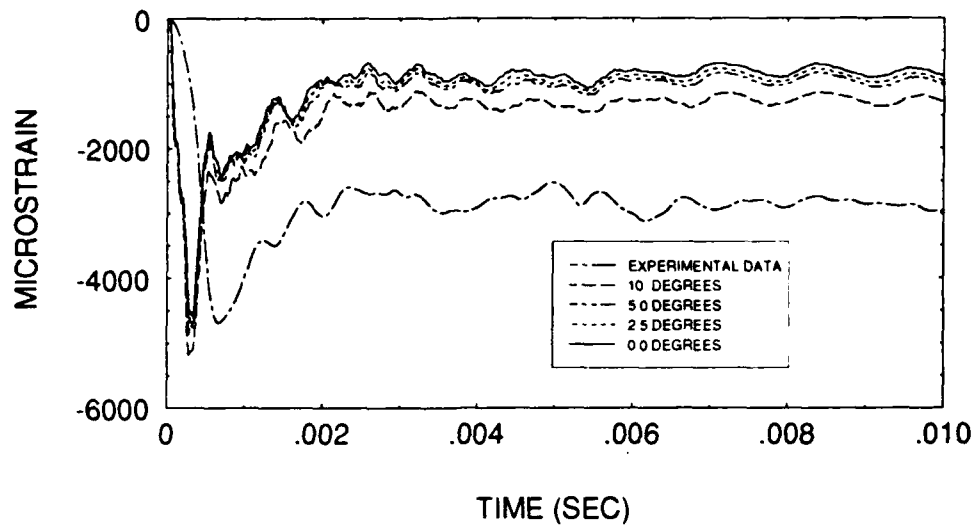
Figure IV.41. Rotation sensitivity results.
(C2 Hoop)
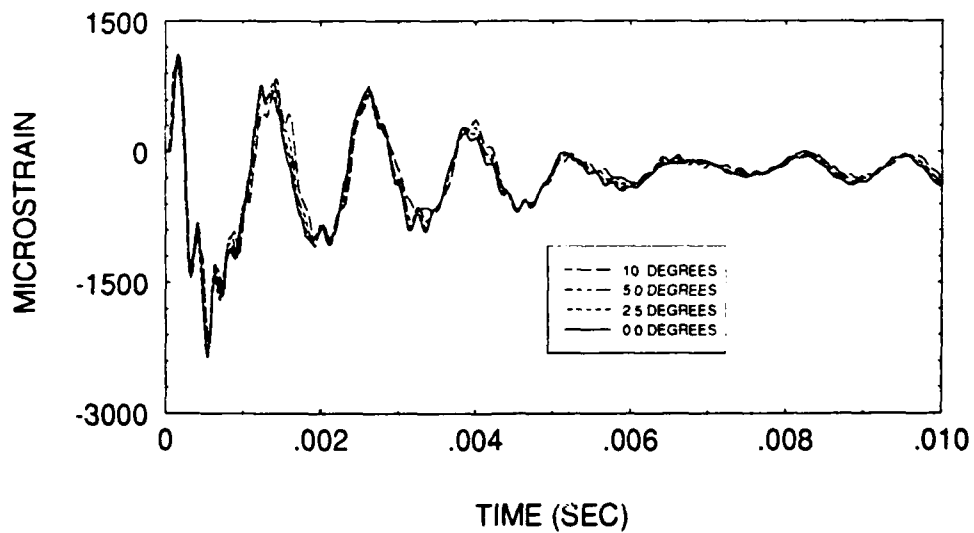
Figure IV.42. Rotation sensitivity results.
(C2 Axial)

71

higher than the hoop strain at position A2 (Figure IV.32) with a rotation of ten degrees. This is also consistent with the experimental data. Similar positive results were obtained for positions A1 and C1 axial strains. It was .further discovered that rotating the cylinder about its axis could further improve the results. However, even though these rotations did improve the results, significant differences still exist between the experimental and numerical strains at the ends of the cylinders. Although it is clear that the model can account for rotational effects, it is also clear that other factors are causing the large differences. Once again, welding affects are suspected to be the probable cause.

The important point to note out of these results is that even small rotations from expected orientation can result in significant errors on in expected results. Therefore extreme care must be taken to ensure that instrumentation cable tension and other unanticipated factors do not cause undetected rotations.

4. PHYSICAL FINDINGS

a. RESPONSE MODES

It was determined that a cylinder subject to a side on explosion will have three primary response modes. The first mode is an accordion motion. The accordion motion results from the compression and subsequent release of the

cylinder in the axial direction. Figure IV.43 shows a plot of points located at the center of each end plate. It is clear
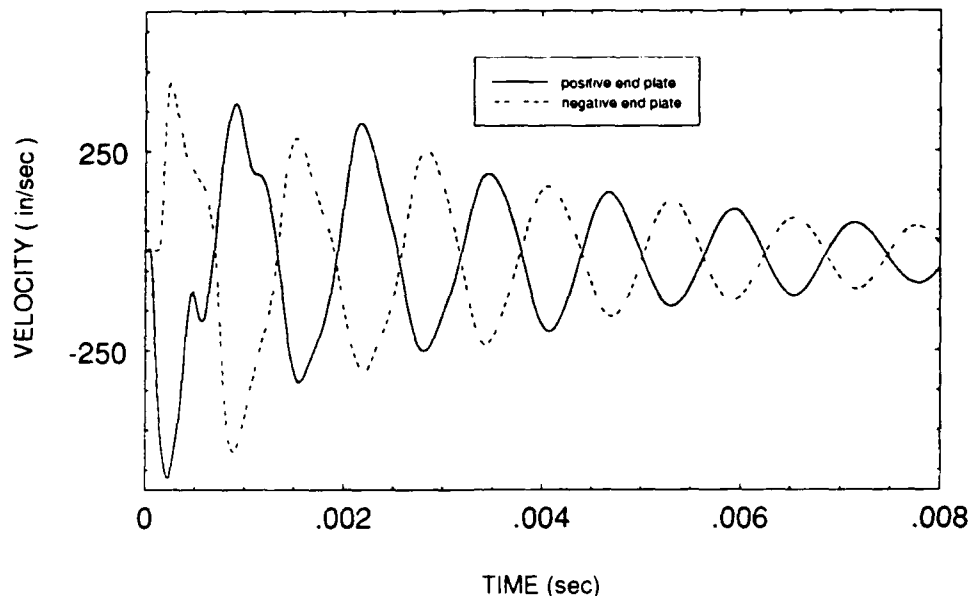
Figure IV.43. Cylinder accordion motion.

that the two end plates are travelling in opposite directions at the same time generating the accordion motion.

The cylinder is also subject to a whipping mode parallel to the direction of shock wave travel. The whipping mode is the most significant motion experienced by the cylinder and is caused as a result of the curvature of the shock wave. In the symmetric situation, the shock wave will come in contact with the center of the cylinder first. This will cause the center to move first, followed by the ends. The cylinder will then move in an oscillatory motion that is a function of the stiffness and mass distribution of the cylinder and the water surrounding the cylinder. Figure IV.44

73
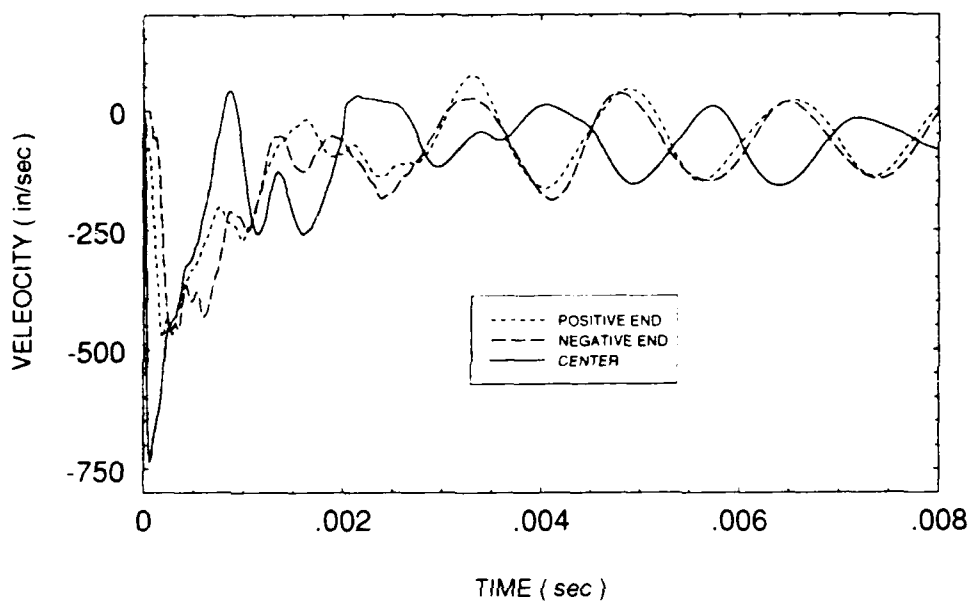
Figure IV.44. Cylinder whipping motion in plane parallel to shock wave direction.

shows a plot of a points located at the center and ends of a line located parallel to the axis on the near side of the cylinder. The plot shows that the end plates are moving in the opposite direction of the cylinder throughout the transient response of the cylinder. Figure IV.45 shows a scale factor 20 drawing of the cylinder at two different times. The cylinder's opposite direction of curvature at the two different times is a result of the whipping motion.

The final response mode noted was a *breathing* motion in the plane perpendicular to the shock wave direction of travel. Although breathing motion also occurred in the direction parallel to the shock wave travel, it was not as obvious since the much larger whipping motion turned out to be

74
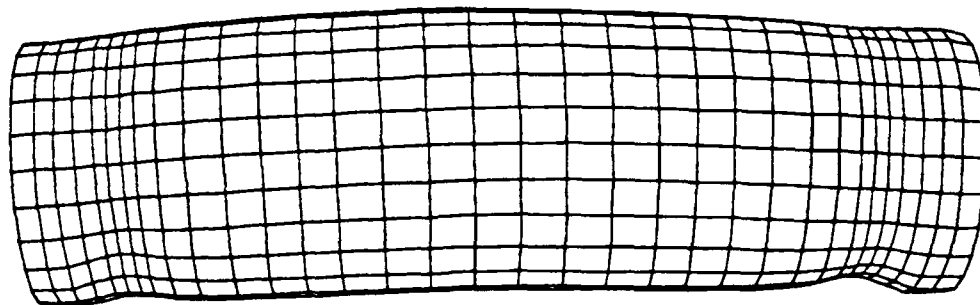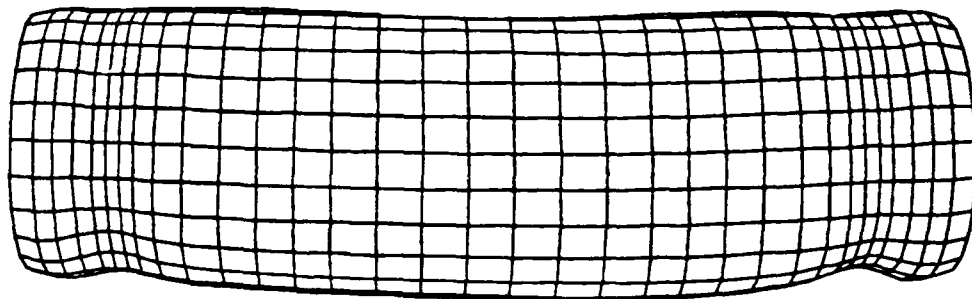
**Figure IV.45.   Cylinder curvature as a result of whipping
motion (scale factor 20).**

the predominant mode in that direction.   Figure IV.46 shows a

plot of two points located at the top and bottom of the

cylinder in a plane perpendicular to the axis at the axial mid

point of the cylinder.   It can be observed that the upper
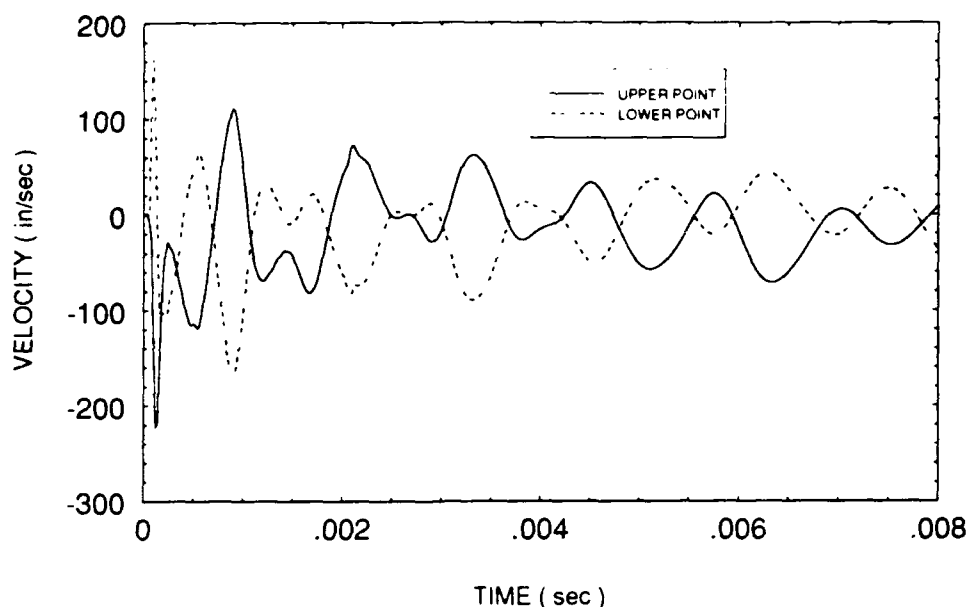
**Figure IV.46. Cylinder breathing motion perpendicular to
the shock wave direction of travel.**

point is moving in a direction opposite to the lower point

throughout the transient response of the cylinder.   The

breathing motion is also caused by the compression and

subsequent release of the cylinder.   Figure IV.47 provides an

illustration of the breathing motion. The two scale factor 40

drawings are for two separate times and show the shell first

bowed inward toward the axis and then outward away from the

axis.

b. ROTATIONAL EFFECTS

Plastic strain fringe plots generated as a result

of the rotation sensitivity analysis revealed some interesting

information on the causes of the strain distribution
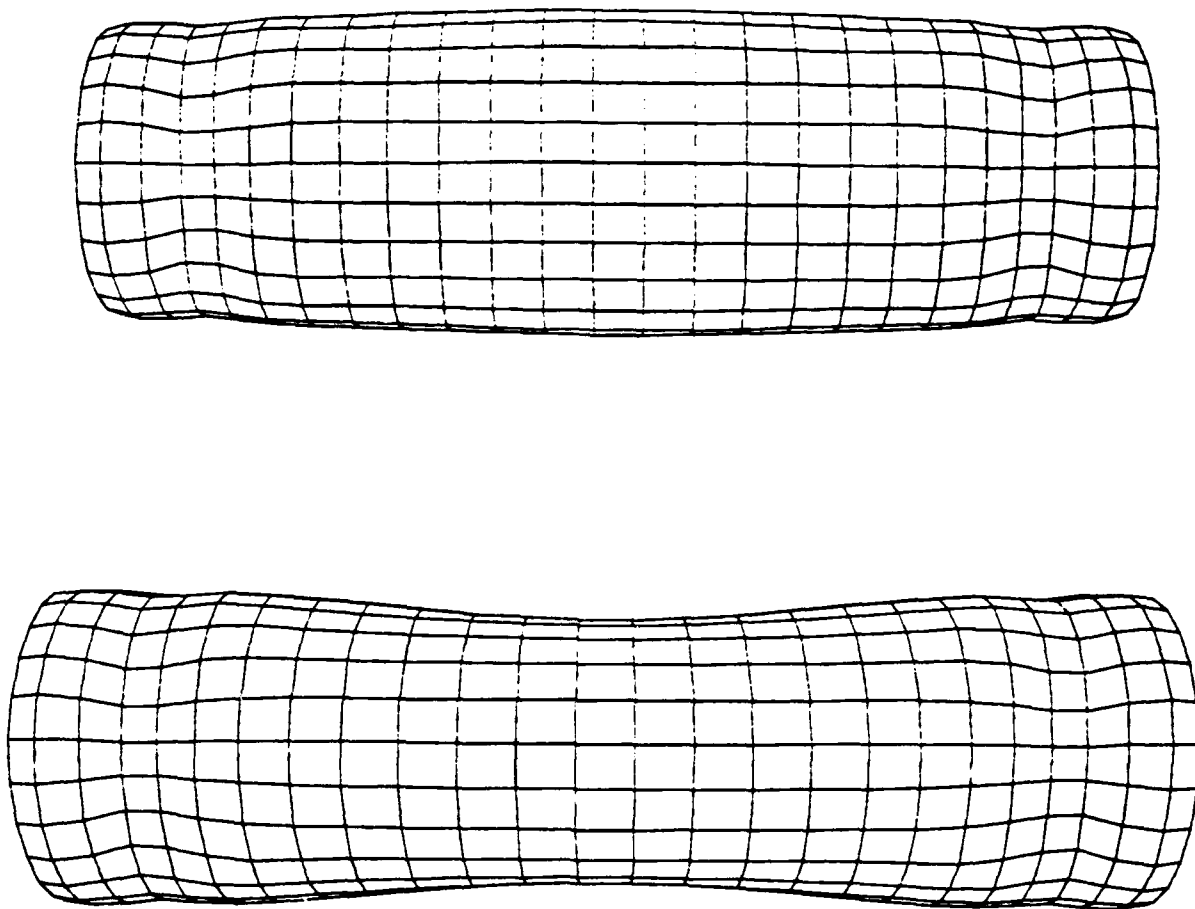
Figure IV.47. Illustration of cylinder breathing mode at two different times (scale factor 40).

experienced by the cylinder. The experimental results included a reduction in the strain at the rear of the cylinder at position B3, a decrease at A2 relative to C2 and an increase at A1 relative to C1. The fringe plots show why this

strain distribution occurs. Figure IV.48 shows the effective plastic strain distribution for a 7.5 degree rotation. The left side of the cylinder is nearest the charge. The results show that the rotation tends to diffuse the strain around the cylinder on the near end while concentrating it at the far end. This causes the distribution noted for positions A1, C1, A2 and C2. At the same time, the high stress region on the reverse side of the cylinder tends to move away from the charge. This placed location B3 in a lower strain region which led to the experimental and numerical results noted at position B3.

THICK   SHELL   MODEL
time •   .59798E-02
fringes of eff. plastic strain
min• 0.000E+00 in element   960
max• 7.104E-03 in element   433

fringe levels
1.089E-03
2.321E-03
3.552E-03
4.783E-03
6.015E-03
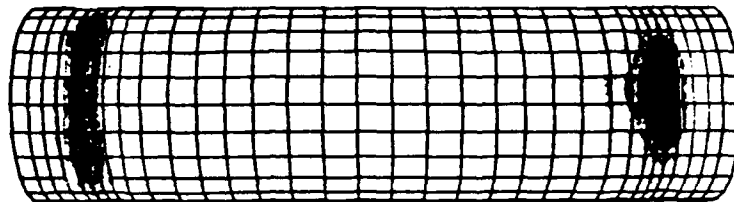
THICK   SHELL   MODEL
time •   .59798E-02
fringes of eff. plastic strain
min• 0.000E+00 in element   960
max• 7.104E-03 in element   433

fringe levels
1.089E-03
2.321E-03
3.552E-03
4.783E-03
6.015E-03
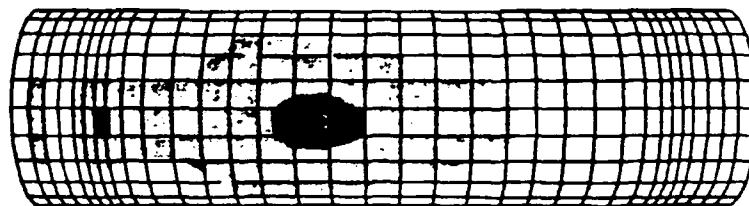
Figure IV.48.   Effective plastic strain distribution for near and remote side of cylinder with 7.5 degrees of rotation.

79

V.   CONCLUSIONS AND RECOMMENDATIONS

A.   CONCLUSIONS.

1.   NUMERICAL MODELLING

Two general conclusions can be reached from the material contained in this report.   First, the USA/DYNA3d connection is successful and can replicate the response of simple analytical models.

Second, numerical modeling can predict the response of a simple cylinder to an underwater explosion.   Far field numerical predictions generally match experimental results if rotation and end effects resulting from fabrication caused material property changes are correctly modelled.   It was found that results in high strain areas are extremely sensitive to shell formulation, mesh design, quadrature rule and integration time increment.   The best results were achieve with brick shell elements.   However, the eight node brick shell required substantially longer computation times to achieve the desired results because of the need to reduce the integration time increment.   In addition, it was found that thin shell formulations can also provide correct results.   However, results for the Belytschko/Lin/Tsay formulation appear to be very sensitive to the number of quadrature points

used for the numerical integration scheme in high strain areas.

2. PHYSICAL ASPECTS

Primary damage areas are near the ends of the cylinder on the side nearest the charge where the stiff, heavy, flat end plates caused a concentration of the effective plastic strain. Damage also occurred on the reverse side as a result of a bending effect similar to that described in the near field results. The cylinder experienced breathing, whipping and accordion response modes.

In addition, it was discovered that rotation tends to diffuse strain on the end nearest the charge while concentrating the strain at the far end on the side nearest the charge. The high strain area located at the center of the cylinder on the reverse side tends to migrate toward the end most remote from the charge.

B. RECOMMENDATIONS.

1. TOPICS FOR ADDITIONAL STUDY.

a. WELDING FABRICATION EFFECTS.

An analysis should be performed to quantify the relative effect that the change in material properties generated by the welding fabrication process has on the numerical results. This analysis could include the measurement of material properties near a weldment. These

properties could then be added as a separate material in the numerical model.

b. EIGHT NODE BRICK SHELL SENSITIVITY ANALYSES.

Although it was fairly clear that the eight node brick shell formulation comes closest to predicting the overall response of the shell, it was also noted that the formulation is very sensitive to integration time increment in areas with high strain. Commonly used thumbrules did not appear to be adequate in this case. In addition, additional analyses need to be performed to determine the mesh sensitivity of the eight node brick shell in this model.

c. FAILURE CRITERIA.

This study was performed on a model with relatively low total plastic strain (less than one percent). In order to deal with larger strains, a failure model must be introduced into the material modelling of the cylinder. The model should include structural instability as well as material rupture criteria.

d. NEAR FIELD EXPERIMENTATION

Although the numerical predictions appear to be physically correct, the physical results obtained using them cannot be assumed completely correct until they are confirmed with experimental results. A study should be conducted to compare near field experimental results with numerical predictions.

2. RECOMMENDATIONS TO IMPROVE TEST CONTROL.

Several factors made the comparison of the numerical to experimental results difficult. If properly controlled, the analysis process could be simplified. First, rotation of the cylinder must be carefully controlled. Second, unless specifically required, high strain gradient areas should be avoided. Placement of the strain gages becomes critical in these locations as does mesh design and integration time increment. If these areas cannot be avoided, additional sensitivity analyses may be required to determine the adequacy of the mesh and integration time increment. Finally, analysis near welded seams should be avoided unless the effects can be quantified. If near weld analysis cannot be avoided, consideration should be given to restoring the heat treatment after the weld process.

LIST OF REFERENCES

1. Boticario, L. A., *Dynamic Response of Cylindrical Shells to Underwater End-On Explosion*, Master's Thesis, Naval Postgraduate School, Monterey, California, 1991.

2. Kwon, Y. W., Fox, P. K. and Shin, Y. S., "Response of a Cylindrical Shell Subject to a Near Field Side-On Explosion," *Proceedings of the 62nd Shock and Vibration Symposium, Volume II*, pp 163 - 178, Pasadena, California, October 1990.

3. Livermore Software Technology Corporation Report 1018, *VEC/DYNA3D User's Manual (Nonlinear Dynamic Analysis of Structures in Three Dimensions)*, by D. W. Stillman and J. O. Hallquist, June 1990.

4. Livermore Software Technology Corporation Report 1019, *LS-INGRID: A Pre-processor and Three-Dimensional Mesh Generator for the Programs LS-DYNA3D, LS-NIKE3D and TOPAZ-3D, version 3.0*, by D. W. Stillman and J. O. Hallquist, June 1991.

5. Livermore Software Technology Corporation Report 1009, *LS-TAURUS, An Interactive Post-Processor for the Programs LS-DYNA3D, LS-NIKE3D and TOPAZ-3D*, by J. O. Hallquist, April 1990.

6. Deruntz, J. A. Jr. and Rankin, C. C., "Applications of the USA-Stags Codes to Underwater Shock Problems, Palo Alto, California, 1990.

7. Geers, T. L., "Residual Potential and Approximate Methods for Three Dimensional Fluid-Structure Interaction Problem," *Journal of the Acoustic Society of America*, v. 49, pp 1505-1510, 1971.

8. Huang, H., Everstine, C. C. and Wang, Y. F., "Retarded Potential for Analysis of Submerged Structures Impinged by Weak Shock Waves," *Computational Methods for Fluid-Structure Interaction Problems*, AMD-Vol 26, American Society of Mechanical Engineers, December 1977.

9. Huang, H., "Transient Interaction of Plane Waves With a Spherical Elastic Shell," *Journal of the Acoustic Society of America*, v. 45, pp 661-670, 1969.

10.   Ugural, A. C. and Fenster, S. K., *Advanced Strength and Applied Elasticity, Second S. I. Edition*, Elsevier Science Publishing Co. Inc., New York, New York, p 398, 1987.

11.   Belytschko, T. and Tsay, C. S., "Explicit Algorithms for Non-Linear Dynamics of Shells," AMD-Vol 48, American Society of Mechanical Engineers, pp 209-231, 1981.

12.   Hughes, T. J. R., *The Finite Element Method. Linear Static and Dynamic Finite Element Analysis,* Prentice Hall, Englewood Cliffs, New Jersey, 1987.

13.   Livermore Software Technology Corporation Report 1009, *LS-DYNA3D Course Notes*, by Hallquist, J. O. and Stillman, D. W., October 1990.

APPENDIX A - SPHERICAL VALIDATION   MODEL

A. INGRID PRE-PROCESSOR INPUT DATA

```
dn3d vec term 5.0 plti 0.01 prti 1000.

mat 1 type 1 e 9.7e+1 pr 0.3 ro 7.79
     shell endmat

lcd 1 2 0.0 0.0 10.0 0.0
lcd 2 2 0.0 0.00025 10.0 0.00025

plan 2

 0 0 0     0 -1  0  0.00001  symm
 0 0 0    -1  0  0  0.00001  symm

start
 -1   6   -11 ;
 -1   6   -11 ;
 -1   6   -11 ;
 -1.  0.   1.
 -1.  0.   1.
 -1.  0.   1.
 sfi -1 -3 ; -1 -3 ; -1 -3 ; sp 0 0 0 1.
 d 0 1 0 0 2 0
 d 1 0 0 2 0 0
 pri -1 -3 ; -1 -3 ; -1 -3 ; 1 -1.0 0. 0. 0.
 thick 0.02
 mate 1
end

end
```

B. INGRID PRE-PROCESSOR OUTPUT DATA

```
    SPHERICAL MODEL VERIFICATION                                          88 large
    1       171          0          0        150          0                    0
    0     0        0              +0C.9                 150
    2   0  151       0      0    0    0     0    0    0     0     0    0    0    0
 2.000E+01 1.000E+03 2.000E-02           0.000E+00 0.000E+00    0       0.000E+00
    0     0    0    0    0    0    0    0    1    0          0    0    0    0
    0     0 0.000E+00
    0     0    0
    1    17.7900E+00    0    00.0000E+00    00.0000E+000.0000E+00    2    0    0
material type # 1   (elastic)
 2.700E+01 0.000E+00 0.000E+00 0.000E+00 0.000E+00 0.000E+00 0.000E+00 0.000E+00
 3.000E-01 0.000E+00 0.000E+00 0.000E+00 0.000E+00 0.000E+00 0.000E+00 0.000E+00
 0.000E+00 0.000E+00 0.000E+00 0.000E+00 0.000E+00 0.000E+00 0.000E+00 0.000E+00
 0.000E+00 0.000E+00 0.000E+00 0.000E+00 0.000E+00 0.000E+00 0.000E+00 0.000E+00
 0.000E+00 0.000E+00 0.000E+00 0.000E+00 0.000E+00 0.000E+00 0.000E+00 0.000E+00
 0.000E+00 0.000E+00 0.000E+00 0.000E+00 0.000E+00 0.000E+00 0.000E+00 0.000E+00
section properties

 0.000E+00 0.000E+00 0.000E+00 0.000E+00 0.000E+00
    1    4.    .0000000000000E+00    .0000000000000E+00  -.1000000000000E+01    7.
    2    2.    .1564342081547E+00    .3438787088953E-17  -.9876884222031E+00    6.
    3    2.    .3090168535703E+00    .6570891175550E-16  -.9510565996170E+00    6.
    4    2.    .4539905680584E+00  -.6570888528572E-16  -.8910064697266E+00    6.
    5    2.    .5877852542011E+00  -.3545041002901E-16  -.8090168237686E+00    6.
    6    2.    .7071068286896E+00    .0000000000000E+00  -.7071068286896E+00    6.
    7    2.   -.1441272742341E-01    .1564342081547E+00  -.9876884222031E+00    5.
    8    2.    .1544903069735E+00    .1544903069735E+00  -.9756404685957E+00    0.
    9    2.    .1560061023456E+00    .1560061023456E+00  -.9400740685632E+00    0.
   10    2.    .1431201263516E+00    .1431201263516E+00  -.8811608004466E+00    0.
   11    2.    .1348078038058E+00    .1348078038058E+00  -.8109869893037E+00    0.
   12    2.    .1207863149176E+00    .1207863149176E+00  -.7017562985420E+00    0.
   13    2.   -.1776001051540E-17    .3090168535703E+00  -.9510565996170E+00    5.
   14    2.    .3061736524195E+00    .3061736524195E+00  -.9400740685632E+00    0.
   15    2.    .2980021708443E-00    .2980021708443E-00  -.9068569348665E+00    0.
   16    2.    .2846010625562E+00    .2846010625562E+00  -.8520765930661E+00    0.
   17    2.    .2563304207977E+00    .2563304207977E+00  -.7775039079905E+00    0.
   18    2.    .2437104401331E+00    .2437104401331E+00  -.6857857704163E+00    0.
   19    2.   -.4539905680584E-16    .4539905680584E+00  -.8910064697266E+00    5.
   20    2.    .4506065813046E+00    .4506065813046E+00  -.8811608004466E+00    0.
   21    0.    .4394280956983E+00    .4394280956983E+00  -.8520765900612E+00    0.
   22    2.    .4001854195736E+00    .4001854195736E+00  -.8143146724695E+00    0.
   23    2.    .3937647312311E+00    .3937647312311E+00  -.7393637293538E+00    0.
   24    2.    .3609513640404E+00    .3609513640404E+00  -.6534363411492E+00    0.
   25    2.   -.5877852542011E-17    .5877852542011E+00  -.8090168237686E+00    5.
   26    2.    .5836555957794E+00    .5836555957794E+00  -.8106853832037E+00    0.
   27    2.    .5697026252747E+00    .5697026252747E+00  -.7775039079655E+00    0.
   28    0.    .5461454331473E+00    .5461454331473E+00  -.7393637293538E+00    0.
   29    0.    .5135421156883E+00    .5135421156883E+00  -.6874019775200E+00    0.
   30    0.    .4727076351784E+00    .4727076351784E+00  -.6031085060027E+00    0.
   31    1.    .7071068286896E+00    .7071068286896E+00  -.7071068286896E+00    5.
   32    0.    .7017562985420E+00    .7017562985420E+00  -.7017562985420E+00    0.
   33    0.    .6857857704163E+00    .6857857704163E+00  -.6857857704163E+00    0.
   34    0.    .6594369411469E+00    .6594369411469E+00  -.6594369411469E+00    0.
   35    0.    .6031085060027E+00    .6031085060027E+00  -.6031085060027E+00    0.
   36    0.    .5773503184313E+00    .5773503184313E+00  -.5773503184313E+00    0.
   37    4.    .0000000000000E+00    .0000000000000E+00   .1000000000000E+01    7.
   38    2.    .1564342081547E+00    .3438787088953E-17   .9876884222031E+00    6.
   39    2.    .3090168535703E+00    .6570891175550E-16   .9510565996170E+00    6.
   40    2.    .4539905680584E+00  -.6570888528572E-16   .8910064697266E+00    6.
   41    2.    .5877852542011E+00  -.3545041002901E-16   .8090168237686E+00    6.
   42    2.    .7071068286896E+00    .0000000000000E+00   .7071068286896E+00    6.
   43    1.   -.1441272742341E-01    .1564342081547E+00   .9876884222031E+00    5.
   44    .    .1544903069735E+00    .1544903069735E+00   .9756404685957E+00    0.
   45    .    .1560061023456E+00    .1560061023456E+00   .9400740685632E+00    0.
```

88

46	0.	.451?0?591?40E+00	.1431921869516E+00	.8811?09???406E+00	0.
47	0.	.56?4855?357794E+00	.1340278238058E+00	.80?8636832?37E+00	0.
48	?.	.?017562?85420E+00	.1227853149176E+00	.7017562?85420E+00	0.
49	1.	-.1??6???15164E-17	.3090168535709E+00	.9510565996170E+00	5.
50	?.	.15?0??1?23436E+00	.30?1736524105E+00	.9400742650033E+00	0.
51	?.	.??29?1???1443E+00	.2980002728443E+00	.9069568348885E+00	0.
52	?.	.4?0??0?4552?0?E+00	.2846010625362E+00	.8520765900612E+00	0.
53	0.	.5697026252747E+00	.2663204967976E+00	.7775039076805E+00	0.
54	0.	.6357857704163E+00	.2437124401331E+00	.6857857704163E+00	0.
55	1.	-.6743750086005E-16	.4539906680584E+00	.8910064697266E+00	5.
56	0.	.1431921869516E+00	.4506085813046E+00	.8811628222466E+00	0.
57	0.	.2846010625362E+00	.4392809569836E+00	.8520765900612E+00	0.
58	0.	.4201654195786E+00	.4201654195786E+00	.8043146729469E+00	0.
59	0.	.5461454391479E+00	.3937847912312E+00	.7393637299538E+00	0.
60	0.	.6594369411469E+00	.3609513640404E+00	.6594369411469E+00	0.
61	1.	-.3439267267305E-17	.5877855420113E+00	.8090168237686E+00	5.
62	0.	.1340278238058E+00	.5836555957794E+00	.8008636832237E+00	0.
63	.	.2663204967976E+00	.5697026252747E+00	.7775039076805E+00	0.
64	.	.3937847912312E+00	.5461454391479E+00	.7393637299538E+00	0.
65	0.	.5135421156883E+00	.5135421156883E+00	.6874219775200E+00	0.
66	0.	.6231085062027E+00	.4727278351784E+00	.6231085062027E+00	0.
67	1.	.0000000000000E+00	.7071068286896E+00	.7071068286896E+00	5.
68	.	.1227853149176E+00	.7017562985420E+00	.7017562985420E+00	0.
69	.	.2437124401331E+00	.6857857704163E+00	.6857857704163E+00	0.
70	.	.3609513640404E+00	.6594369411469E+00	.6594369411469E+00	0.
71	.	.4727278351784E+00	.6231085062027E+00	.6231085062027E+00	0.
72	.	.5773503184319E+00	.5773503184319E+00	.5773503184319E+00	0.
73	1.	.4011630007073E-17	.8090168237686E+00	-.5877854824065E+00	5.
74	.	.1340?78?...E+00	.8008636832237E+00	-.5836555957794E+00	0.
75	0.	.2663204967976E+00	.7775039076805E+00	-.5697026252747E+00	0.
76	.	.3937847912312E+00	.7393637299538E+00	-.5461454391479E+00	0.
77	0.	.5135421156883E+00	.6874219779153E+00	-.5135421750930E+00	0.
78	.	.6231085062027E+00	.6231085062027E+00	-.4727278947?8?E+00	0.
79	1.	.6?47?687?9374E-16	.8910064697266E+00	-.4539206381561E+00	5.
80	.	.143?...E+00	.8811628222466E+00	-.4506?8551?...E+00	0.
81	.	.2846?...E+00	.8520765900612E+00	-.43?2809569836E+00	0.
82	1.	.4?0165?8?77?2E+00	.8043146133403E+00	-.4201654?8977?2E+00	0.
83	.	.5461454391479E+00	.7393637299538E+00	-.3937848210303E+00	0.
84	.	.6594369411469E+00	.6594369411469E+00	-.3609513640450E+00	0.
85	1.	.?5?47?6?4?0?7?E-16	.9510565996170E+00	-.3090168237686E+00	5.
86	.	.15?...E+00	.9400743246073E+00	-.3061735928059E+00	0.
87	.	...E+00	.9069568348885E+00	-.2980000130097E+00	0.
88	0.	.4?0?...936?E+00	.8520765304565E+00	-.2846010327339E+00	0.
89	.	.5?...?43E+00	.7775039076805E+00	-.2663204669951E+00	0.
90	.	...41??E+00	.6857857704163E+00	-.2437124252319E+00	0.
91	1.	...5656E-16	.9876842220031E+00	-.1564341793514E+00	5.
92	.	.1544?...9735E+00	.9758409261702E+00	-.1544002622?00E+00	0.
93	.	...E+00	.9400743246073E+00	-.15006?6?7?9?1E+00	0.
94	.	...47E+00	.8811628222466E+00	-.1431921?...E+00	0.
95	0.	.5836555957794E+00	.8008636832237E+00	-.13402777311?2?E+00	0.
96	0.	.7017562985420E+00	.7017562985420E+00	-.1227852776647E+00	0.
97	1.	.000000000000E+00	.1000000000000E+01	.0000000000000E+00	5.
98	0.	.1544342081547E+00	.9876884222031E+00	-.4917976482540E-21	0.
99	0.	.3090168535709E+00	.9510565996170E+00	-.1728606165154E-17	0.
100	.	.4539?...?84E+00	.8910064697266E+00	-.6743750086005E-16	0.
101	0.	.5877855420113E+00	.8090168237686E+00	-.3439267267305E-17	0.
102	0.	.7071?...?46E+00	.7071068286896E+00	.0000000000000E+00	0.
103	1.	.3439?7?088965?E-17	.9876884222031E+00	.1564342081547E+00	5.
104	0.	.15449030?755E+00	.9758408565657E+00	.1544903069735E+00	0.
105	0.	.?0?17?654105E+00	.9400742650033E+00	.1500601023455E+00	0.
106	0.	.450?...?46E+00	.8811628222466E+00	.1431921869516E+00	0.
107	.	.56?4855?5?7?4E+00	.8008636832237E+00	.1340278238058E+00	0.
108	0.	.7017562985420E+00	.7017562985420E+00	.1227853149176E+00	0.
109	1.	.?670?3117?5?0E-15	.9510565996170E+00	.3090168535709E+00	5.
110	0.	.15?0??1?3436E+00	.9400742650033E+00	.3061735624105E+00	0.
111	.	...441E+00	.?685?6?346?5?E+00	...2980??2728443E+00	0.
112	.	...E+00	.9?...?41?E+00	.2846?1??35?E+00	0.
113	.	...47?E+00	.77750??1?68?5E+00	.2663204967976E+00	0.

114	0.	.6857857704160E+00	.6857857704160E+00	.2437124401331E+00	0.
115	1.	-.4870828829572E-16	.8912064697266E+00	.4539906080584E+00	5.
116	0.	.1431921869515E+00	.8811628222466E+00	.4506085813046E+00	0.
117	0.	.2846010205201E+00	.8520765900610E+00	.4392809569636E+00	0.
118	0.	.4201654195766E+00	.8043146709463E+00	.4201654195786E+00	0.
119	0.	.5461454391473E+00	.7393637299538E+00	.3937847910310E+00	0.
120	0.	.6594369411469E+00	.6594369411469E+00	.3609513640404E+00	0.
121	1.	-.3545041002901E-16	.8090168237686E+00	.5877854420113E+00	5.
122	0.	.1340278238058E+00	.8008636832237E+00	.5836555957794E+00	0.
123	0.	.2663204967976E+00	.7775039076805E+00	.5697026252747E+00	0.
124	0.	.3937847910310E+00	.7393637299538E+00	.5461454391479E+00	0.
125	0.	.5135421156883E+00	.6874219775200E+00	.5135421156883E+00	0.
126	0.	.6231085062027E+00	.6231085062027E+00	.4727278351784E+00	0.
127	2.	.8090168237686E+00	.4211630207073E-17	-.5877854824066E+00	6.
128	0.	.8008636832237E+00	.1340278238058E+00	-.5836555957794E+00	0.
129	0.	.7775039076805E+00	.2663204967976E+00	-.5697026252747E+00	0.
130	0.	.7393637299538E+00	.3937847910312E+00	-.5461454391479E+00	0.
131	0.	.6874219172153E+00	.5135421156883E+00	-.5135421752930E+00	0.
132	2.	.8410064697266E+00	.8047658708374E-16	-.4539906380561E+00	6.
133	0.	.8811628222466E+00	.1431921720505E+00	-.4506085515023E+00	0.
134	0.	.8520765900610E+00	.2846010605362E+00	-.4392809569636E+00	0.
135	0.	.8043146133423E+00	.4201653897762E+00	-.4201653897762E+00	0.
136	0.	.7393637299538E+00	.5461454391473E+00	-.3337848010335E+00	0.
137	2.	.6874219775193E+00	-.8047667972797E-16	-.3090169037686E+00	6.
138	0.	.6403040807SE+00	.1500601003438E+00	-.3061735908059E+00	0.
139	0.	.5980024386955E+00	.2980024934320E+00	-.2980022135327E+00	0.
140	0.	.5520715304565E+00	.4392809569895E+00	-.2846010327333E+00	0.
141	0.	.5607016825E+00	.5607016848793E+00	-.2663204669950E+00	0.
142	2.	.4517790110305E-16	-.4141770110305E-16	-.1564741783524E+00	6.
143	0.	.9756449061703E+00	.1544903069735E+00	-.1544903622700E+00	0.
144	0.	.6403040807SE+00	.3061730026042E+00	-.1500600574611E+00	0.
145	0.	.5511083034665E+00	.4506085813041E+00	-.1431921403430E+00	0.
146	0.	.5807053352407E+00	.5836555957734E+00	-.1340277711103E+00	0.
147	2.	.1177030700006E-11	.1000000000006E+00	.0000700000000E+00	5.
148	0.	.9870288410C011E+00	.1564341061547E+00	-.4317976480547E-01	0.
149	0.	.9810809809617E+00	.3090169837109E+00	-.1703606161154E-17	0.
150	0.	.9410040497049E+00	.4539906080584E+00	-.6743750096015E-16	0.
151	0.	.6603044802706E+00	.5877854420113E+00	-.3439067367365E-17	0.
152	2.	.6074569420035E+00	.6438757068950E-17	.1564341781547E+00	6.
153	0.	.9756449065077E+00	.1544903069735E+00	.1544903069735E+00	0.
154	0.	.6403040603SE-01	.3061739854145E+00	.1500601013436E+00	0.
155	0.	.5511083214678E+00	.4506085813041E+00	.1431921669510E+00	0.
156	0.	.8008636832237E+00	.5836555957794E+00	.1340278239058E+00	0.
157	2.	.6874219775170E+00	.6570891175550E-16	.3090168535709E+00	6.
158	0.	.6403040603032E+00	.1500601003436E+00	.3061736504145E+00	0.
159	0.	.5980024348685E+00	.2980024708443E+00	.2980002713443E+00	0.
160	0.	.5520765900610E+00	.4392809569936E+00	.2846010605362E+00	0.
161	0.	.7775039076805E+00	.5697026250747E+00	.2663204967976E+00	0.
162	2.	.7421649275454E+00	-.6570891973957E-16	.4539903680544E+00	6.
163	0.	.8811628203446E+00	.1431921669516E+00	.4506085813046E+00	0.
164	0.	.8520765900610E+00	.2846010605362E+00	.4392809569636E+00	0.
165	0.	.8043146729469E+00	.4201654195786E+00	.4201654195786E+00	0.
166	0.	.7393637299538E+00	.5461454391479E+00	.3937847910310E+00	0.
167	2.	.8090168237686E+00	-.3545041002901E-16	.5877854420113E+00	6.
168	0.	.8008636832237E+00	.1340278238058E+00	.5836555957794E+00	0.
169	0.	.7775039076805E+00	.2663204967976E+00	.5697026252747E+00	0.
170	0.	.7393637299538E+00	.3937847910310E+00	.5461454391479E+00	0.
171	0.	.6874219775200E+00	.5135421156883E+00	.5135421156883E+00	0.

```
    1        1        1        7        8        2
2.000E-02 2.000E-02 2.000E-02 2.000E-02
    2        1        2        8        9        3
2.000E-02 2.000E-02 2.000E-02 2.000E-02
    3        1        3        9       10        4
2.000E-02 2.000E-02 2.000E-02 2.000E-02
    4        1        4       10       11        5
2.000E-02 2.000E-02 2.000E-02 2.000E-02
    5        1        5       11       12        6
2.000E-02 2.000E-02 2.000E-02 2.000E-02
```

```
       6      1        7        13       14            8
2.000E-02 2.000E-02 2.000E-02 2.000E-02
       7      1        8        14       15            9
2.000E-02 2.000E-02 2.000E-02 2.000E-02
       8      1        9        15       16           10
2.000E-02 2.000E-02 2.000E-02 2.000E-02
       9      1       10        16       17           11
2.000E-02 2.000E-02 2.000E-02 2.000E-02
      10      1       11        17       18           12
2.000E-02 2.000E-02 2.000E-02 2.000E-02
      11      1       13        19       20           14
2.000E-02 2.000E-02 2.000E-02 2.000E-02
      12      1       14        20       21           15
2.000E-02 2.000E-02 2.000E-02 2.000E-02
      13      1       15        21       22           16
2.000E-02 2.000E-02 2.000E-02 2.000E-02
      14      1       16        22       23           17
2.000E-02 2.000E-02 2.000E-02 2.000E-02
      15      1       17        23       24           18
2.000E-02 2.000E-02 2.000E-02 2.000E-02
      16      1       19        25       26           20
2.000E-02 2.000E-02 2.000E-02 2.000E-02
      17      1       20        26       27           21
2.000E-02 2.000E-02 2.000E-02 2.000E-02
      18      1       21        27       28           22
2.000E-02 2.000E-02 2.000E-02 2.000E-02
      19      1       22        28       29           23
2.000E-02 2.000E-02 2.000E-02 2.000E-02
      20      1       23        29       30           24
2.000E-02 2.000E-02 2.000E-02 2.000E-02
      21      1       24        30       31           26
2.000E-02 2.000E-02 2.000E-02 2.000E-02
      22      1       25        32       33           27
2.000E-02 2.000E-02 2.000E-02 2.000E-02
      23      1       27                 34           28
2.000E-02 2.000E-02 2.000E-02 2.000E-02
      24      1       28        34       35           29
2.000E-02 2.000E-02 2.000E-02 2.000E-02
      25      1       29        35       36           30
2.000E-02 2.000E-02 2.000E-02 2.000E-02
      26      1       37        43       44           38
2.000E-02 2.000E-02 2.000E-02 2.000E-02
      27      1       38        44       45           39
2.000E-02 2.000E-02 2.000E-02 2.000E-02
      28      1       39        45       46           40
2.000E-02 2.000E-02 2.000E-02 2.000E-02
      29      1       40        46       47           41
2.000E-02 2.000E-02 2.000E-02 2.000E-02
      30      1       41        47       48           42
2.000E-02 2.000E-02 2.000E-02 2.000E-02
      31      1       43        49       50           44
2.000E-02 2.000E-02 2.000E-02 2.000E-02
      32      1       44        50       51           45
2.000E-02 2.000E-02 2.000E-02 2.000E-02
      33      1       45        51       52           46
2.000E-02 2.000E-02 2.000E-02 2.000E-02
      34      1       46        52       53           47
2.000E-02 2.000E-02 2.000E-02 2.000E-02
      35      1       47        53       54           48
2.000E-02 2.000E-02 2.000E-02 2.000E-02
      36      1       49        55       56           50
2.000E-02 2.000E-02 2.000E-02 2.000E-02
      37      1       50        56       57           51
2.000E-02 2.000E-02 2.000E-02 2.000E-02
      38      1       51        57       58           52
2.000E-02 2.000E-02 2.000E-02 2.000E-02
      39      1       52        58       59           53
2.000E-02 2.000E-02 2.000E-02 2.000E-02
```

91

```
    40     1        5?        5?        60      54
2.000E-02 2.000E-02 2.000E-02 2.000E-02
    41     1        5?        51        62      56
2.000E-02 2.000E-02 2.000E-02 2.000E-02
    42     1        5?        62        6?      57
2.000E-02 2.000E-02 2.000E-02 2.000E-02
    43     1        57        63        64      58
2.000E-02 2.000E-02 2.000E-02 2.000E-02
    44     1        58        64        65      59
2.000E-02 2.000E-02 2.000E-02 2.000E-02
    45     1        5?        65        66      60
2.000E-02 2.000E-02 2.000E-02 2.000E-02
    46     1        61        67        68      62
2.000E-02 2.000E-02 2.000E-02 2.000E-02
    47     1        62        68        69      63
2.000E-02 2.000E-02 2.000E-02 2.000E-02
    48     1        63        69        70      64
2.000E-02 2.000E-02 2.000E-02 2.000E-02
    49     1        64        70        71      65
2.000E-02 2.000E-02 2.000E-02 2.000E-02
    50     1        65        71        72      66
2.000E-02 2.000E-02 2.000E-02 2.000E-02
    51     1        ??        73        74      3?
2.000E-02 2.000E-02 2.000E-02 2.000E-02
    52     1        ??        74        75      ??
2.000E-02 2.000E-02 2.000E-02 2.000E-02
    5?     1        ??        75        7?      ?4
2.000E-02 2.000E-02 2.000E-02 2.000E-02
    54     1        ?4        7?        77      ?5
2.000E-02 2.000E-02 2.000E-02 2.000E-02
    5?     1        ??        77        78      3?
2.000E-02 2.000E-02 2.000E-02 2.000E-02
    5?     1        ??        7?        ??      74
2.000E-02 2.000E-02 2.000E-02 2.000E-02
    5?     1        74        ??        ?1      75
2.000E-02 2.000E-02 2.000E-02 2.000E-02
    5?     1        ??        ?1        ??      7?
2.000E-02 2.000E-02 2.000E-02 2.000E-02
    5?     1        7?        ?0        ??      77
2.000E-02 2.000E-02 2.000E-02 2.000E-02
    ??     1        ??        ??        ?4      7?
2.000E-02 2.000E-02 2.000E-02 2.000E-02
    ?1     1        7?        ?5        ??      ?0
2.000E-02 2.000E-02 2.000E-02 2.000E-02
    ?2     1        ??        ??        87      ?1
2.000E-02 2.000E-02 2.000E-02 2.000E-02
    ??     1        ??        ??        88      8?
2.000E-02 2.000E-02 2.000E-02 2.000E-02
    ?4     1        ??        ??        89      8?
2.000E-02 2.000E-02 2.000E-02 2.000E-02
    65     1        83        8?        90      84
2.000E-02 2.000E-02 2.000E-02 2.000E-02
    6?     1        ?5        ?1        92      8?
2.000E-02 2.000E-02 2.000E-02 2.000E-02
    ?7     1        ??        ?2        ??      97
2.000E-02 2.000E-02 2.000E-02 2.000E-02
    68     1        8?        93        94      ?8
2.000E-02 2.000E-02 2.000E-02 2.000E-02
    69     1        8?        ?4        ?5      8?
2.000E-02 2.000E-02 2.000E-02 2.000E-02
    70     1        8?        ?5        96      9?
2.000E-02 2.000E-02 2.000E-02 2.000E-02
    71     1        91        ?7        98      92
2.000E-02 2.000E-02 2.000E-02 2.000E-02
    72     1        ??        ??        ??      93
2.000E-02 2.000E-02 2.000E-02 2.000E-02
    7?     1        ??        ??        ??      ?4
2.000E-02 2.000E-02 2.000E-02 2.000E-02
```

92

```
 74      1       94      ...     101      95
2.000E-02 2.000E-02 2.000E-02 2.000E-02
 75      1       95      101     102      96
2.000E-02 2.000E-02 2.000E-02 2.000E-02
 76      1       97      ...     104      98
2.000E-02 2.000E-02 2.000E-02 2.000E-02
 77      1       98      ..4     105      99
2.000E-02 2.000E-02 2.000E-02 2.000E-02
 78      1       99      105     106     100
2.000E-02 2.000E-02 2.000E-02 2.000E-02
 79      1      100      106     107     101
2.000E-02 2.000E-02 2.000E-02 2.000E-02
 80      1      101      107     108     102
2.000E-02 2.000E-02 2.000E-02 2.000E-02
 81      1      103      109     110     104
2.000E-02 2.000E-02 2.000E-02 2.000E-02
 82      1      104      110     111     105
2.000E-02 2.000E-02 2.000E-02 2.000E-02
 83      1      105      111     112     106
2.000E-02 2.000E-02 2.000E-02 2.000E-02
 84      1      106      112     113     107
2.000E-02 2.000E-02 2.000E-02 2.000E-02
 85      1      107      113     114     108
2.000E-02 2.000E-02 2.000E-02 2.000E-02
 86      1      109      115     116     110
2.000E-02 2.000E-02 2.000E-02 2.000E-02
 87      1      110      116     117     111
2.000E-02 2.000E-02 2.000E-02 2.000E-02
 88      1      111      117     118     112
2.000E-02 2.000E-02 2.000E-02 2.000E-02
 89      1      112      118     119     113
2.000E-02 2.000E-02 2.000E-02 2.000E-02
 90      1      113      114     120     114
2.000E-02 2.000E-02 2.000E-02 2.000E-02
 91      1      115      121     122     116
2.000E-02 2.000E-02 2.000E-02 2.000E-02
 92      1      116      122     123     117
2.000E-02 2.000E-02 2.000E-02 2.000E-02
 93      1      117      123     124     118
2.000E-02 2.000E-02 2.000E-02 2.000E-02
 94      1      118      124     125     119
2.000E-02 2.000E-02 2.000E-02 2.000E-02
 95      1      119      125     126     120
2.000E-02 2.000E-02 2.000E-02 2.000E-02
 96      1      101      97      68      122
2.000E-02 2.000E-02 2.000E-02 2.000E-02
 97      1      102      68      69      123
2.000E-02 2.000E-02 2.000E-02 2.000E-02
 98      1      103      69      70      124
2.000E-02 2.000E-02 2.000E-02 2.000E-02
 99      1      104      70      71      125
2.000E-02 2.000E-02 2.000E-02 2.000E-02
100      1      105      71      72      126
2.000E-02 2.000E-02 2.000E-02 2.000E-02
101      1      107      128      12
2.000E-02 2.000E-02 2.000E-02 2.000E-02
102      1       12      128     129      18
2.000E-02 2.000E-02 2.000E-02 2.000E-02
103      1       13      129     130      24
2.000E-02 2.000E-02 2.000E-02 2.000E-02
104      1       24      130     131      30
2.000E-02 2.000E-02 2.000E-02 2.000E-02
105      1       30      131      78      36
2.000E-02 2.000E-02 2.000E-02 2.000E-02
106      1      127      132     133     128
2.000E-02 2.000E-02 2.000E-02 2.000E-02
107      1             133     134     129
2.000E-02 2.000E-02 2.000E-02 2.000E-02
```

93

```
   108     1      109      134      135      130
2.000E-02 2.000E-02 2.000E-02 2.000E-02
   109     1      130      135      136      131
2.000E-02 2.000E-02 2.000E-02 2.000E-02
   110     1      131      136       84       79
2.000E-02 2.000E-02 2.000E-02 2.000E-02
   111     1      132      137      138      133
2.000E-02 2.000E-02 2.000E-02 2.000E-02
   112     1      133      138      139      134
2.000E-02 2.000E-02 2.000E-02 2.000E-02
   113     1      134      139      140      135
2.000E-02 2.000E-02 2.000E-02 2.000E-02
   114     1      135      140      141      136
2.000E-02 2.000E-02 2.000E-02 2.000E-02
   115     1      136      141       90       84
2.000E-02 2.000E-02 2.000E-02 2.000E-02
   116     1      137      142      143      138
2.000E-02 2.000E-02 2.000E-02 2.000E-02
   117     1      138      143      144      139
2.000E-02 2.000E-02 2.000E-02 2.000E-02
   118     1      139      144      145      140
2.000E-02 2.000E-02 2.000E-02 2.000E-02
   119     1      140      145      146      141
2.000E-02 2.000E-02 2.000E-02 2.000E-02
   120     1      141      146       96       90
2.000E-02 2.000E-02 2.000E-02 2.000E-02
   121     1      142      147      148      143
2.000E-02 2.000E-02 2.000E-02 2.000E-02
   122     1      143      148      149      144
2.000E-02 2.000E-02 2.000E-02 2.000E-02
   123     1      144      149      151      145
2.000E-02 2.000E-02 2.000E-02 2.000E-02
   124     1      145      151      151      146
2.000E-02 2.000E-02 2.000E-02 2.000E-02
   125     1      146      151      152       96
2.000E-02 2.000E-02 2.000E-02 2.000E-02
   126     1      147      152      153      148
2.000E-02 2.000E-02 2.000E-02 2.000E-02
   127     1      148      153      154      149
2.000E-02 2.000E-02 2.000E-02 2.000E-02
   128     1      149      154      155      150
2.000E-02 2.000E-02 2.000E-02 2.000E-02
   129     1      150      155      156      151
2.000E-02 2.000E-02 2.000E-02 2.000E-02
   130     1      151      156      108      102
2.000E-02 2.000E-02 2.000E-02 2.000E-02
   131     1      152      157      158      153
2.000E-02 2.000E-02 2.000E-02 2.000E-02
   132     1      153      158      159      154
2.000E-02 2.000E-02 2.000E-02 2.000E-02
   133     1      154      159      160      155
2.000E-02 2.000E-02 2.000E-02 2.000E-02
   134     1      155      160      161      156
2.000E-02 2.000E-02 2.000E-02 2.000E-02
   135     1      156      161      114      108
2.000E-02 2.000E-02 2.000E-02 2.000E-02
   136     1      157      162      163      158
2.000E-02 2.000E-02 2.000E-02 2.000E-02
   137     1      158      163      164      159
2.000E-02 2.000E-02 2.000E-02 2.000E-02
   138     1      159      164      165      160
2.000E-02 2.000E-02 2.000E-02 2.000E-02
   139     1      160      165      166      161
2.000E-02 2.000E-02 2.000E-02 2.000E-02
   140     1      161      166      120      114
2.000E-02 2.000E-02 2.000E-02 2.000E-02
   141     1      162      167      168      163
2.000E-02 2.000E-02 2.000E-02 2.000E-02
```

```
    142      1      1.0      1.6      169      164
2.000E-02 2.000E-02 2.000E-02 2.000E-02
    143      1      1.4      1.6      170      165
2.000E-02 2.000E-02 2.000E-02 2.000E-02
    144      1      16F      173      171      169
2.000E-02 2.000E-02 2.000E-02 2.000E-02
    145      1      16      171      126      123
2.000E-02 2.000E-02 2.000E-02 2.000E-02
    146      1      167      42      48      168
2.000E-02 2.000E-02 2.000E-02 2.000E-02
    147      1      168      48      54      169
2.000E-02 2.000E-02 2.000E-02 2.000E-02
    148      1      169      54      60      170
2.000E-02 2.000E-02 2.000E-02 2.000E-02
    149      1      170      60      66      171
2.000E-02 2.000E-02 2.000E-02 2.000E-02
    150      1      171      66      72      126
2.000E-02 2.000E-02 2.000E-02 2.000E-02
```

```
*----------------------- LOAD CURVE DEFINITIONS -----------------------*

      1      2
0.000E+0       . E-
0.000E+ .      . E+

      1      3
. . E+       . . E-4
. . E+ 1 1.  E- 4
```

```
*----------------- PRESSURE BOUNDARY CONDITION CARDS -----------------*

1           4           7           8       1-1.000E+00-1.000E+00-1.000E+00-1.000E+00
1           8          13          14       6-1.000E+00-1.000E+00-1.000E+00-1.000E+00
1          14          19          20      14-1.000E+00-1.000E+00-1.000E+00-1.000E+00
1          19          25          26      20-1.000E+00-1.000E+00-1.000E+00-1.000E+00
1          25          31          32      26-1.000E+00-1.000E+00-1.000E+00-1.000E+00
1                      13          41       3-1.000E+00-1.000E+00-1.000E+00-1.000E+00
1                      15          41       9-1.000E+00-1.000E+00-1.000E+00-1.000E+00
1          34                              15-1.000E+00-1.000E+00-1.000E+00-1.000E+00
1          23                              21-1.000E+00-1.000E+00-1.000E+00-1.000E+00
1          32                      5       27-1.000E+00-1.000E+00-1.000E+00-1.000E+00
1                                          4-1.000E+00-1.000E+00-1.000E+00-1.000E+00
1                              16          10-1.000E+00-1.000E+00-1.000E+00-1.000E+00
1          10                      22      16-1.000E+00-1.000E+00-1.000E+00-1.000E+00
1          11                      32      22-1.000E+00-1.000E+00-1.000E+00-1.000E+00
1                              34          28-1.000E+00-1.000E+00-1.000E+00-1.000E+00
1          14                      11      5-1.000E+00-1.000E+00-1.000E+00-1.000E+00
1                                  17      11-1.000E+00-1.000E+00-1.000E+00-1.000E+00
1                                          23-1.000E+00-1.000E+00-1.000E+00-1.000E+00
1          14          14          35      29-1.000E+00-1.000E+00-1.000E+00-1.000E+00
1          5          11          12       6-1.000E+00-1.000E+00-1.000E+00-1.000E+00
1          11          17          18      12-1.000E+00-1.000E+00-1.000E+00-1.000E+00
1          17          23          24      18-1.000E+00-1.000E+00-1.000E+00-1.000E+00
1          23          29          30      24-1.000E+00-1.000E+00-1.000E+00-1.000E+00
1          24          35          37      30-1.000E+00-1.000E+00-1.000E+00-1.000E+00
1          43          37          38      44-1.000E+00-1.000E+00-1.000E+00-1.000E+00
1          49          43          44      50-1.000E+00-1.000E+00-1.000E+00-1.000E+00
1          55          44          50      56-1.000E+00-1.000E+00-1.000E+00-1.000E+00
1          61          55          56      62-1.000E+00-1.000E+00-1.000E+00-1.000E+00
1          67          61          62      68-1.000E+00-1.000E+00-1.000E+00-1.000E+00
1          44          34          39      45-1.000E+00-1.000E+00-1.000E+00-1.000E+00
1          50          44          45      51-1.000E+00-1.000E+00-1.000E+00-1.000E+00
1          56          50          51      57-1.000E+00-1.000E+00-1.000E+00-1.000E+00
1          62          56          57      63-1.000E+00-1.000E+00-1.000E+00-1.000E+00
1          69          62          63      69-1.000E+00-1.000E+00-1.000E+00-1.000E+00
1          45          39          4       46-1.000E+00-1.000E+00-1.000E+00-1.000E+00
1          51          45          46      52-1.000E+00-1.000E+00-1.000E+00-1.000E+00
1          57          51          52      58-1.000E+00-1.000E+00-1.000E+00-1.000E+00
```

```
1      63      57      54      64-1.000E+00-1.000E+00-1.000E+00-1.000E+00
1      69      63      64      70-1.000E+00-1.000E+00-1.000E+00-1.000E+00
1      46      40      41      47-1.000E+00-1.000E+00-1.000E+00-1.000E+00
1      52      46      47      53-1.000E+00-1.000E+00-1.000E+00-1.000E+00
1      58      52      53      59-1.000E+00-1.000E+00-1.000E+00-1.000E+00
1      64      58      54      65-1.000E+00-1.000E+00-1.000E+00-1.000E+00
1      70      64      65      71-1.000E+00-1.000E+00-1.000E+00-1.000E+00
1      47      41      42      48-1.000E+00-1.000E+00-1.000E+00-1.000E+00
1      53      47      48      54-1.000E+00-1.000E+00-1.000E+00-1.000E+00
1      59      53      54      60-1.000E+00-1.000E+00-1.000E+00-1.000E+00
1      65      59      60      66-1.000E+00-1.000E+00-1.000E+00-1.000E+00
1      71      65      66      72-1.000E+00-1.000E+00-1.000E+00-1.000E+00
1      31      73      74      32-1.000E+00-1.000E+00-1.000E+00-1.000E+00
1      73      79      80      74-1.000E+00-1.000E+00-1.000E+00-1.000E+00
1      79      85      86      80-1.000E+00-1.000E+00-1.000E+00-1.000E+00
1      85      91      92      86-1.000E+00-1.000E+00-1.000E+00-1.000E+00
1      91      97      98      92-1.000E+00-1.000E+00-1.000E+00-1.000E+00
1      97     103     104      98-1.000E+00-1.000E+00-1.000E+00-1.000E+00
1     103     109     110     104-1.000E+00-1.000E+00-1.000E+00-1.000E+00
1     109     115     116     110-1.000E+00-1.000E+00-1.000E+00-1.000E+00
1     115     121     122     116-1.000E+00-1.000E+00-1.000E+00-1.000E+00
1     121      97      98     122-1.000E+00-1.000E+00-1.000E+00-1.000E+00
1                            33-1.000E+00-1.000E+00-1.000E+00-1.000E+00
1      74                    75-1.000E+00-1.000E+00-1.000E+00-1.000E+00
1                            81-1.000E+00-1.000E+00-1.000E+00-1.000E+00
1                            87-1.000E+00-1.000E+00-1.000E+00-1.000E+00
1                            93-1.000E+00-1.000E+00-1.000E+00-1.000E+00
1                            99-1.000E+00-1.000E+00-1.000E+00-1.000E+00
1                           105-1.000E+00-1.000E+00-1.000E+00-1.000E+00
1                           111-1.000E+00-1.000E+00-1.000E+00-1.000E+00
1                           117-1.000E+00-1.000E+00-1.000E+00-1.000E+00
1                           123-1.000E+00-1.000E+00-1.000E+00-1.000E+00
1                            34-1.000E+00-1.000E+00-1.000E+00-1.000E+00
1                            76-1.000E+00-1.000E+00-1.000E+00-1.000E+00
1                            82-1.000E+00-1.000E+00-1.000E+00-1.000E+00
1                            88-1.000E+00-1.000E+00-1.000E+00-1.000E+00
1                            94-1.000E+00-1.000E+00-1.000E+00-1.000E+00
1                           100-1.000E+00-1.000E+00-1.000E+00-1.000E+00
1                           106-1.000E+00-1.000E+00-1.000E+00-1.000E+00
1                           112-1.000E+00-1.000E+00-1.000E+00-1.000E+00
1                           118-1.000E+00-1.000E+00-1.000E+00-1.000E+00
1                           124-1.000E+00-1.000E+00-1.000E+00-1.000E+00
1                            35-1.000E+00-1.000E+00-1.000E+00-1.000E+00
1                            77-1.000E+00-1.000E+00-1.000E+00-1.000E+00
1                            83-1.000E+00-1.000E+00-1.000E+00-1.000E+00
1      96                    89-1.000E+00-1.000E+00-1.000E+00-1.000E+00
1                            95-1.000E+00-1.000E+00-1.000E+00-1.000E+00
1                           101-1.000E+00-1.000E+00-1.000E+00-1.000E+00
1                           107-1.000E+00-1.000E+00-1.000E+00-1.000E+00
1                           113-1.000E+00-1.000E+00-1.000E+00-1.000E+00
1     116     124     125     119-1.000E+00-1.000E+00-1.000E+00-1.000E+00
1     124             71     125-1.000E+00-1.000E+00-1.000E+00-1.000E+00
1                            36-1.000E+00-1.000E+00-1.000E+00-1.000E+00
1                            84     78-1.000E+00-1.000E+00-1.000E+00-1.000E+00-1.000E+00
1      83              80     84-1.000E+00-1.000E+00-1.000E+00-1.000E+00
1      89      95      96     90-1.000E+00-1.000E+00-1.000E+00-1.000E+00
1      95     101     102     96-1.000E+00-1.000E+00-1.000E+00-1.000E+00
1     101     107     108    102-1.000E+00-1.000E+00-1.000E+00-1.000E+00
1     107     113     114    108-1.000E+00-1.000E+00-1.000E+00-1.000E+00
1     113     119     120    114-1.000E+00-1.000E+00-1.000E+00-1.000E+00
1     119     125     126    120-1.000E+00-1.000E+00-1.000E+00-1.000E+00
1     125             72    126-1.000E+00-1.000E+00-1.000E+00-1.000E+00
1     127             12    128-1.000E+00-1.000E+00-1.000E+00-1.000E+00
1     132     127     128    133-1.000E+00-1.000E+00-1.000E+00-1.000E+00
1     137     132     133    138-1.000E+00-1.000E+00-1.000E+00-1.000E+00
1     142             113    143-1.000E+00-1.000E+00-1.000E+00-1.000E+00
1     147     142     143    148-1.000E+00-1.000E+00-1.000E+00-1.000E+00
1     152     147     148    153-1.000E+00-1.000E+00-1.000E+00-1.000E+00
```

96

```
1    157   152   153   158-1.000E+00-1.000E+00-1.000E+00-1.000E+00
1    162   157   158   163-1.000E+00-1.000E+00-1.000E+00-1.000E+00
1    168   162   163   169-1.000E+00-1.000E+00-1.000E+00-1.000E+00
1    42    17    18    48-1.000E+00-1.000E+00-1.000E+00-1.000E+00
1                      129-1.000E+00-1.000E+00-1.000E+00-1.000E+00
1          124   125   134-1.000E+00-1.000E+00-1.000E+00-1.000E+00
1    133         134   139-1.000E+00-1.000E+00-1.000E+00-1.000E+00
1    143   138   139   144-1.000E+00-1.000E+00-1.000E+00-1.000E+00
1    148   143   144   149-1.000E+00-1.000E+00-1.000E+00-1.000E+00
1    153   148   149   154-1.000E+00-1.000E+00-1.000E+00-1.000E+00
1    158   153   154   159-1.000E+00-1.000E+00-1.000E+00-1.000E+00
1    163   158   159   164-1.000E+00-1.000E+00-1.000E+00-1.000E+00
1    168   163   164   169-1.000E+00-1.000E+00-1.000E+00-1.000E+00
1    48    165   169   54-1.000E+00-1.000E+00-1.000E+00-1.000E+00
1    129   18    24    130-1.000E+00-1.000E+00-1.000E+00-1.000E+00
1    134   129   130   135-1.000E+00-1.000E+00-1.000E+00-1.000E+00
1    139   134   135   140-1.000E+00-1.000E+00-1.000E+00-1.000E+00
1    144         140   145-1.000E+00-1.000E+00-1.000E+00-1.000E+00
1    149   144   145   150-1.000E+00-1.000E+00-1.000E+00-1.000E+00
1    154   149   150   155-1.000E+00-1.000E+00-1.000E+00-1.000E+00
1    159   154   155   160-1.000E+00-1.000E+00-1.000E+00-1.000E+00
1    164   159   160   165-1.000E+00-1.000E+00-1.000E+00-1.000E+00
1    169   164   165   170-1.000E+00-1.000E+00-1.000E+00-1.000E+00
1    54          17    50-1.000E+00-1.000E+00-1.000E+00-1.000E+00
1                      131-1.000E+00-1.000E+00-1.000E+00-1.000E+00
1                      136-1.000E+00-1.000E+00-1.000E+00-1.000E+00
1          135   136   141-1.000E+00-1.000E+00-1.000E+00-1.000E+00
1    145   140   141   146-1.000E+00-1.000E+00-1.000E+00-1.000E+00
1          145   146   151-1.000E+00-1.000E+00-1.000E+00-1.000E+00
1    156   151   152   156-1.000E+00-1.000E+00-1.000E+00-1.000E+00
1                      161-1.000E+00-1.000E+00-1.000E+00-1.000E+00
1                      166-1.000E+00-1.000E+00-1.000E+00-1.000E+00
1                      171-1.000E+00-1.000E+00-1.000E+00-1.000E+00
1                      56-1.000E+00-1.000E+00-1.000E+00-1.000E+00
1    131                78-1.000E+00-1.000E+00-1.000E+00-1.000E+00
1                      84-1.000E+00-1.000E+00-1.000E+00-1.000E+00
1    141         84    90-1.000E+00-1.000E+00-1.000E+00-1.000E+00
1    144               96-1.000E+00-1.000E+00-1.000E+00-1.000E+00
1                      102-1.000E+00-1.000E+00-1.000E+00-1.000E+00
1                      108-1.000E+00-1.000E+00-1.000E+00-1.000E+00
1                      114-1.000E+00-1.000E+00-1.000E+00-1.000E+00
1                124    120-1.000E+00-1.000E+00-1.000E+00-1.000E+00
1                      126-1.000E+00-1.000E+00-1.000E+00-1.000E+00
1                      90-1.000E+00-1.000E+00-1.000E+00-1.000E+00
1                       8
1                       14
1
1    45    51    52    26
1                       3
1    14    14    15    15
1                21    21
1    26    22    33    27
1    3           4      4
1    9     15    16    10
1    15          22    16
1    21    27    28    22
1    27    33    34    28
1    4     10    11    5
1    10    16    17    11
1    16    22    23    17
1          24    22    23
1    28    34    35    29
1                       6
1                       12
1          11          18
1                       24
```

97

1	29		56	30
1	43			44
1	42	43	44	50
1	55	42		56
1	61	55		
1				
1	44	38		45
1	50	44	45	51
1	56	50	51	57
1	62	56	57	63
1	68	62	58	69
1	45		40	46
1	51	45	46	52
1	57	51	52	58
1	63	57	58	64
1	62		64	72
1	46	40	41	47
1			47	53
1	58		53	59
1	64	56	59	65
1				
1	47			48
1				54
1				
1				
1				
1			98	
1				
1				
1				
1				
1				93
1				
1				88
1				94
1				100
1	105	111	112	106
1	111	117	119	112
1	117		124	118
1	123			124
1	34		77	35
1	76	82	83	77
1	92		89	83
1	88	94	95	89
1	94	100	101	95
1	130			101
1	106	112	113	107
1	112	118	119	113
1	118	124	115	119
1				125
1				
1			44	78

1	33	65		84
1	42	45	45	90
1	48	111	120	96
1	101	117	113	102
1	107	113	124	108
1	113	117	117	114
1	117	115	115	115
1	123	71	72	126
1	127	7	10	128
1	133	127	128	133
1	137	132	133	138
1	142	137	138	143
1	147	142	143	148
1	152	147	148	153
1	157	152	153	158
1	162	157	158	163
1	167	162	163	168
1	43	167	178	48
1	104	11	18	129
1	133	128	129	134
1	138	133	134	139
1	143	138	139	144
1	148	143	144	149
1	153	147	148	154
1	158	153	154	159
1	163	158	159	164
1	168	163	164	169
1	44	165	175	54
1	120	133	144	132
1	134	134	135	138
1	139	134	135	143
1	144	143	144	148
1	147	147	148	153
1	154	152	153	158
1	154	157	158	163
1	159	164	165	168
1	54	164	174	72
1	136	138	139	138
1	138	139	140	141
1	147	144	145	146
1	173	148	149	151
1	158	153	154	156
1	163	158	159	161
1	168	163	164	166
1	173	168	130	171
1	45	173	55	78
1	135	135	44	84
1	141	141	44	90
1	147	141	47	96
1	151	146	96	102
1	155	151	102	108
1	161	156	108	114
1	165	161	114	120
1	171	166	120	126
1	66	171	156	72

C.   FLUMAS PRE-PROCESSOR DATA

```
FLUMAS DATA FOR SPHERICAL SHELL QUARTER MODEL
sph.flu sph.geo sph.nom sph.daa $ FLUNAM GEONAM GRDNAM DAANAM
T T F T                         $ PRTGMT PRTTRN PRTAMF CALCAM
T F F T                         $ EIGMAF TWODIM HAFMOD QUAMOD
F F T T                         $ PCHCDS NASTAM STOMAS STOINV
F F F F                         $ FRWTFL FRWTGE FRWTGR FRESUR
F T F F                         $ RENUMB STOGMT ROTGEO ROTQUA
F F T F                         $ PRTCOE STRMAS SPHERE ROTSYM
F F F F                         $ OCTMOD CAVFLU FRWTFV EFUDGE
DYNA                            $ MAINKY
0 171 0 150                     $ NSTRC  NSTRF  NGEN   NGENF
0 0 0                           $ NBRA   NCYL   NCAV
1. 1.                           $ RHO    CEE
10                              $ NVEC
1. 1. 1. 1.                     $ CQ(1)  CQ(2)  CQ(3)  CQ(4)
1                               $ NSRADI
1. 1. 1 150 1                   $ RAD1   RAD2   JBEG   JEND   JINC
0                               $ NSORDR
1.                              $ SPHRAD
```

D.   AUGMAT PRE-PROCESSOR DATA

```
AUGMAT DATA FOR SPHERICAL SHELL QUARTER MODEL
sph.nom sph.flu sph.geo sph.pre  $ STRNAM FLUNAM GEONAM PRENAM
F F F F                          $ FRWTGE FRWTST FRWTFL PLNWAV
F F T T                          $ FLUSKY DAAFRM SYMCON DOFTAB
F F F T                          $ PRTGMT PRTTRN PRTSTF PRTAUG
F F F                            $ MODTRN STRLCL INTWAT
DYNA                             $ MAINKY
1.                               $ DAA2
171 513 3 3                      $ NSTR   NSFR   NFRE   NFTR
1                                $ NSETLC
0 1 150 1                        $ NDICOS JSTART JSTOP  JINC
4                                $ NUMCON
1    1 121   6                   $ ICON   NSTART NSTOP  NINC
2    1   6   1                   $ ICON   NSTART NSTOP  NINC
2   37  42   1                   $ ICON   NSTART NSTOP  NINC
2  127 167   5                   $ ICON   NSTART NSTOP  NINC
```

E.   TIMINT PRE-PROCESSOR INPUT DATA

```
TIMINT DATA FOR SPHERICAL SHELL QUARTER MODEL
sph.pre sph.pos $ PRENAM POSNAM
sph.rst         $ RESNAM
0. 0.  10000.   $ XC      YC      ZC
 0. 0. 1.       $ SX      SY      SZ
F F F F         $ EXPWAV SPLINE VARLIN PACKET
F F F F         $ HYPERB BUBPUL REFSEC EXPLOS
2               $ JPHIST
1. 0.           $ PNORM
50.             $ DTHIST
1.E-6 1.E-6     $ PHIST
1 0             $ NTINT   NCHGAL
0. .00025       $ STRTIM DELTIM
1000 1000       $ NSAVER NRESET NSODFL
0 0 0 0         $ LOCBEG LOCRES LOCWRT NSTART
F               $ DISPLA
```

APPENDIX B - INFINITE CYLINDER VALIDATION INPUT DATA

A. INGRID PRE-PROCESSOR INPUT DATA

INFINITE CYLINDER MODEL

```
dn3d vec term 5.0 plti 0.01 prti 1000.

mat 1 type 1 e 9.813e+1 pr 0.3 ro 7.85
    shell quad 0 thick 0.010 endmat

lcd 1 2 0.0 0.0 10.0 0.0
lcd 2 2 0.0 0.000025 10.0 0.000025

plan 3

 0 0   0      0 -1  0  0.00001  symm
 0 0 -.0005    0  0 -1  0.001   symm
 0 0  .0005    0  0  1  0.001   symm

start
 -1   6   -11 ;
 -1   6   -11 ;
  1 2 ;
 -1.  0.  1.
 -1.  0.  1.
 -.0005   .0005
 a 1 1 0 3 3 0 3 1.0
 d 0 1 0 0 2 0
 pri -1 -3 ; -1 -3 ; ; 1 -1.0 0. 0. 0.
 mate 1
end

end
```

104

```
INFINITE CYLINDER MODEL                                                    88 large
    1       42                        0          20        0                 0
    0       0         0         0
            0         0        e20.9                     20
    2    0   2.      0          0     0     0     0     0     0     0     0   0   0
 5.000E+00 1.000E+00 1.000E-02               0.000E+00 0.000E+00      0      0.000E+00
    0       0         0         0         2     0     0     1     0         0     0     0     0
    0       0 0.000E+00
    0       0         0
    1    10.8500E+00       0     00.0000E+00      00.0000E+000.0000E+00      2     0     0
material type # 1  (elastic)
 9.813E+01 0.000E+00 0.000E+00 0.000E+00 0.000E+00 0.000E+00 0.000E+00 0.000E+00
 3.000E-01 0.000E+00 0.000E+00 0.000E+00 0.000E+00 0.000E+00 0.000E+00 0.000E+00
 0.000E+00 0.000E+00 0.000E+00 0.000E+00 0.000E+00 0.000E+00 0.000E+00 0.000E+00
 0.000E+00 0.000E+00 0.000E+00 0.000E+00 0.000E+00 0.000E+00 0.000E+00 0.000E+00
 0.000E+00 0.000E+00 0.000E+00 0.000E+00 0.000E+00 0.000E+00 0.000E+00 0.000E+00
 0.000E+00 0.000E+00 0.000E+00 0.000E+00 0.000E+00 0.000E+00 0.000E+00 0.000E+00
section properties
                 0
 1.000E-00 1.000E-01 1.000E-02 1.000E-02 0.000E+00                   .
     1     5.  -.1    .1  .0000000E-01   .0000000000000E+00 -.5000000237487E-03     7.
     2     5.  -.9876883625984E+00   .1564344763756E+00 -.5000000237487E-03     4.
     3     5.  -.9510565400124E+00   .3090170323849E+00 -.5000000237487E-03     4.
     4     5.  -.8910065488491E+00   .4539905488491E+00 -.5000000237487E-03     4.
     5     3.  -.8090170235840E+00   .5877853035927E+00 -.5000000237487E-03     4.
     6     3.  -.7071068286846E+00   .7071068286846E+00 -.5000000237487E-03     4.
     7     5.   .0000000000036E+00   .0000000000036E+00 -.5000000237487E-03     7.
     8     5.  -.9876883625984E+00   .1564344763756E+00  .5000000237487E-03     4.
     9     5.  -.9510565400124E+00   .3090170323849E+00  .5000000237487E-03     4.
    10     3.  -.8910065488491E+00   .4539905488491E+00  .5000000237487E-03     4.
    11     3.  -.8090170235840E+00   .5877853035927E+00  .5000000237487E-03     4.
    12     3.  -.7071068286846E+00   .7071068286846E+00  .5000000237487E-03     4.
    13     5.  -.5877853035927E+00   .8090170621872E+00 -.5000000237487E-03     4.
    14     3.  -.4539905488491E+00   .8910065485435E+00 -.5000000237487E-03     4.
    15     3.  -.3090170323849E+00   .9510565400124E+00 -.5000000237487E-03     4.
    16     3.  -.1564344763756E+00   .9876883541414E+00 -.5000000237487E-03     4.
    17     5.   .0000000000000E+00   .1000000000000E+01 -.5000000237487E-03     4.
    18     3.  -.5877853035927E+00   .8090170621872E+00  .5000000237487E-03     4.
    19     3.  -.4539905488491E+00   .8910065485435E+00  .5000000237487E-03     4.
    20     3.  -.3090170323849E+00   .9510565400124E+00  .5000000237487E-03     4.
    21     3.  -.1564344763756E+00   .9876883541414E+00  .5000000237487E-03     4.
    22     3.   .0000000000000E+00   .1000000000000E+01  .5000000237487E-03     4.
    23     3.   .1564344763756E+00   .9876883625984E+00 -.5000000237487E-03     4.
    24     3.   .3090170323849E+00   .9510565400124E+00 -.5000000237487E-03     4.
    25     3.   .4539905488491E+00   .8910065293331E+00 -.5000000237487E-03     4.
    26     3.   .5877853035927E+00   .8090170025826E+00 -.5000000237487E-03     4.
    27     5.   .7071068286846E+00   .7071068286846E+00 -.5000000237487E-03     4.
    28     3.   .1564344763756E+00   .9876883625984E+00  .5000000237487E-03     4.
    29     3.   .3090170323849E+00   .9510565400124E+00  .5000000237487E-03     4.
    30     3.   .4539905488491E+00   .8910065293331E+00  .5000000237487E-03     4.
    31     3.   .5877853035927E+00   .8090170025826E+00  .5000000237487E-03     4.
    32     3.   .7071068286846E+00   .7071068286846E+00  .5000000237487E-03     4.
    33     5.   .0000000000000E+01   .0000000000000E+00 -.5000000237487E-03     7.
    34     3.   .9876883625984E+00   .1564344763756E+00 -.5000000237487E-03     4.
    35     3.   .9510565400124E+00   .3090170323849E+00 -.5000000237487E-03     4.
    36     3.   .8910065293331E+00   .4539905488491E+00 -.5000000237487E-03     4.
    37     3.   .8090170025826E+00   .5877853035927E+00 -.5000000237487E-03     4.
    38     5.   .1000000000000E+01   .0000000000000E+00  .5000000237487E-03     7.
    39     3.   .9876883625984E+00   .1564344763756E+00  .5000000237487E-03     4.
    40     3.   .9510565400124E+00   .3090170323849E+00  .5000000237487E-03     4.
    41     3.   .8910065293331E+00   .4539905488491E+00  .5000000237487E-03     4.
    42     3.   .8090170025826E+00   .5877853035927E+00  .5000000237487E-03     4.
     1       1         1         7         8         2
 1.000E+00 1.000E-01     .  .  E-   1.000E-02
         0         1        20         4         5         3
```

105

```
1.000E-02 1.000E-02 1.000E-02 1.000E-02
      3       1       8       9      10       4
1.000E-02 1.000E-02 1.000E-02 1.000E-02
      4       1       9      10      11       5
1.000E-02 1.000E-02 1.000E-02 1.000E-02
      5       1      10      11      12       6
1.000E-02 1.000E-02 1.000E-02 1.000E-02
      6       1       6      12      18      13
1.000E-02 1.000E-02 1.000E-02 1.000E-02
      7       1      13      18      19      14
1.000E-02 1.000E-02 1.000E-02 1.000E-02
      8       1      14      19      20      15
1.000E-02 1.000E-02 1.000E-02 1.000E-02
      9       1      15      20      21      16
1.000E-02 1.000E-02 1.000E-02 1.000E-02
     10       1      16      21      22      17
1.000E-02 1.000E-02 1.000E-02 1.000E-02
     11       1      17      22      28      23
1.000E-02 1.000E-02 1.000E-02 1.000E-02
     12       1      23      28      29      24
1.000E-02 1.000E-02 1.000E-02 1.000E-02
     13       1      24      29      30      25
1.000E-02 1.000E-02 1.000E-02 1.000E-02
     14       1      25      30      31      26
1.000E-02 1.000E-02 1.000E-02 1.000E-02
     15       1      26      31      32      27
1.000E-02 1.000E-02 1.000E-02 1.000E-02
     16       1      33      38      39      34
1.000E-02 1.000E-02 1.000E-02 1.000E-02
     17       1      34      39      40      35
1.000E-02 1.000E-02 1.000E-02 1.000E-02
     18       1      35      40      41      36
1.000E-02 1.000E-02 1.000E-02 1.000E-02
     19       1      36      41      42      37
1.000E-02 1.000E-02 1.000E-02 1.000E-02
     20       1      37      42      32      37
1.000E-02 1.000E-02 1.000E-02 1.000E-02
*
*----------------------- LOAD CURVE DEFINITIONS ------------------------*
*
      1       2
0.000E+00 0.000E+00
1.000E+01 0.000E+00
      2       2
0.000E+00 0.000E+00
1.000E+01 0.000E+00
*
*---------------- PRESSURE BOUNDARY CONDITION CARDS ----------------*
*
      1       1       7       8       2-1.000E+00-1.000E+00-1.000E+00-1.000E+00
      1       2       8       9       3-1.000E+00-1.000E+00-1.000E+00-1.000E+00
      1       3       9      10       4-1.000E+00-1.000E+00-1.000E+00-1.000E+00
      1       4      10      11       5-1.000E+00-1.000E+00-1.000E+00-1.000E+00
      1       5      11      12       6-1.000E+00-1.000E+00-1.000E+00-1.000E+00
      1       6      12      18      13-1.000E+00-1.000E+00-1.000E+00-1.000E+00
      1      13      18      19      14-1.000E+00-1.000E+00-1.000E+00-1.000E+00
      1      14      19      20      15-1.000E+00-1.000E+00-1.000E+00-1.000E+00
      1      15      20      21      16-1.000E+00-1.000E+00-1.000E+00-1.000E+00
      1      16      21      22      17-1.000E+00-1.000E+00-1.000E+00-1.000E+00
      1      17      22      28      23-1.000E+00-1.000E+00-1.000E+00-1.000E+00
      1      23      28      29      24-1.000E+00-1.000E+00-1.000E+00-1.000E+00
      1      24      29      30      25-1.000E+00-1.000E+00-1.000E+00-1.000E+00
      1      25      30      31      26-1.000E+00-1.000E+00-1.000E+00-1.000E+00
      1      26      31      32      27-1.000E+00-1.000E+00-1.000E+00-1.000E+00
      1      38      33      34      39-1.000E+00-1.000E+00-1.000E+00-1.000E+00
      1      39       4      35      40-1.000E+00-1.000E+00-1.000E+00-1.000E+00
      1       4      35      36      41-1.000E+00-1.000E+00-1.000E+00-1.000E+00
      1      41      36      37      42-1.000E+00-1.000E+00-1.000E+00-1.000E+00
```

106

```
1      42     37     27     32-1.000E+00-1.000E+00-1.000E+00-1.000E+00
1       1      2      1      2
1       2      3      3      3
1       3      4      4      4
1       4      5      5      5
1       5      6      6      6
1       6     12     13     13
1      13     18     19     14
1      14     19     20     15
1      15     20     21     16
1      16     21     22     17
1      17     22     28     23
1      23     28     29     24
1      24     29     30     25
1      25     30     31     26
1      26     31     32     27
1      38     33     34     39
1      39     34     35     40
1      40     35     36     41
1      41     36     37     42
1      42     37     37     32
```

C.   FLUMAS PRE-PROCESSOR INPUT DATA

```
FLUMAS DATA FOR INFINITE CYLINDER MODEL
cyl.flu cyl.geo cyl.nom  cyl.daa $ FLUNAM GEONAM GRDNAM DAANAM
T T T T                         $ PRTGMT PRTTRN PRTAMF CALCAM
T T T F                         $ EIGMAF TWODIM HAFMOD QUAMOD
F F T T                         $ PCHCDS NASTAM STOMAS STOINV
F F F F                         $ FRWTFL FRWTGE FRWTGR FRESUR
F T F F                         $ RENUMB STOGMT ROTGEO ROTQUA
F F F F                         $ PRTCOE STRMAS SPHERE ROTSYM
F F F F                         $ OCTMOD CAVFLU FRWTFV EFUDGE
DYNA                            $ MAINKY
0 42 0 20                       $ NSTRC  NSTRF  NGEN   NGENF
0 0 0                           $ NBRA   NCYL   NCAV
1. 1.                           $ RHO    CEE
10                              $ NVEC
1. 1.                           $ CQ(1)  CQ(2)
0.  0. -1.  0.                  $ DHALF  CXHF   CYHF   CZHF
1                               $ NSRADI
0. 1.  1   20 1               $ RAD1   RAD2   JBEG   JEND   JINC
1                               $ NSORDR
1  1   20  1                    $ NORD   JBEG   JEND   JINC
```

D.   AUGMAT PRE-PROCESSOR DATA

```
AUGMAT DATA FOR INFINITE CYLINDER MODEL
cyl.nom cyl.flu cyl.geo cyl.pre $ STRNAM FLUNAM GEONAM PRENAM
F F F F                         $ FRWTGE FRWTST FRWTFL PLNWAV
F F T T                         $ FLUSKY DAAFRM SYMCON DOFTAB
T T F T                         $ PRTGMT PRTTRN PRTSTF PRTAUG
F F F                           $ MOCTRN STRLCL INTWAT
DYNA                            $ MAINKY
0.75                            $ DAA2
42 126 3 3                      $ NSTR   NSFR   NFRE   NFTR
1                               $ NSETLC
0 1 20 1                        $ NDICOS JSTART JSTOP JINC
2                               $ NUMCON
2  1   7   6                    $ ICON   NSTART NSTOP NINC
2 33  38   5                    $ ICON   NSTART NSTOP NINC
```

E.   TIMINT PRE-PROCESSOR DATA

```
TIME INTEGRATION DATA FOR INFINITE CYLINDER MODEL
cyl.pre cyl.pos              $ PRENAM POSNAM
cyl.rst                      $ RESNAM
10000.     0.0000  0.000000  $ XC      YC       ZC
1.0000     0.0000  0.000000  $ SX      SY       SZ
F F F F                      $ EXPWAV SPLINE  VARLIN  PACKET
F F F F                      $ HYPERB BUBPUL  REFSEC  EXPLOS
2                            $ JPHIST
1. 0.                        $ PNORM   HYDPRE
50.                          $ DTHIST
1.e-6 1.e-6                  $ PHIST(1) PHIST(2)
1 0                          $ NTINT   NCHGAL
0. 0.00025                   $ STRTIM DELTIM
10000 10000                  $ NSAVER NRESET NSODFL
0 0 0 0                      $ LOCBEG LOCRES LOCWRT NSTART
F                            $ DISPLA
```

110

APPENDIX C - UNDEX TEST REPORT

DYNAMIC TESTING, INC.

DTI-R-TSG
DTI91-183
4 September 1991

United States Naval Postgraduate School
Department of Mechanical Engineering
Monterey, California   93943-5100

Attention: Dr. Young Shin

Subject: Cylinder Test Results, DTI Job No. 131

Enclosure: *(1)*   Instrumentation Time-Histories, Test No. 1
(2)   Instrumentation Time-Histories, Test No. 2
(3)   Test Photographs
(4)   Data Provided in ASCII Format

Gentlemen:

Dynamic Testing, Inc. (DTI), is pleased to provide the following results for the cylinder tests conducted at our facility on 20 and 22 August 1991.

The first test, conducted on Tuesday, 20 August 1991, using a 60-pound HBX cylindrical charge, consisted of one cylinder oriented for an end-on shot with a 28-foot standoff at a depth of 12 feet. There were a total of 7 strain gauges per axis for a total of 14 strain gauges. One free-field pressure gauge was located 28 feet from the charge, but was positioned in such a way that no reflection from the cylinder occurred. There were three pair of strain gauges located in the center of the cylinder, one at B1, B2, and B3. Two pair of strain gauges were located 4.5 inches from each end oriented at A1, A3, C1, and C3. Before the test it was noted that gauge A1C was not working properly, so we oriented the cylinder so that the end, designated C, was toward the blast (see Figure 1).

The strain gauges were oriented to monitor longitudinal and circumferential strains. Predicted analysis indicated a .2 percent strain at 30 feet. No visual damage was observed.

The second test, conducted Thursday, 22 August 1991, using a 60-pound HBX cylindrical charge, consisted of one cylinder oriented for a side shot with a 25-foot standoff at a depth of 12 feet. There were a total of 7 strain gauges per axis for a total of 14 strain gauges. One free-field pressure gauge was located 25 feet from the charge, and positioned so no reflection from the cylinder occurred. There were three pair of strain gauges located in the center of the cylinder, one at B1, B2, and B3. Two pair of strain gauges were located 4.5 inches from each end oriented at A1, A2, C1, and C2 (see above).

The strain gauges were oriented to monitor longitudinal and circumferential strains. Predicted analysis indicated a .48 percent strain at 25 feet. No visual damage was observed.
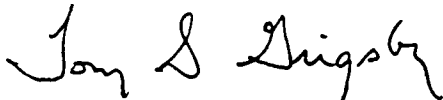
The test configuration consisted of one cylinder being suspended by the crane and one charge suspended from a float (see Figures 2a and 2b for test configurations).

We trust you will find the enclosed satisfactory. It was a pleasure working with you on this project.

If you have any questions or comments, please do not hesitate to contact Mr. Randy Fairfield or the undersigned.

Sincerely,

DYNAMIC TESTING, INC.

Tony S. Grigsby
Instrumentation Technician

TSG:mal

cc: G.G. Amir
      G.D. Snyder
      R.D. Fairfield
      W.G. Lyon
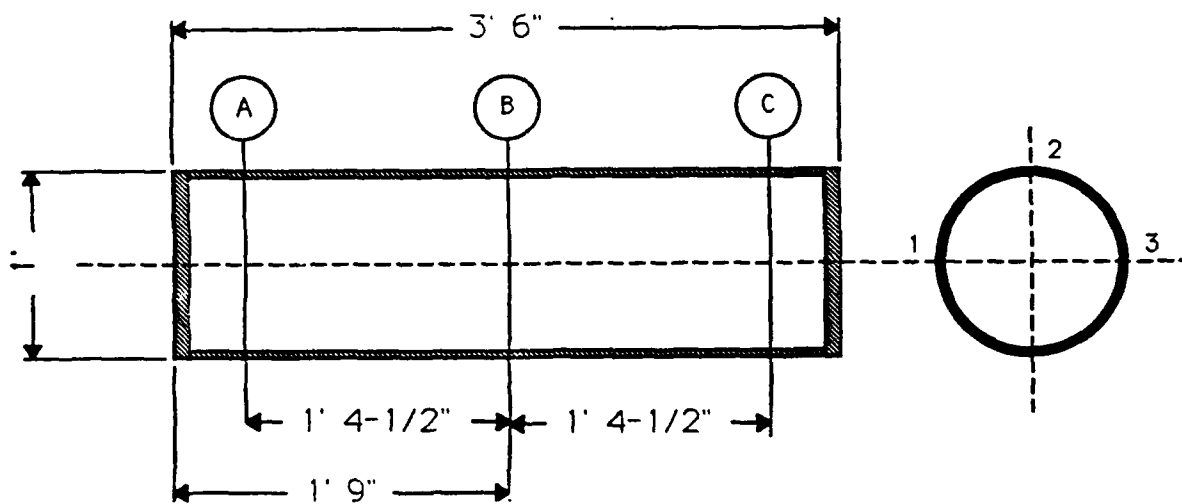
Figure 1. Cylinder Orientation Prior to Test No. 1
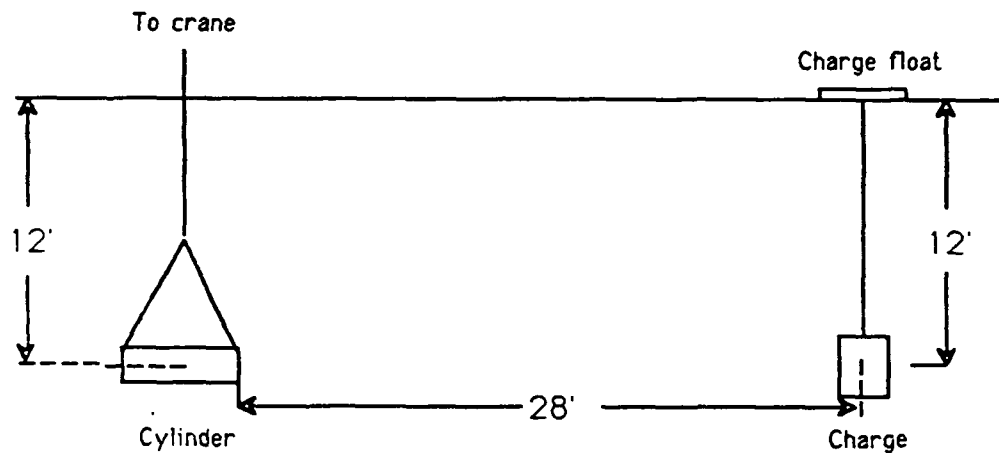
Figure 2a. *Test Configuration for Test No. 1*
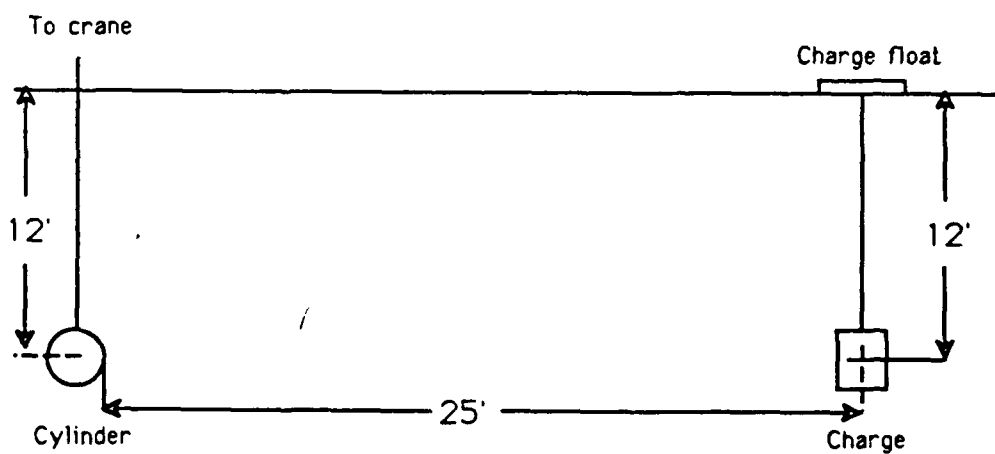
Figure 2b. *Test Configuration for Test No. 2*

Test No. 1

NPS PRECISION UNDEX TESTING
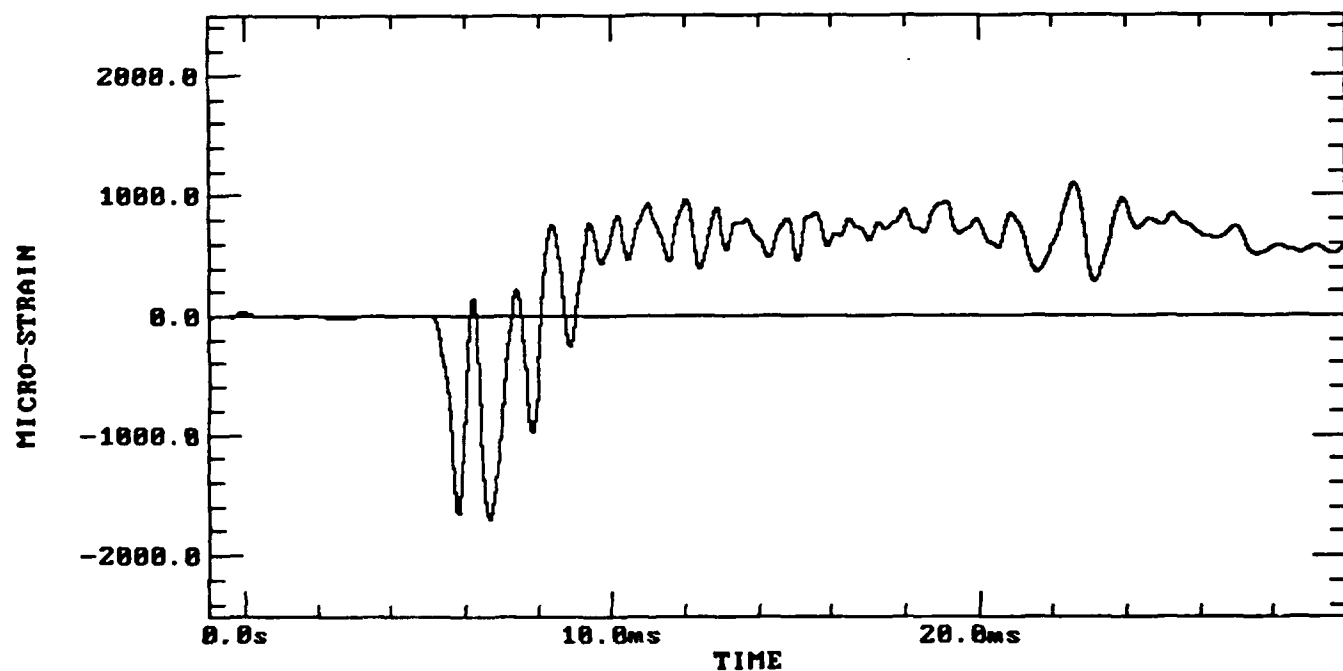
TEST 1

ZERO REPRESENTS DETONATION TIME

TIME HISTORY OF GAUGE A1L

FILTERED AT 2000 HZ LOW PASS

NPS PRECISION UNDEX TESTING

TEST 1

ZERO REPRESENTS DETONATION TIME
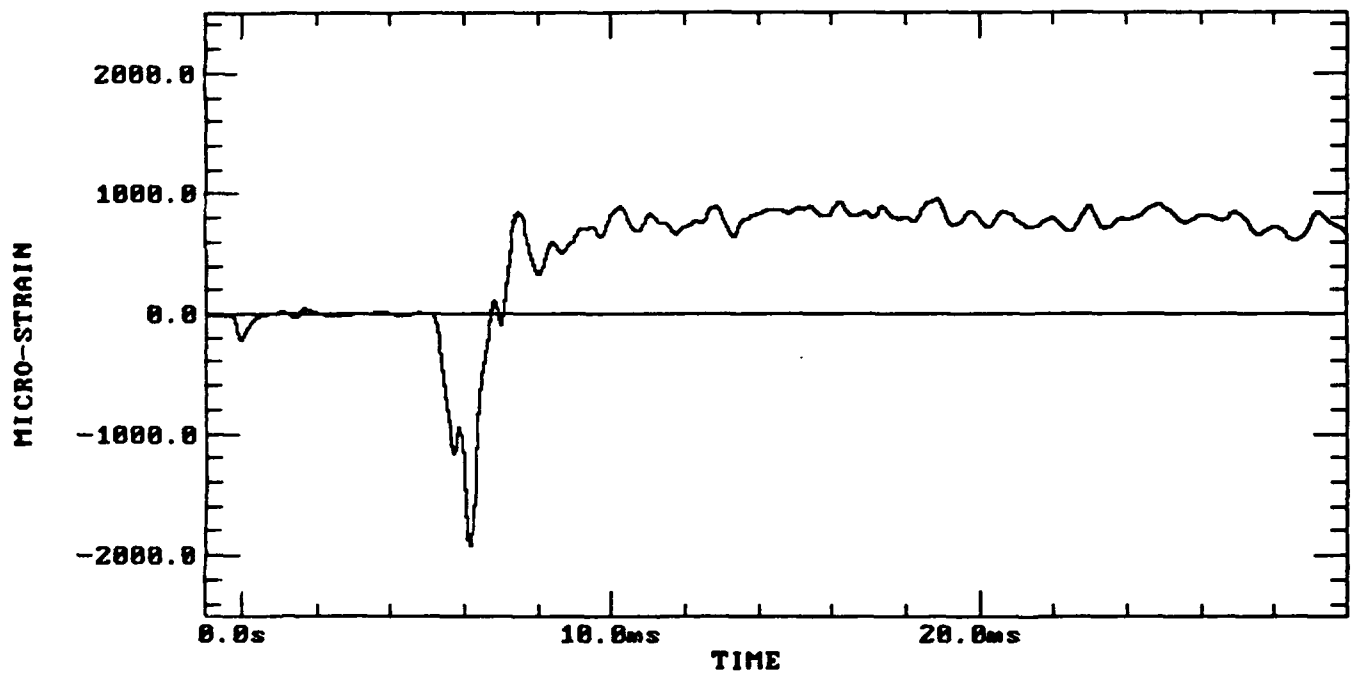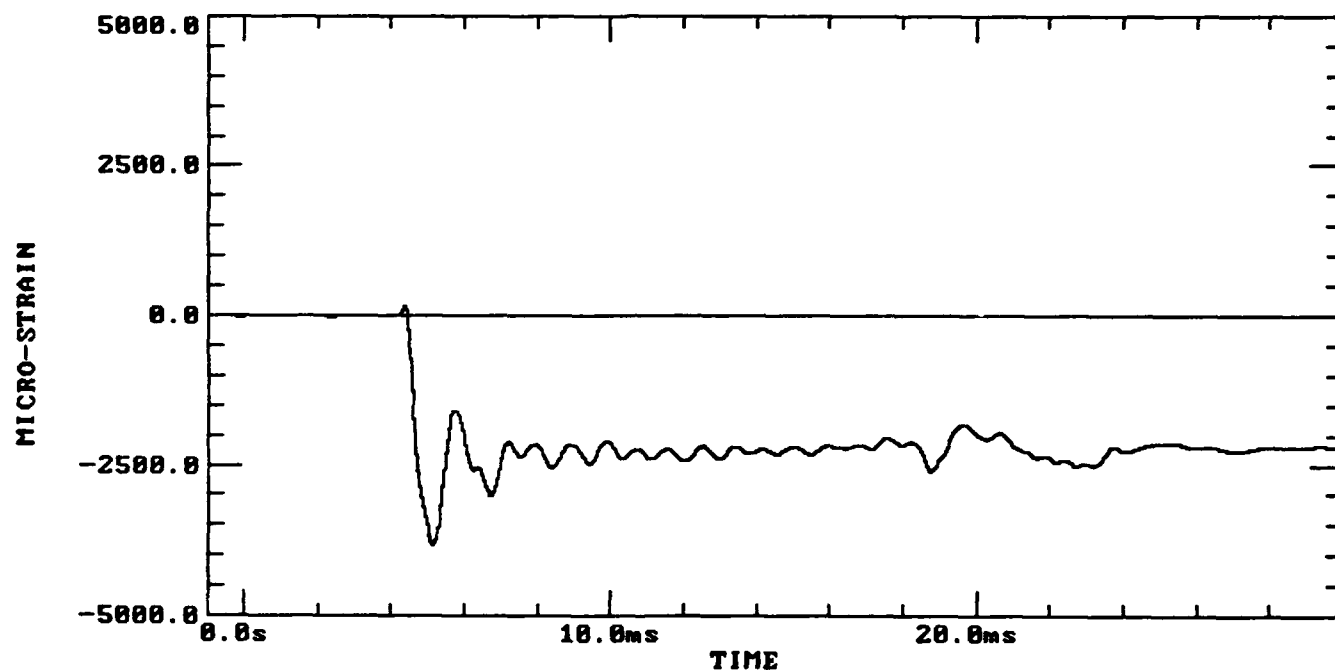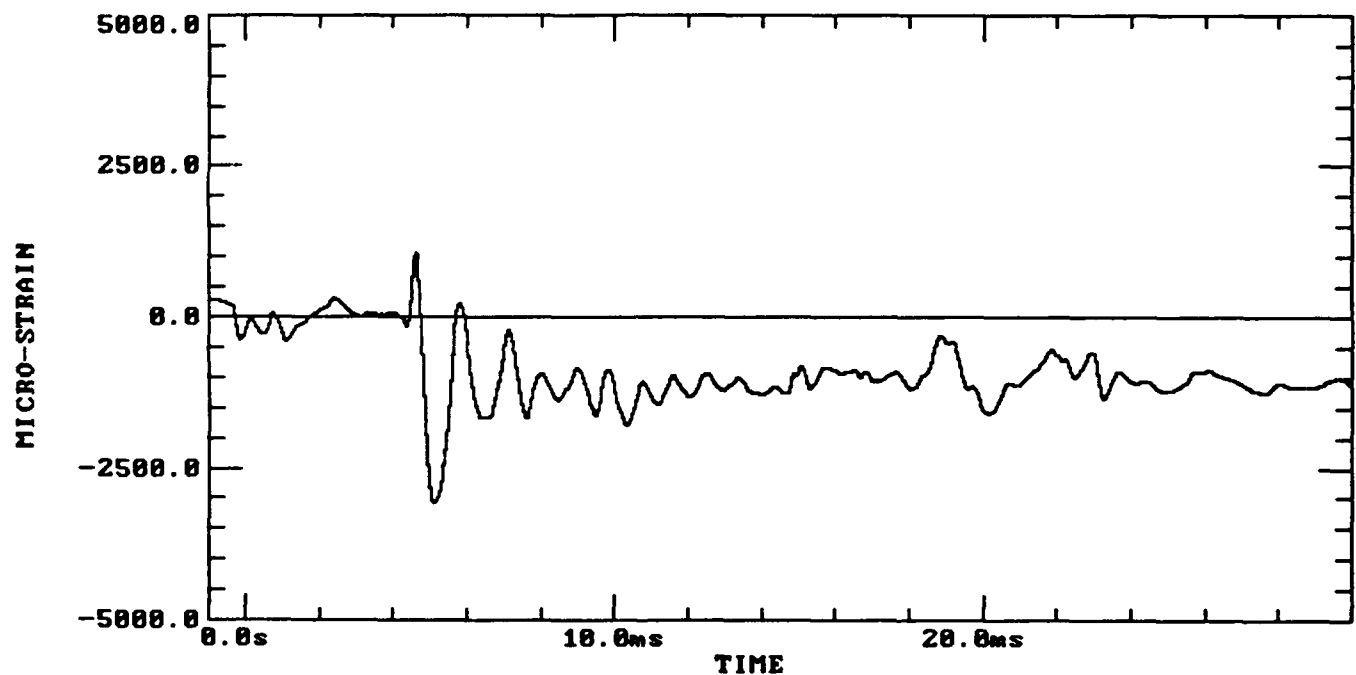

TIME HISTORY OF GAUGE A3L

FILTERED AT 2000 HZ LOW PASS

NPS PRECISION UNDEX TESTING

TEST 1

ZERO REPRESENTS DETONATION TIME
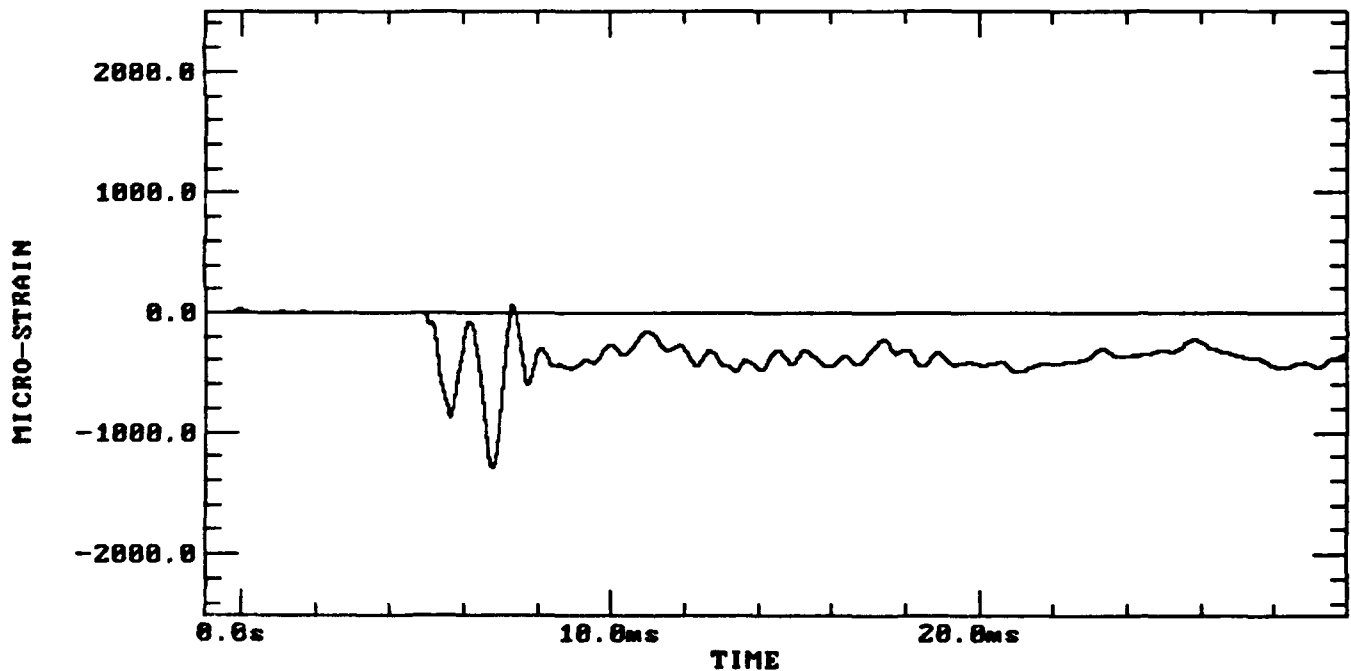
TIME HISTORY OF GAUGE C1L

FILTERED AT 2000 HZ LOW PASS

NPS PRECISION UNDEX TESTING

TEST 1
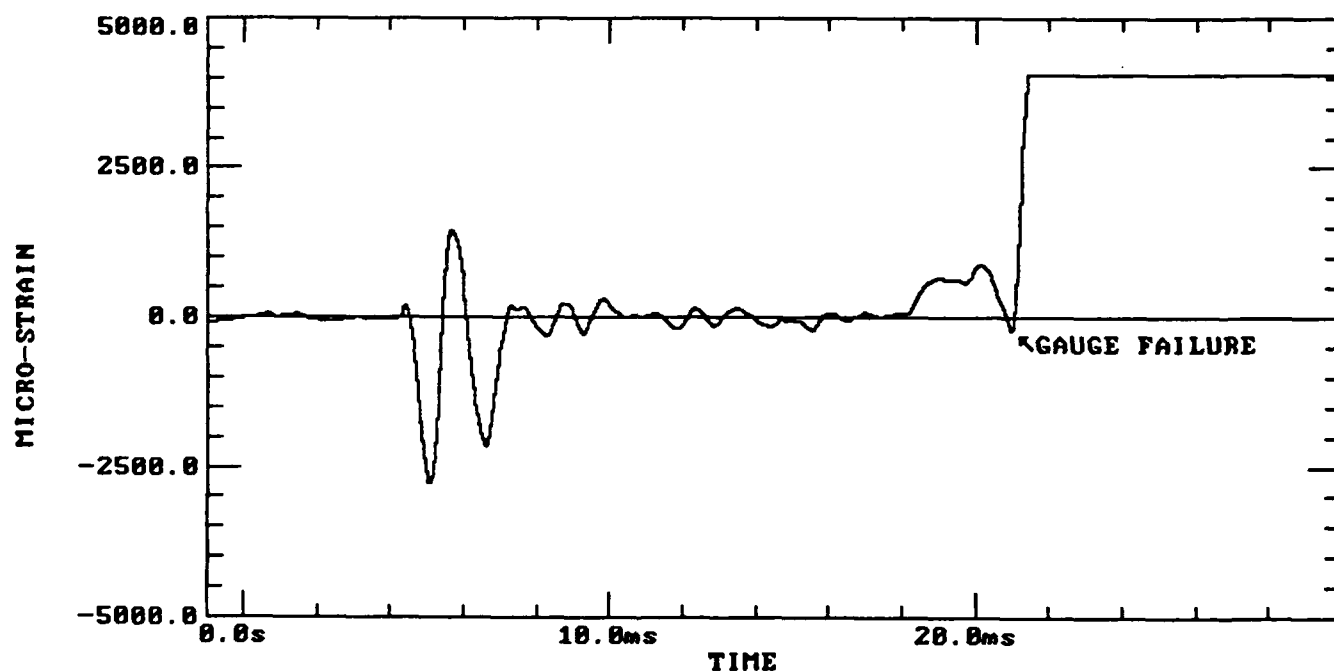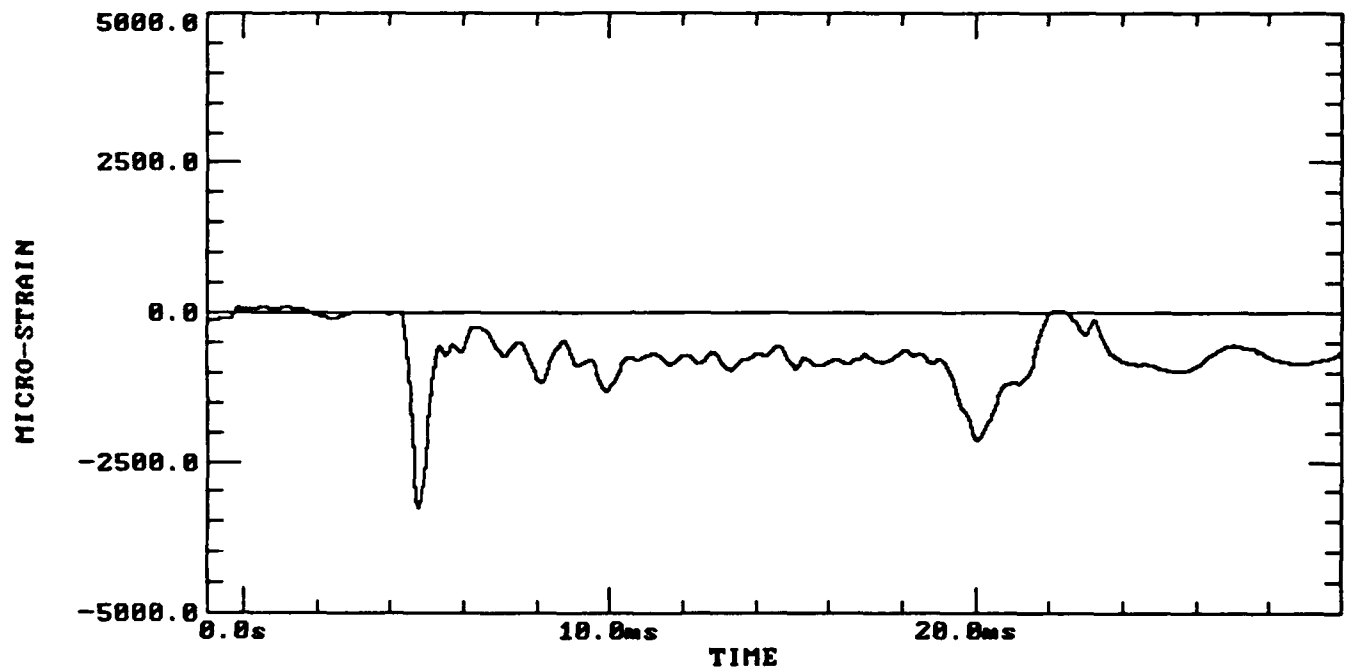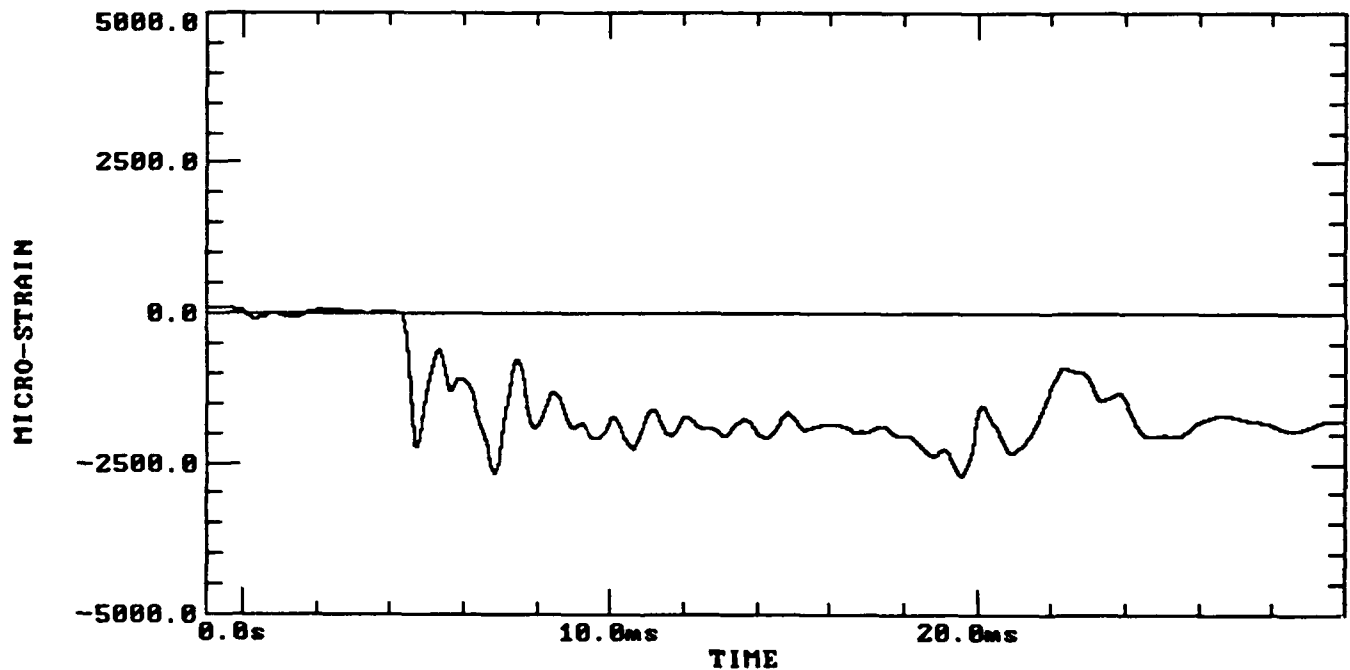
ZERO REPRESENTS DETONATION TIME
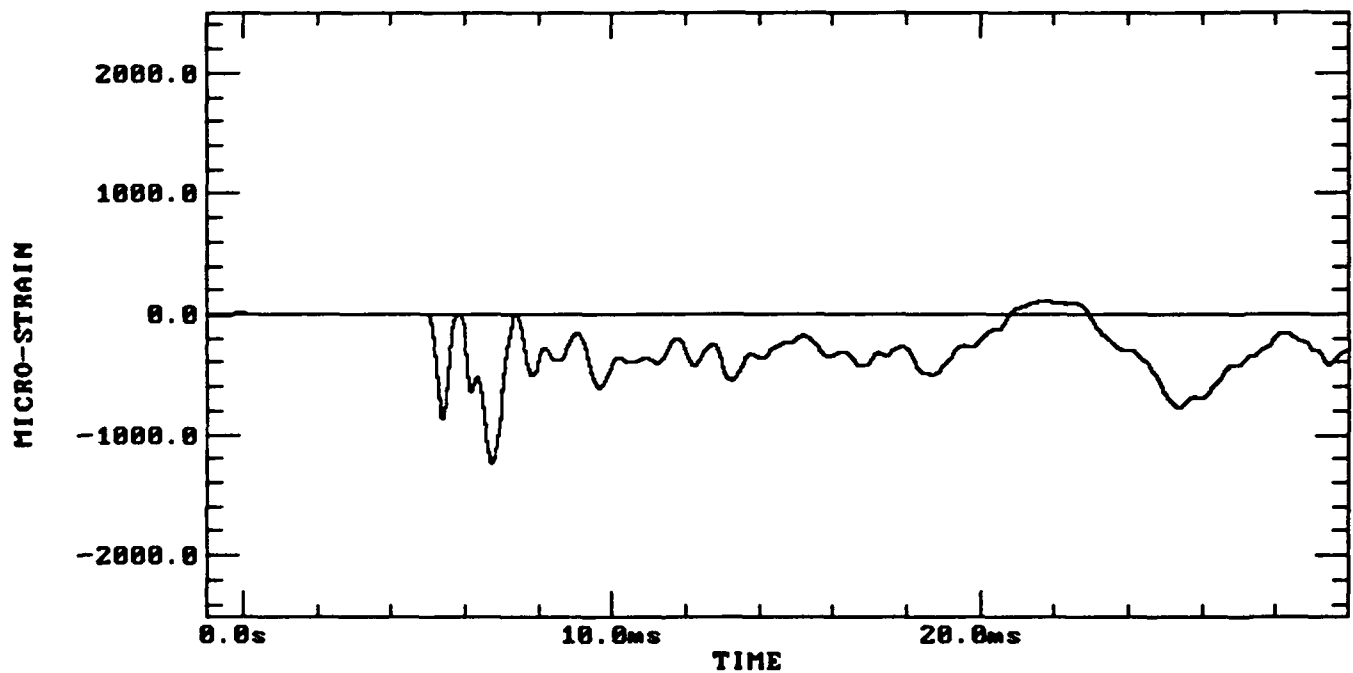
TIME HISTORY OF GAUGE B2L

FILTERED AT 2000 HZ LOW PASS

NPS PRECISION UNDEX TESTING

TEST 1

ZERO REPRESENTS DETONATION TIME
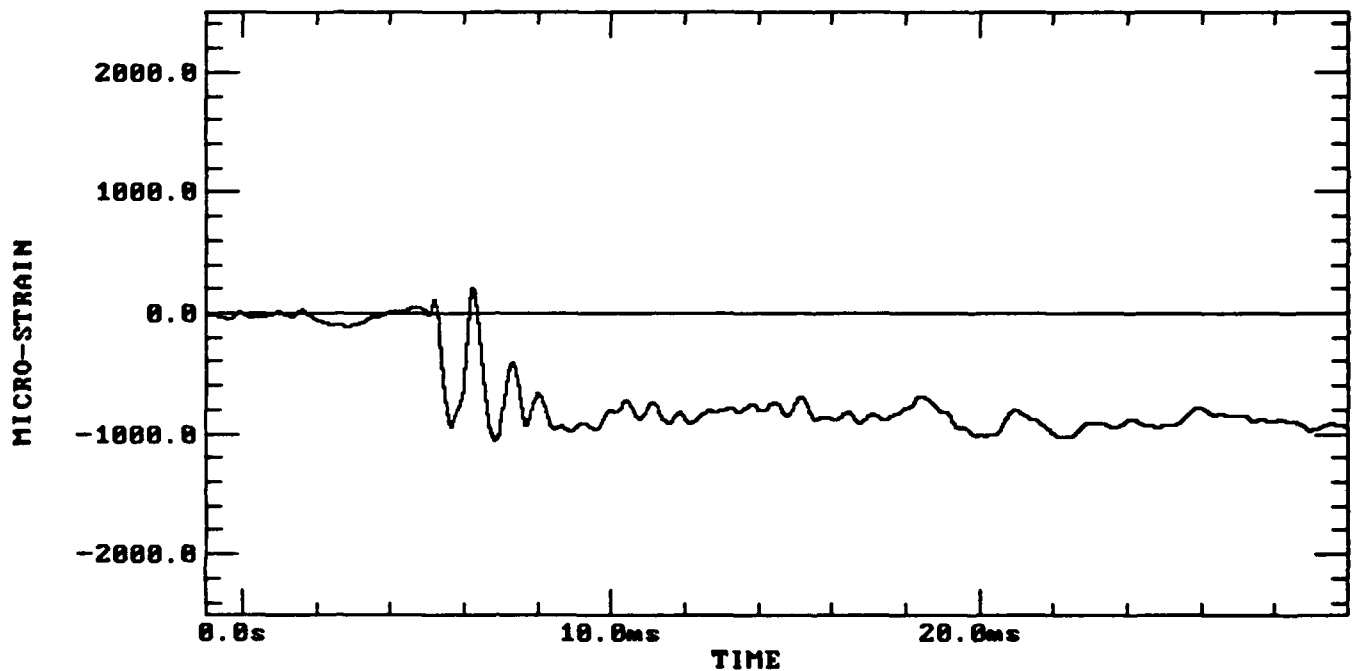
TIME HISTORY OF GAUGE C3L

FILTERED AT 2000 HZ LOW PASS

NPS PRECISION UNDEX TESTING

TEST 1

ZERO REPRESENTS DETONATION TIME
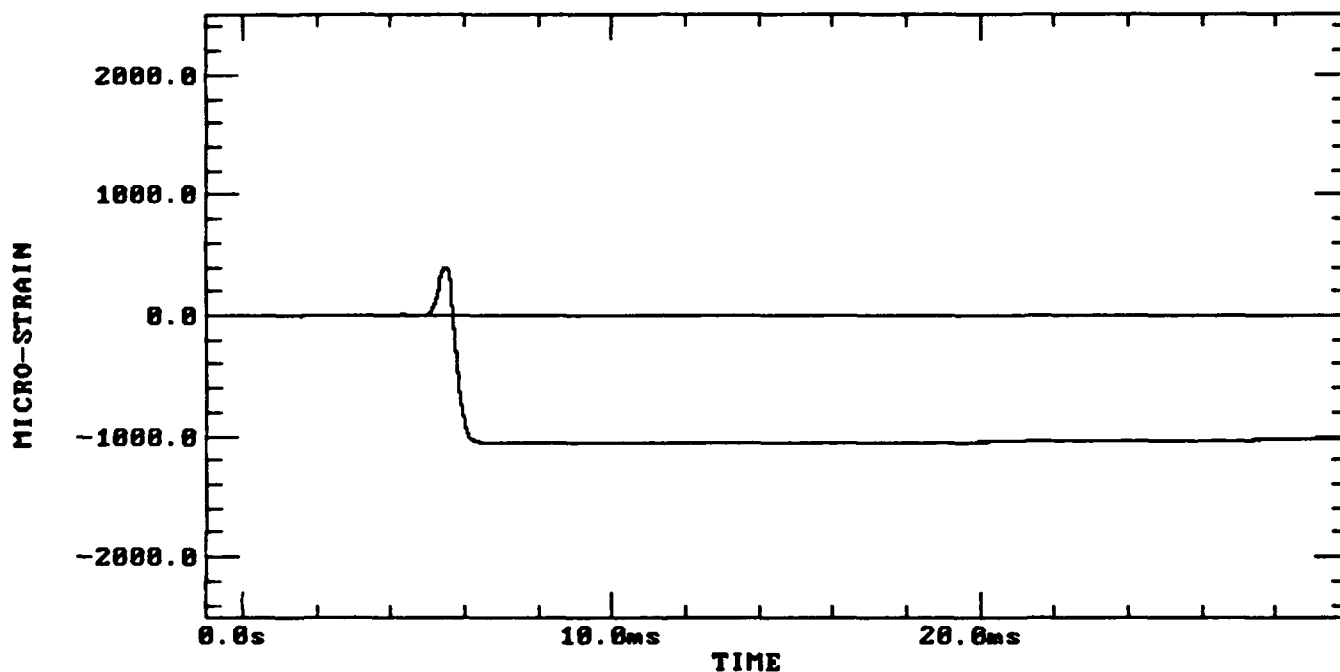
TIME HISTORY OF GAUGE A3C

FILTERED AT 2000 HZ LOW PASS

NPS PRECISION UNDEX TESTING

TEST 1

ZERO REPRESENTS DETONATION TIME

TIME HISTORY OF GAUGE B1C

FILTERED AT 2000 HZ LOW PASS

NPS PRECISION UNDEX TESTING

TEST 1

ZERO REPRESENTS DETONATION TIME

TIME HISTORY OF GAUGE B2C

FILTERED AT 2000 HZ LOW PASS

NPS PRECISION UNDEX TESTING

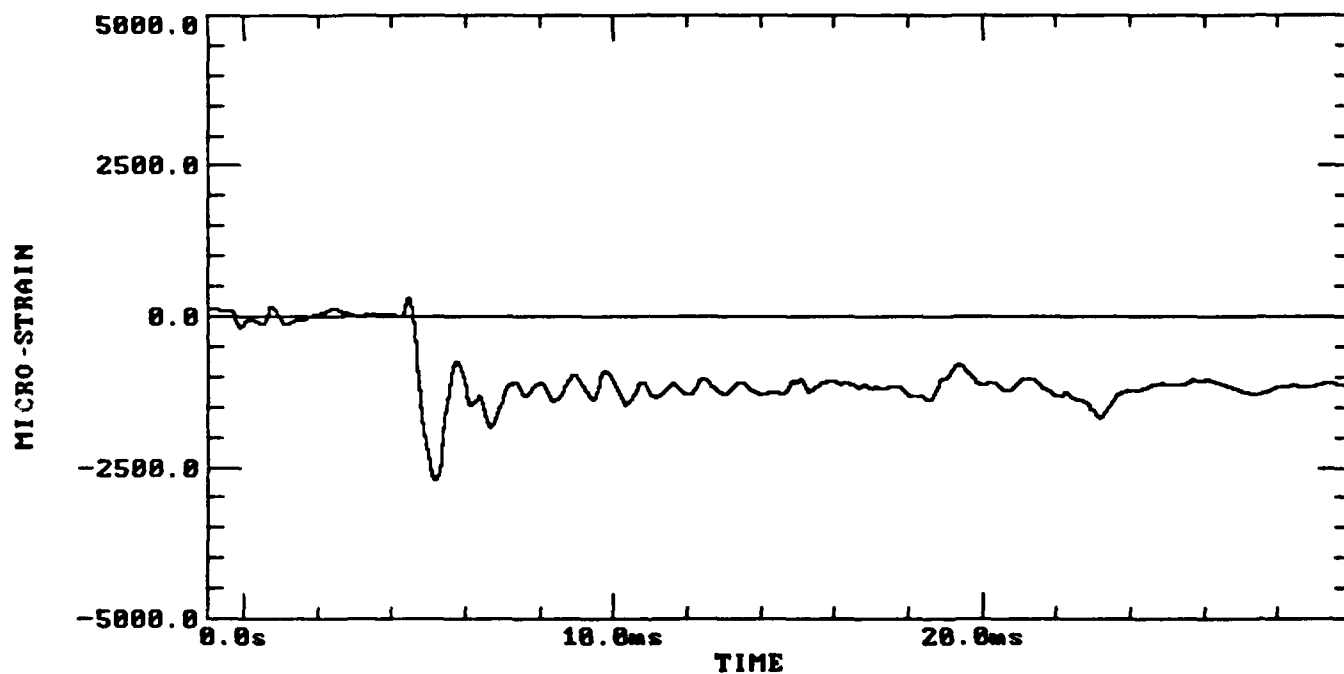**TEST 1**

ZERO REPRESENTS DETONATION TIME
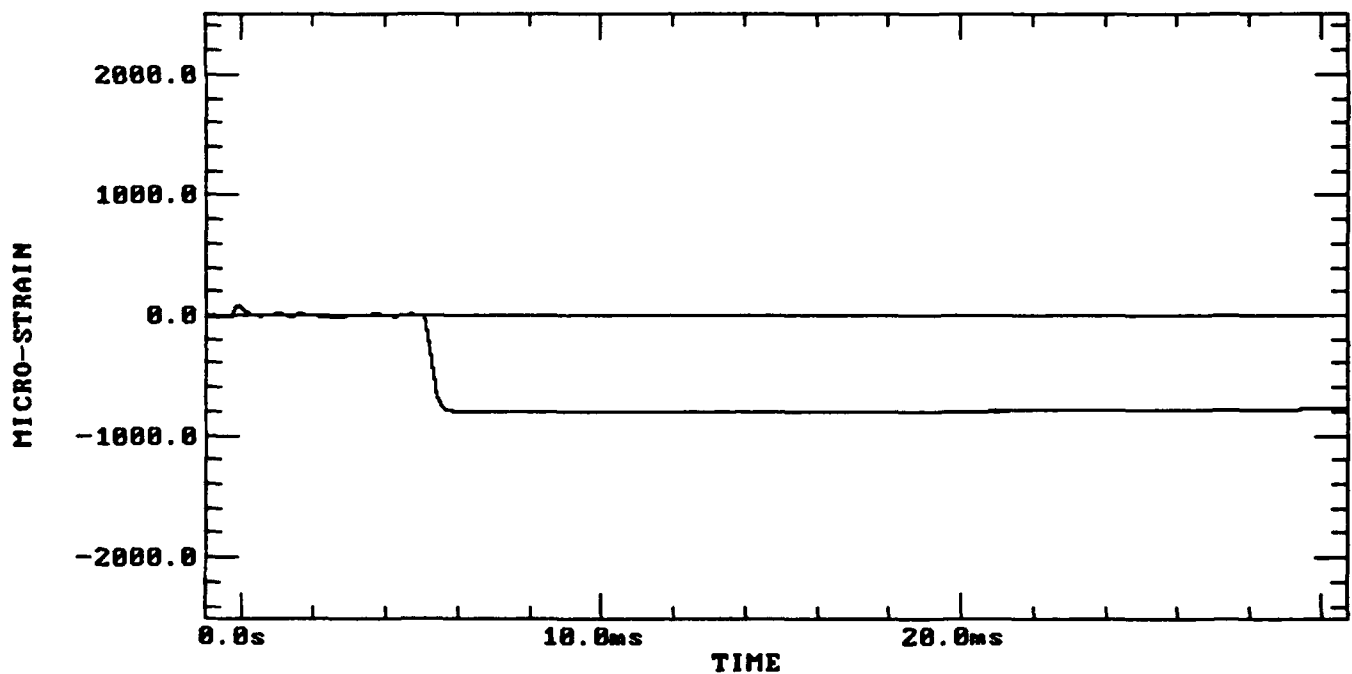
TIME HISTORY OF GAUGE B3C

FILTERED AT 2000 HZ LOW PASS

NPS PRECISION UNDEX TESTING
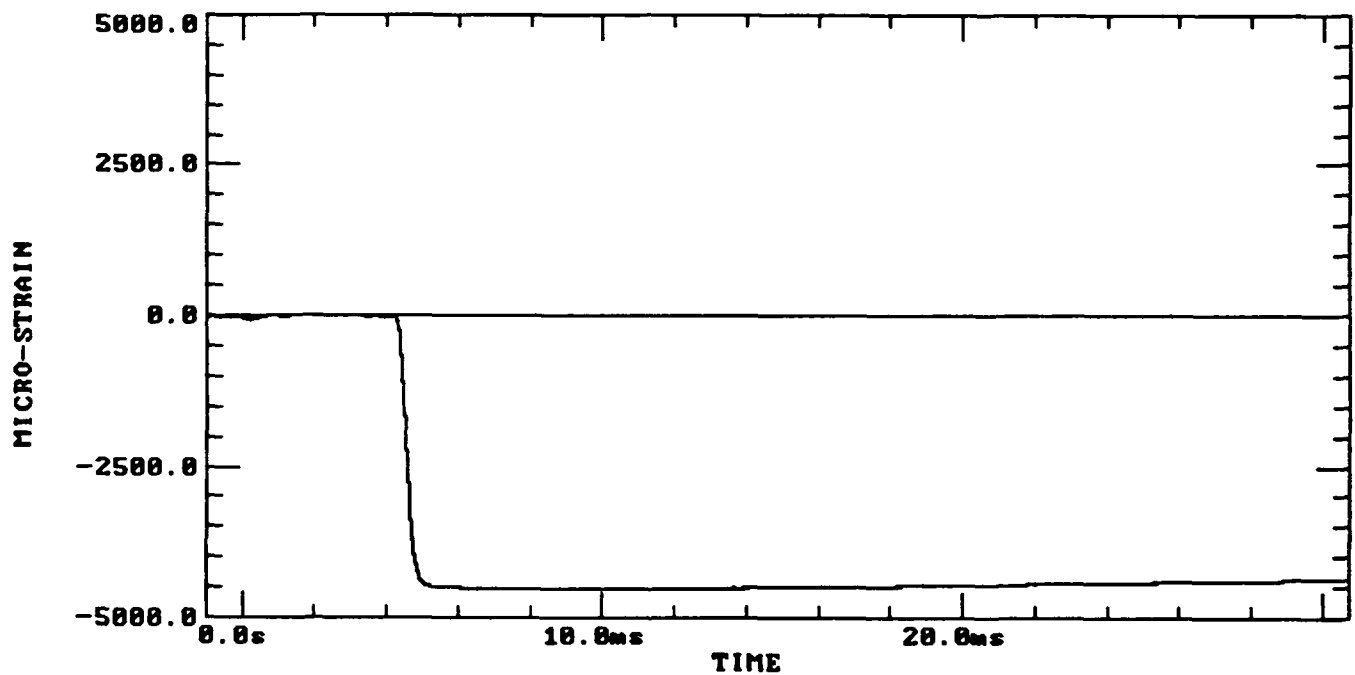
TEST 1

ZERO REPRESENTS DETONATION TIME

TIME HISTORY OF GAUGE C1C

FILTERED AT 2000 HZ LOW PASS

NPS PRECISION UNDEX TESTING

TEST 1

ZERO REPRESENTS DETONATION TIME
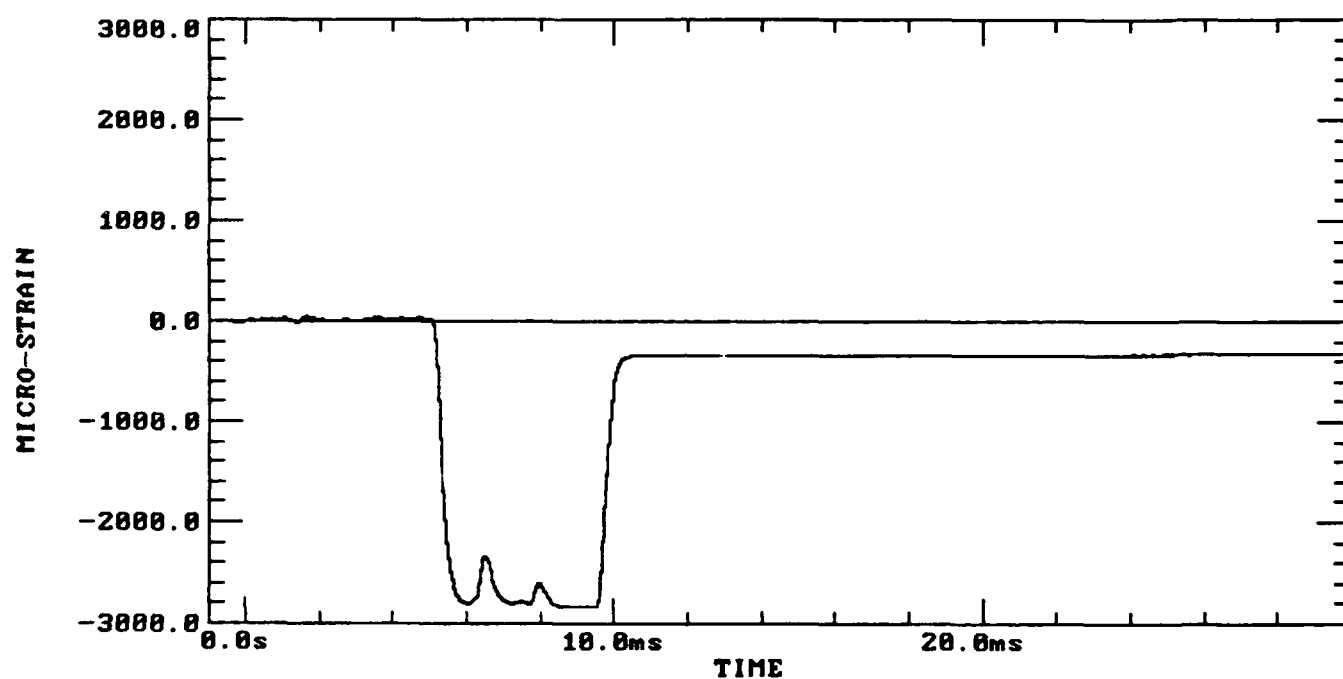
TIME HISTORY OF GAUGE C3C

FILTERED AT 2000 HZ LOW PASS

Test No. 2

NPS PRECISION UNDEX TESTING

TEST 2

ZERO REPRESENTS DETONATION TIME

TIME HISTORY OF GAUGE A1L

FILTERED AT 2000 HZ LOW PASS

NPS PRECISION UNDEX TESTING

TEST 2

ZERO REPRESENTS DETONATION TIME

TIME HISTORY OF GAUGE A2L

FILTERED AT 2000 HZ LOW PASS

NPS PRECISION UNDEX TESTING

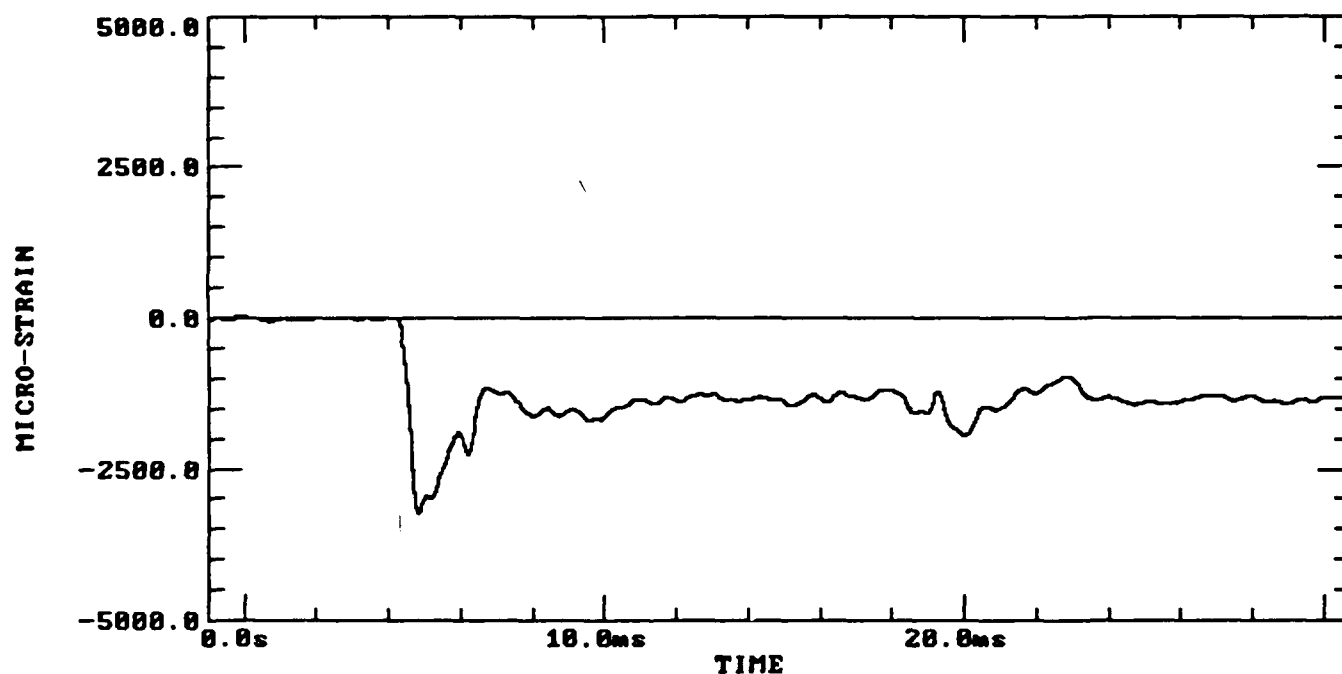**TEST 2**

ZERO REPRESENTS DETONATION TIME

TIME HISTORY OF GAUGE B1L

FILTERED AT 2000 HZ LOW PASS

NPS PRECISION UNDEX TESTING

TEST 2

ZERO REPRESENTS DETONATION TIME

TIME HISTORY OF GAUGE B2L

FILTERED AT 2000 HZ LOW PASS

NPS PRECISION UNDEX TESTING

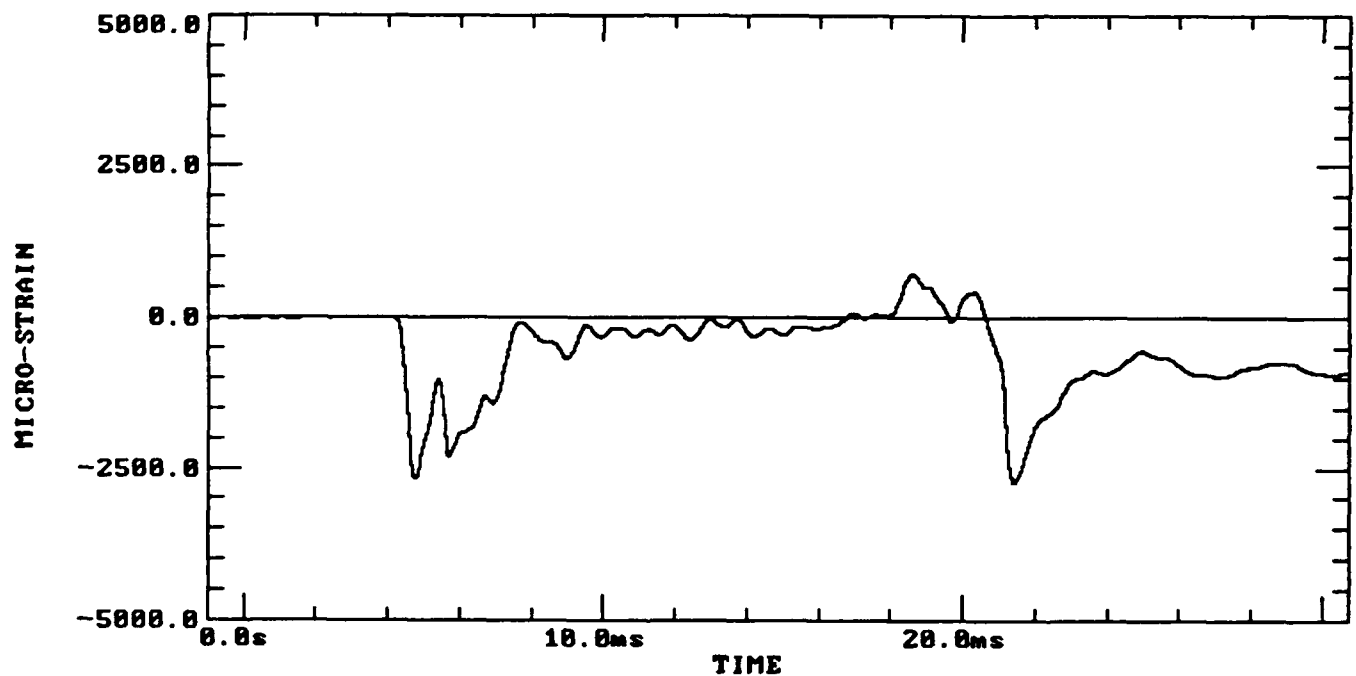**TEST 2**

ZERO REPRESENTS DETONATION TIME

TIME HISTORY OF GAUGE B3L

FILTERED AT 2000 HZ LOW PASS

NPS PRECISION UNDEX TESTING

TEST 2

ZERO REPRESENTS DETONATION TIME

TIME HISTORY OF GAUGE C1L

FILTERED AT 2000 HZ LOW PASS

NPS PRECISION UNDEX TESTING

TEST 2

ZERO REPRESENTS DETONATION TIME

TIME HISTORY OF GAUGE A1C

FILTERED AT 2000 HZ LOW PASS

NPS PRECISION UNDEX TESTING

TEST 2

ZERO REPRESENTS DETONATION TIME

TIME HISTORY OF GAUGE A2C

FILTERED AT 2000 HZ LOW PASS

NPS PRECISION UNDEX TESTING
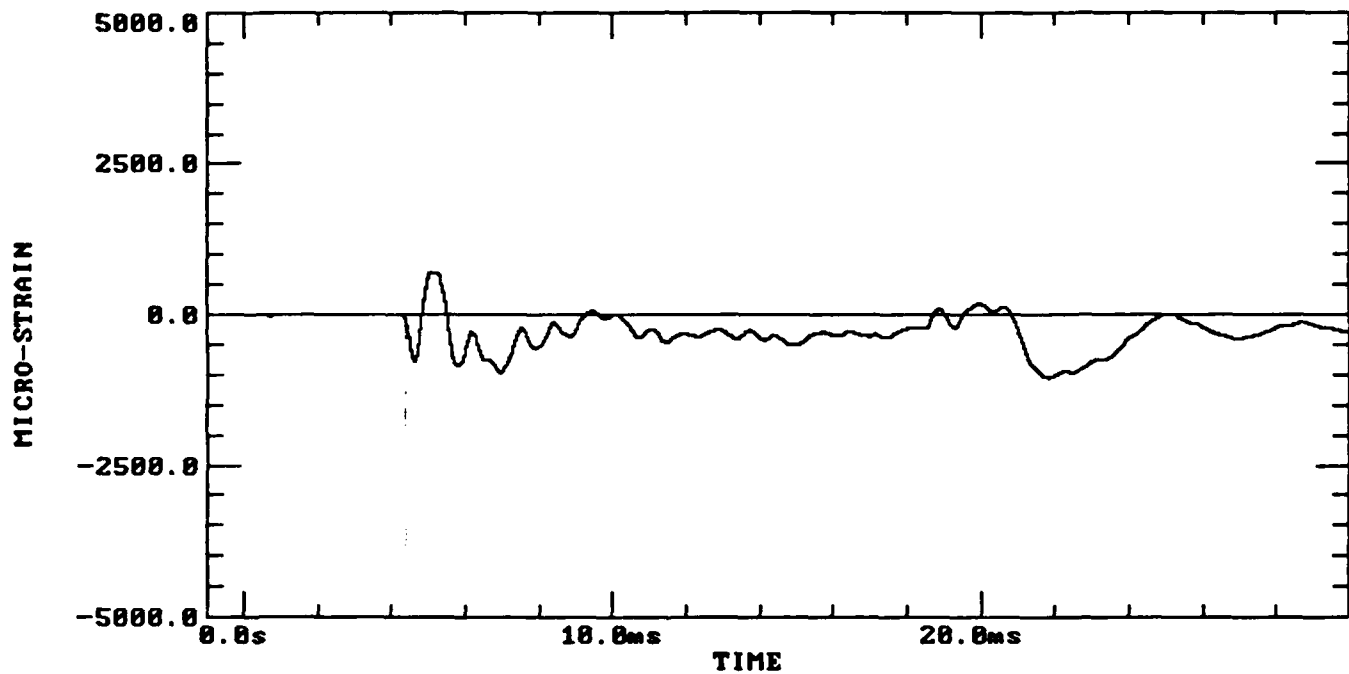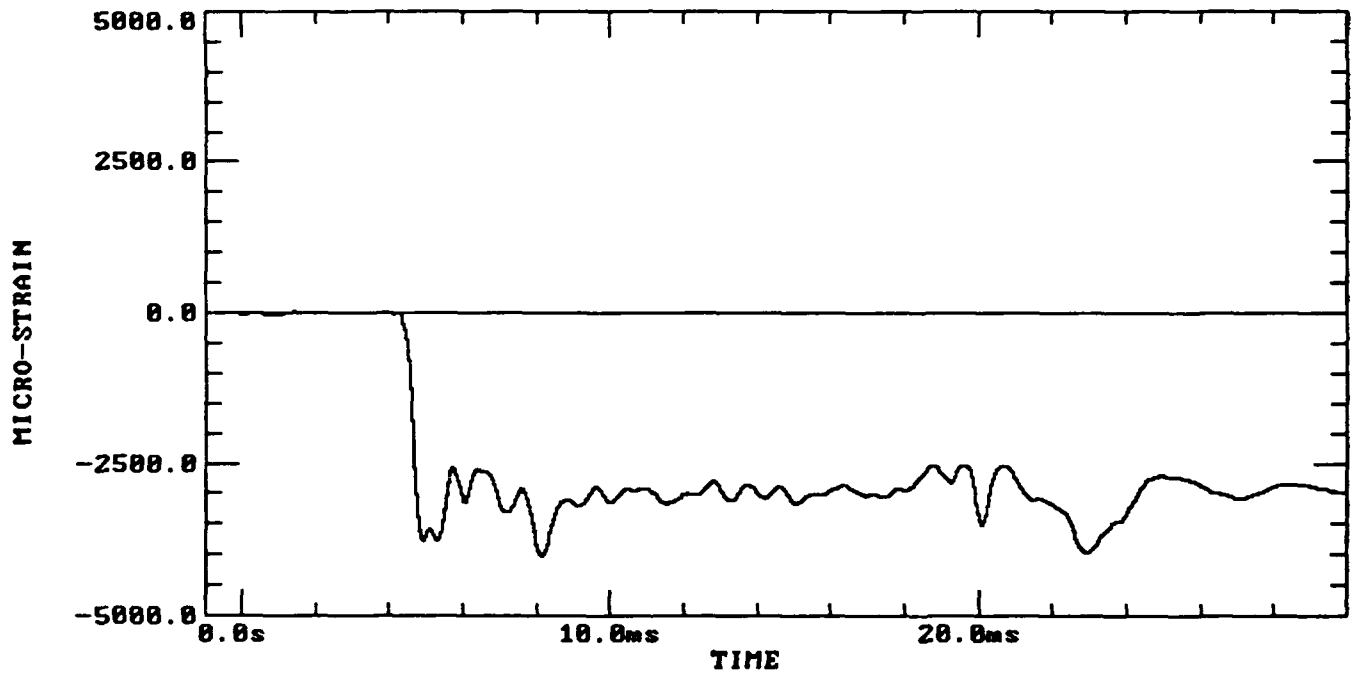
TEST 2

ZERO REPRESENTS DETONATION TIME

TIME HISTORY OF GAUGE B1C

FILTERED AT 2000 HZ LOW PASS

NPS PRECISION UNDEX TESTING

TEST 2

ZERO REPRESENTS DETONATION TIME

TIME HISTORY OF GAUGE B2C

FILTERED AT 2000 HZ LOW PASS

NPS PRECISION UNDEX TESTING

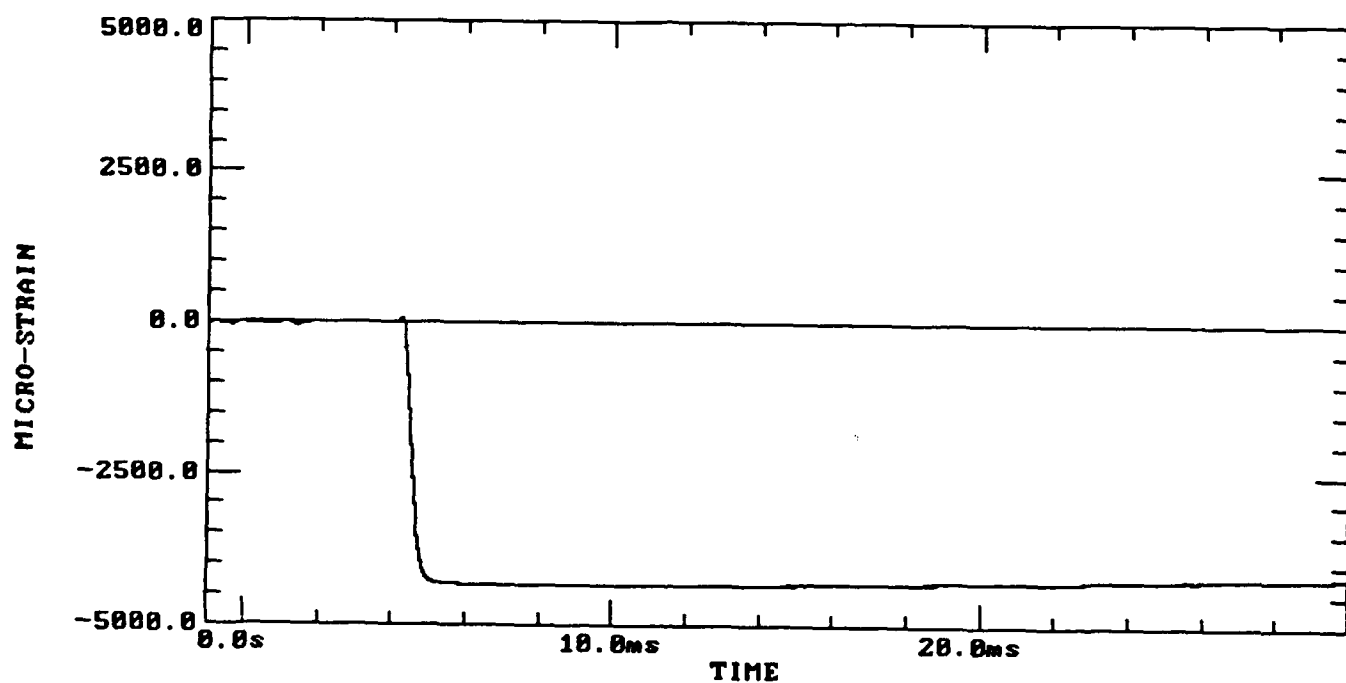**TEST 2**

ZERO REPRESENTS DETONATION TIME

TIME HISTORY OF GAUGE B3C

FILTERED AT 2000 HZ LOW PASS

NPS PRECISION UNDEX TESTING

TEST 2

ZERO REPRESENTS DETONATION TIME

TIME HISTORY OF GAUGE C1C

FILTERED AT 2000 HZ LOW PASS

NPS PRECISION UNDEX TESTING

TEST 2

ZERO REPRESENTS DETONATION TIME
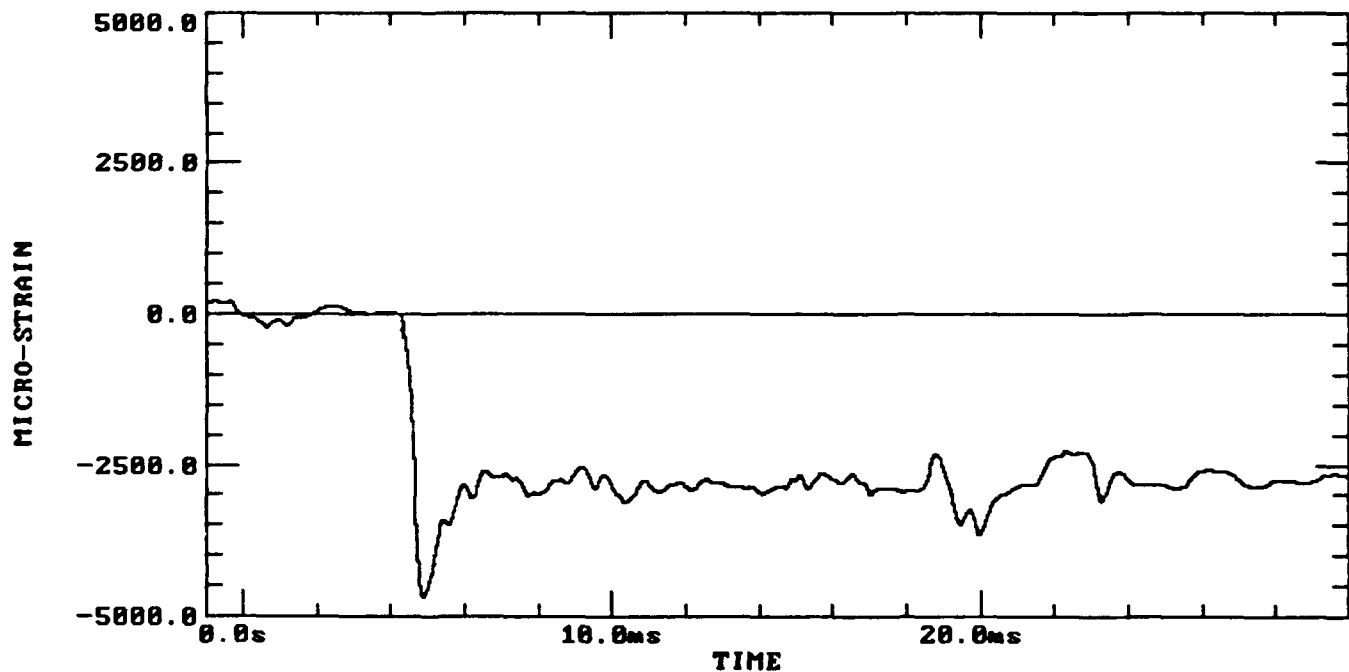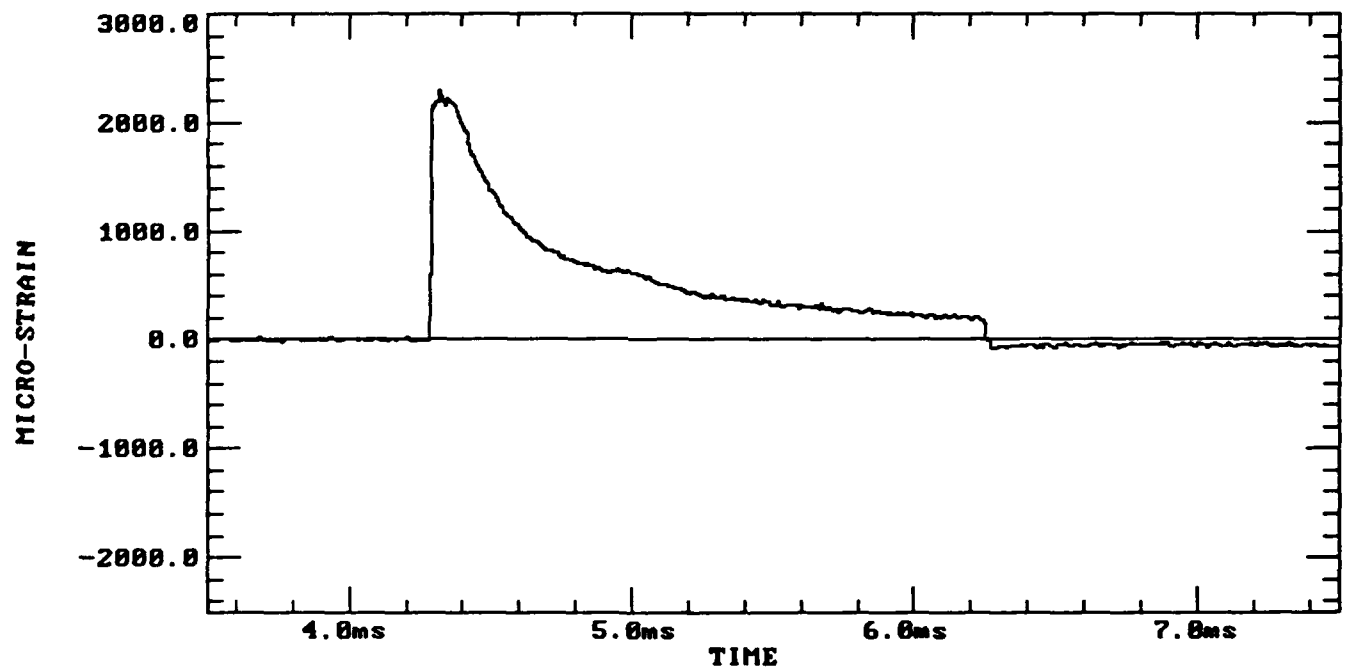

TIME HISTORY OF GAUGE C2C

FILTERED AT 2000 HZ LOW PASS

NPS PRECISION UNDEX TESTING

TEST 2

ZERO REPRESENTS DETONATION TIME

TIME HISTORY OF GAUGE P1

UNFILTERED

INITIAL DISTRIBUTION LIST

No. of Copies

1. Defense Technology Information Center   2
    Cameron Station
    Alexandria, Virginia 22304-6145

2. Library, Code 52   2
    Naval Postgraduate School
    Monterey, California 93943-5002

3. Professor Y. W. Kwon, Code ME/Kw   2
    Department of Mechanical Engineering
    Naval Postgraduate School
    Monterey, California 93943

4. Professor Y. S. Shin, Code ME/Sg   2
    Department of Mechanical Engineering
    Naval Postgraduate School
    Monterey, California 93943

5. Dr. Thomas T. Tsai   1
    Defense Nuclear Agancy
    6801 Telegraph Road
    Alexandria, Virginia 22310

6. Dr. Kent Goering   1
    Defense Nuclear Agancy
    6801 Telegraph Road
    Alexandria, Virginia 22310

7. Mr. Douglas Bruder   1
    Defense Nuclear Agancy
    6801 Telegraph Road
    Alexandria, Virginia 22310

8. Dr. Phillip B. Abraham   1
    Office of Naval Research
    Mechanics Division, Code 1132
    800 North Quincy Street
    Arlington, Virginia 22217-5000

9. Mr. Gene Remmers, ONT-23   1
    Director, Office of Naval Technology
    800 N. Quincy Street
    Arlington, Virginia 22217-5000

10. LCDR Padraic K. Fox   1
    RR 3, Box 181
    Watertown, South Dakota 57201